FOURIER TRANSFORM ION CYCLOTRON RESONANCE MASS SPECTROMETRY INSTRUMENTATION DESIGN AND DEVELOPMENT: REDUCTION OF ION CLOUD DE-PHASING AND TIME-OF-FLIGHT DISCRIMINATION

By

Nathan Kenneth Kaiser

**A dissertation submitted in partial fulfillment of
the requirements for the degree of**

DOCTOR OF PHILOSOPHY

**WASHINGTON STATE UNIVERSITY
Department of Chemistry**

December 2007

To the Faculty of Washington State University:

The members of the Committee appointed to examine the dissertation of NATHAN KENNETH KAISER find it satisfactory and recommend that it be accepted.

_____
Chair

_____

_____

ACKNOWLEDGEMENTS

The work presented here could not have been accomplished without the support and dedication of many individuals. I would like to thank my committee chair and advisor Dr. James E. Bruce for giving me the opportunity to work in his lab and for providing the resources necessary to conduct cutting-edge scientific research. He not only helped to develop my interest for mass spectrometry with his never ending enthusiasm and crazy ideas and to become an independent researcher but also to grow as a person. I also would like to thank all my committee members Dr. William F. Siems, Dr. Herbert H. Hill, and Dr. Ken Nash.

I am grateful for the support I received from Gordon Anderson and David Prior at Pacific Northwest National Laboratory, their advice on electronics and design of various aspects of the instrument proved **extremely** valuable. I would also like to thank the Technical Services at WSU, in particular all the people at the Machine shop who offered very useful advice and were responsible for fabricating many of the components for the FTICR mass spectrometer I helped build.

I would also like to acknowledge all members of the Bruce group present and past, for all their support and valuable suggestions. In particular I would like to thank Sisi Wu and Kai Zhang for helping with the initial development of the instrument, and Gunnar Skulason for all his advice and expertise with electronics and instrument design.

FOURIER TRANSFORM ION CYCLOTRON RESONANCE MASS SPECTROMETRY INSTRUMENTATION DESIGN AND DEVELOPMENT: REDUCTION OF ION CLOUD DE-PHASING AND TIME-OF-FLIGHT DISCRIMINATION

Abstract

By Nathan Kenneth Kaiser, Ph.D.
Washington State University
December 2007

Chair: James E. Bruce

Fourier Transform Ion Cyclotron Resonance (FTICR) mass spectrometers are the instruments of choice for analysis of biological ions produced through electrospray ionization. FTICR mass spectrometers offer highest possible resolution and greatest mass measurement accuracy of any current mass spectrometer. Though FTICR mass spectrometers are the highest performance mass spectrometers available, it is a relatively new technique and still not fully understood in terms of ion dynamics during image current detection. Thus, there are still many improvements to be made to FTICR instrumentation. In this research, we explore a novel way to improve ion current detection and develop instrumentation to overcome the shortcomings of the current ion injection methods.

We have developed a new technique called Electron Promoted Ion Coherence or EPIC to improve duration of the detected time-domain signals. The EPIC technique consists of

injecting a high density beam of electrons through the center of the ICR cell during detection. De-phasing of ion packets during image current detection leads to loss of signal. In principle, the longer the signal is detected the greater the instrument performance. With EPIC, we have been able to detect image current for up to 70 seconds as well as obtain isotopic fine structure. Both experimental and theoretical studies were carried out to establish a theory on how EPIC improves image current detection. The basis of the enhancement is from the alteration of the radial electric fields with the application of the electron beam.

A novel FTICR mass spectrometer which utilizes a 3 Tesla magnet has been developed in our laboratory. There are number of novel features implemented in this instrument, such as a flared capillary inlet tube, electrodynamic ion funnel, Restrained Ion Population Transfer (RIPT) ion guide and a Trapping Ring Electrode Cell (TREC). The RIPT ion guide was developed to eliminate time-of-flight mass discrimination, as well as transfer ions of low kinetic energy to the ICR cell. TREC was designed to allow tuning of radial electric fields during the ICR experiment to improve overall performance.

TABLE OF CONTENTS

Page

LISTS OF TABLES

Chapter 2

Chapter 6

LISTS OF FIGURES

Chapter 2: Figures

Chapter 3: Figures

Chapter 4: Figures

Chapter 5 Figures

Chapter 6 Figures

Chapter 7

Dedication

This dissertation is dedicated to:
my Dad and Mom,
my two brothers Gabe and Chad,
and my sister Kelli

CHAPTER 1

Introduction

Research Objectives

Mass spectrometry has become an indispensable tool for the analysis of complex biological samples, especially in the area of proteomics. Proteomics is the area of research that explores the dynamically changing proteome. It is an analysis of all proteins which are expressed, the quantity of protein present, and location of proteins, which may change based the state of the organism. For example, a certain protein or set of proteins may be differentially-expressed if a particular disease is present. Identification of these proteins may lead to biomarker discovery. To find biomarkers and fully understand protein function more sensitive and accurate methods for protein identification are needed.

The driving force behind my research was to develop new technology which will allow us to dig deeper with more confidence into the proteome. The focus of my research was on the development of novel Fourier transform ion cyclotron resonance mass spectrometry instrumentation for the task mentioned above. My research can be narrowed down to two primary research objectives: (i) modification of electric fields inside the ICR cell during ion measurement to reduce ion cloud de-phasing, and (ii) development of a novel ion transfer technique to transmit ions of low kinetic energy to the ICR cell and eliminate time of flight effects.

Fourier Transform Ion Cyclotron Resonance Mass Spectrometry

The first ion cyclotron [1] instrument to determine the mass of an ion was called the "omegatron", developed in 1949 by Hipple *et. al*. [2]. This instrument detected ion current by continually exciting ion cyclotron motion until the ion physically hit a detector plate. The first commercially available ICR system called the Syrotron, by Varian Associates, did not become available until 1965. This instrument had low resolution and could only detect one mass-to-charge ratio (*m*/*z)* at a time. It operated with fixed frequency detection which required slow scanning of the magnetic field strength to obtain a range of *m*/*z* values. Despite these limitations this instrument proved to be an extremely useful for studying gas phase ion-molecule reaction and rate constants [3-5].

In 1965, Cooley and Tukey developed a fast algorithm which made it possible to Fourier transform a large data set in less than a minute on a minicomputer [6]. By the early 1970's Fourier transform methods had been applied to obtain an entire spectrum at once for IR [7] and NMR [8] spectroscopy. Ion cyclotron resonance mass spectrometry [9] had been used for a number of years before Fourier transform was first applied by Comisarow and Marshall in 1974 [10, 11]. The introduction of Fourier transform to ion cyclotron resonance mass spectrometry allowed the instrument to become a powerful analytical tool. The technique offers 10-100 times higher mass resolution, and mass measurement accuracy than any other mass analysis technique [12]. Up to 12,449 spectral peaks have been assigned in a single mass spectrum [13]. Greater than 8 million resolving power has been shown on 8.6 kDa protein [14]. Routine sub-part-per-million mass measurement accuracy has been achieved [15-17].

The high performance capability of this instrument is enabled by its non-destructive ion detection technique. It utilizes image current detection in which ions spinning on their excited cyclotron orbit induce a charge on two opposed detection plates. The induced charge from the detection plates is sent through a differential amplifier to produce an electrical signal. Therefore, as an ion spins on its excited cyclotron orbit, the signal amplitude varies with time and results in an oscillating signal. Fourier transformation of the digital time-domain signal converts the oscillating signal to the frequency domain. The mass-to-charge ratio of the ion is inversely proportional to its cyclotron frequency as shown in equation 1.

$$(1) \quad \omega_c = \frac{qB_o}{m}$$

ω_c is the "unperturbed" cyclotron frequency, q is the charge, m is the mass, and B_o is the magnetic field strength. The amplitude of the induced charge is dependent upon the number of ions and their proximity to the detection plates. The image charge induced by an ion of charge q, is given in equation 2

$$(2) \quad \Delta Q = -\frac{2qy}{d}$$

ΔQ is the difference in image charge on two opposed infinitely extended parallel conductive plates. y is the ion cyclotron radius, and d is the distance between the plates. Therefore, the ICR signal is proportional to the total induced current as shown in equation 3 [18, 19]. The ICR signal increases with cyclotron radius and ion charge. Therefore, multiply charged ions will produce a larger signal than singly charged ions if

the ion packets contained the same number of ions. It is important to note that the ICR signal is independent of frequency and magnetic field strength.

$$(3)\ \frac{d\Delta Q}{dt} = -2q\frac{\left(dy/dt\right)}{d}$$

It is also possible to calculate the minimum number of ions that need to be present to produce a detectable signal. For an undamped signal in a single 1-second acquisition period the minimum number of ions can be calculated as follows.

$$(4)\ N = \frac{CV_{d(p-p)}}{qA_1(r)}$$

Where C is the capacitance of the detection circuit, $V_{d(p-p)}$ is the peak-to-peak amplitude of the detected voltage, and $A_1(r)$ is a coefficient that is approximately proportional to r [20]. Therefore, to produce an observable signal for ions which have a small number of charges one would need either to have many ions present or sum a number of scans since the signal-to-noise ratio increases with $(n)^{1/2}$. It has also been shown that is possible to detect a single ion with an FTICR mass spectrometer if a there are a large number of charges present [21].

Ions initially contained in the ICR cell do not produce an observable electrical signal by themselves for two reasons. First, the cyclotron radius would be too small to induce a charge on the detection plates. Second, ions of the same m/z species need to be orbiting in-phase with each other. For ions of the same m/z located randomly about the same cyclotron orbit in the ICR cell, any given ion and its induced current on a detection

plate will be cancelled by a charge induced on the opposite detection plate by ions that are 180^o out of phase. The net difference in detected charge between the two plates is zero. In order to detect ICR signal, the ions cyclotron motion is excited by applying an oscillating electric field at the cyclotron frequency of a particular *m*/*z* value. This increases the ion cyclotron radius creating an ion packet with phase coherence. The final excited cyclotron radius depends upon the excitation voltage and duration. For a single *m*/*z* species only one frequency needs to be applied to excite coherent cyclotron motion. However, the advantage of FTICR-MS is the ability to simultaneously detect a large number of species over a broad *m*/*z* range. Thus, all species need to be excited to a detectable cyclotron radius simultaneously. The simultaneous excitation of a number of cyclotron frequencies is called broadband excitation. Broadband excitation is usually accomplished by performing a frequency sweep or "chirp" excitation [11, 22, 23]. The post-excitation radius can be determined by equation 5 [24].

$$(5)\quad r_{excite} = \frac{V_{p-p}\beta_{dipolar}\sqrt{\frac{1}{sweep\_rate}}}{2dB_o}$$

were r_{excite} is the post-excitation radius (m), $V_{p\text{-}p}$ is the amplitude of the RF voltage (peak-to-peak in Volts), $\beta_{dipolar}$ is the geometry scaling factor for a particular ICR cell design [25], d is the ICR cell diameter (m), and *sweep_rate* is in Hz/s. This provides relatively uniform excitation over a broad frequency range. However, there is limited mass selectivity near the beginning and end of the frequency sweep. Another common type of frequency excitation is Stored Wave Inverse Fourier Transform or SWIFT [26-28]. SWIFT provides a more uniform excitation profile than "chirp" and results in improved

accuracy and precision [29]. With SWIFT the desired excitation profile is generated by first creating the desired excitation spectrum in the mass-domain converting it to the frequency-domain followed by inverse Fourier transform to generate the desired excitation waveform.

Ions need to be confined in three dimensions in order to observe their cyclotron frequencies for an extended time period. Ions are trapped in an ICR cell in the *x*-*y* direction by a strong spatially uniform magnetic field and along the *z*-axis by electrostatic potentials applied to trapping electrodes. The axial confinement of a single ion in a magnetic field results in primarily three types of ion motion, (1) cyclotron motion, (2) magnetron motion, and (3) trapping motion. Cyclotron frequency results from the motion of a charged particle in a magnetic field. Magnetron motion results from the outward directed radial force of the electrostatic potential needed to confine the ions axially. This causes the ions to acquire a drift orbit within the ICR cell at a constant electrostatic potential. Trapping motion is the ion oscillation along the *z*-axis of the cell resulting from the potential well formed by the potentials applied to the trapping electrodes. The different motions that arise have frequencies that differ by several orders of magnitudes.

Cyclotron frequency >> Trapping frequency >> Magnetron frequency

For a 1000 *m*/*z* species in a 7 Tesla magnet field with 1 volt applied to the trapping electrodes the cyclotron frequency will be approximately 100 kHz, the trapping frequency will be approximately 3 kHz, while the magnetron frequency will be on the order of 10-20 Hz.

Below is the set of equations that is used to derive the observed cyclotron frequency. Ion motion perpendicular to a spatially uniform magnetic field will result in a

vector cross product between the ion velocity and the magnetic field, which results in the Lorentz force that is perpendicular to the direction of the magnetic field. In a strong spatially homogenous magnetic field the path of the ion is continually altered by Lorentz forces such that the trajectory is circular.

(6) $Force = mass \cdot acceleration = m\frac{dv}{dt} = qv \times B$

Angular acceleration perpendicular to the magnetic field is equal to

(7) $v^2{}_{xy} / r$

Substituting equation 7 into the acceleration component of equation 6 one gets

(8) $\frac{mv^2{}_{xy}}{r} = qv_{xy}B_o$

the equation for angular frequency

(9) $\omega = \frac{v_{xy}}{r}$

Solving for angular velocity and substitution into equation 8 results in the following

(10) $m\omega^2 r = qB_o\omega r$

This equation is reduced to the following "unperturbed" cyclotron frequency

(1) $\omega_c = \frac{qB_o}{m}$

However, the addition of electric fields needed to confine ions to a finite space produces a radial force describe as

(11) $Radial\_force = qE(r) = \frac{qV_{trap}\alpha}{a^2}r$

Were q is the charge, V_{trap} is the trap plate potential, α is an ICR cell geometry factor, a is the distance between trap plates, and r is the radius. This outward directed electric force opposes the inward-directed Lorentz force, therefore they have opposite signs. With the presence of this outward-directed force we can combine equations 10 and 11 to obtain the equation for motion in a static magnetic field and we assume a three-dimensional axial quadrupolar electrostatic potential is created by the trap electrodes.

(12) $Force = m\omega^2 r = qB_o\omega r - \frac{qV_{trap}\alpha}{a^2}r$

This equation can be reduced as follows

(13) $\omega^2 - \frac{qB_o\omega}{m} + \frac{qV_{trap}\alpha}{ma^2} = 0$

Thus, two important things are a direct result of this relationship: 1) in a perfectly three dimensional axial quadrupolar electric field the observed frequency is independent of radius and 2) the expression reduces to a quadratic equation. When this equation is

solved it produces two separate frequencies in place of the "unperturbed" cyclotron frequency.

(14) $\omega_{+} = \frac{\omega_c}{2} + \sqrt{\left(\frac{\omega_c}{2}\right)^2 - \frac{\omega_z^2}{2}}$ "reduced" cyclotron frequency

(15) $\omega_{-} = \frac{\omega_c}{2} - \sqrt{\left(\frac{\omega_c}{2}\right)^2 - \frac{\omega_z^2}{2}}$ "magnetron" frequency

The trapping oscillation can be described as

(16) $\omega_z = \sqrt{\frac{2qV_{trap}\alpha}{ma^2}}$ "Trapping" frequency

One of the figures of merit which allows FTICR mass spectrometry to stand above other types of mass spectrometers is the ability to provide ultra-high accuracy mass measurements. The mass-to-charge ratio of an ion is inversely proportional to the cyclotron frequency of that ion; however, there are other factors which cause perturbations to the cyclotron frequency which degrades the performance of the instrument if not carefully controlled [30]. The magnetron frequency reduces the unperturbed cyclotron frequency so that the observed cyclotron frequency can be expressed by equation 17.

(17) $\omega_{+} = \omega_c - \omega_{-}$

Where ω_c is the "unperturbed" cyclotron frequency, ω_+ is the reduced cyclotron frequency and ω_- is the magnetron frequency. The inclusion of trapping potentials produces an outward-directed radial electric field which effectively reduces the ion cyclotron frequency. The observed cyclotron frequency can be converted to a mass-to-charge ratio simply by matching the observed cyclotron frequencies to masses of known elemental composition. The coefficients are usually fit to the data by a simple least-squares best fit, whose coefficients are generated directly form the data. The two most common frequency-to-mass formulas in use were derived by Ledford *et al.* [31, 32] who assumed that the $m/z < (m/z)_{\text{critical}}$ were $(m/z)_{\text{critical}}$ is the value at which the magnetron and reduced cyclotron converge. The other calibration equation developed by Francl. *et al*. [33] assumes that the $m/z << (m/z)_{\text{critical}}$. Shi *et. al*. [34] showed that the mass measurement accuracy resulting from these two calibration functions (and their interconversion) are indistinguishable.

(18) $$\frac{m}{z} = \frac{A}{\nu_+} + \frac{B}{\nu^2_+}$$ Ledford *et al*.

(19) $$\frac{m}{z} = \frac{A}{\nu_+ - B}$$ Francl *et al*.

Though these are the two most common mass calibration equations, many more investigators have taken these equations and expanded them to take into account factors which may cause perturbations to the calibration [35]. Since FTICR measurements are usually carried out with a large number of trapped ions it is necessary to consider static and dynamic effects of ion-ion repulsion. Increasing the number of ions decreases the

observed cyclotron frequency [36]. This frequency shift based on the number of ions is called the "space charge" effect. Therefore, when performing accurate mass measurements it is necessary trap the same number of ions in every data acquisition period. This can be accomplished with automated gain control [37, 38]. If the number of ions injected into the ICR cell does vary, the frequency can be corrected for by performing internal calibration [39-42]. Since space charge results in a constant frequency shift across the entire spectrum a single peak can be used to shift all frequencies [43]. A calibration curve can also be established to account for frequency shifts as a function of ion intensity [17, 44]. A post calibration method has also been developed to correct for space charge frequency shifts when multiple charge states are present by adjusting the calibration equation so the deconvolved isotope envelopes overlay exactly [45, 46]. However, recently it has been shown that an ion cloud experiences different interactions with other ion clouds. Thus, ion packets with a lower number of ions will have more of a frequency shift than a packet that contains a large number of ions [47]. This idea has been used to modify the calibration equations to increase the mass measurement accuracy [48-50].

Ion-ion interactions can also lead to peak coalescence between two closely spaced peaks if too many ions are present [51]. This is a problem when determining isotopic fine structure within the isotope envelope [52, 53]. Isotopic fine structure can provide information such as the number of sulfur atoms present in the molecule [54]. The peak coalescence phenomenon is also a problem for large proteins that are highly charged since the frequency difference between isotope peaks becomes small [55]. When performing high resolution measurements, it is also possible for the frequency to shift

during ion detection. It is most common to see a frequency shift to high *m*/*z* because as the ion cloud encounters collisions the cyclotron radius decreases and the space charge increases. The spatial distribution of ions decreases as the cyclotron radius decreases. A number of corrections have been developed to correct for the time based frequency shift [56, 57].

There are three ideal types of electric fields within the ICR cell that need to be generated to form the ideal cell [58]. (1) When the RF voltage is applied to the excite plates, the electric field lines should be parallel to the excite plates. If these electric field lines are not completely parallel to the direction of the magnetic field, ions will gain velocity in the *z*-direction Thus, ejection of ions along the *z*-axis during excitation when the excitation frequency is twice the trapping frequency or the cyclotron frequency plus twice the trapping frequency can occur [59, 60]. For optimized excitation profile, the open coupled cell [61], infinity cell [62], and electric field shimming electrode cell were designed [63, 64]. These cells are desirable since they eliminate *z*-axis ejection during excitation, and are able to excite ions to the same cyclotron radius more reliably. (2) To obtain a frequency that is independent of ion position in the cell, the trapping electric fields should form a three dimensional quadrupolar potential inside the ICR cell. This can be achieved with a hyperbolic geometry cell [65, 66]. Deviations to these non-ideal electric fields results in frequency perturbations due to static electric fields [67-70]. A number of ICR cells have been designed to reduce frequency perturbations from static electric fields [63, 64, 67, 71]. (3) Azimuthal quadrupolar R.F. potential is applied for ion axialization [72], the generation of this type of electric field converts magnetron motion to cyclotron motion in the presence of a collision gas [73, 74]. This technique of

quadrupolar axialization improves virtually every aspect of FTICR instrument performance, and allows accurate remeasurment of ions which improves signal-to-noise ratio and lowering the detection limit [75-79]. Since most instruments create ions external to the magnetic field, the trap design must also consider open access for externally generated ions [80, 81]. There is usually a trade-off in one of these electrical fields during ICR cell design. However, there are a number of cells that have been developed to optimize one or more the ideal electric fields [82-85]. However, Marshall and coworkers, designed a matrix-shimmed ICR cell that consisted of 150 electrodes that was able to produce any desired electric field inside the ICR cell, though was unable to produce the desired performance from the ICR cell [86]. The ICR cells employed in commercial instruments have been designed to minimize *z*-axis ejection during ion excitation [61, 62].

Calculation of a single molecule in an ICR cell in a static magnetic field has been done to get an approximation of ion motion [68]. Though a single ion has been detected with FTICR [21, 87, 88] most experiments are carried out with large number of ions. Therefore, Coulombic interactions of ions become extremely important in describing a model for ion motion within the ICR cell. The increase in the number of ions greatly increases the complexity of ion motion compared to a single ion. These models need to account for Coulombic frequency shifts, sideband generation, spectral line broadening as well as coalescence of closely spaced peaks [30, 89-96]. Therefore, realistic modeling of ion motion is needed to fully understand ion motion inside an ICR cell [97, 98]. Rapid degradation of FTICR signal is still a major problem and a better understanding of the

mechanisms which causes ion cloud de-phasing is needed for FTICR to reach its full potential.

Attributions

Chapters 2-6 were written based on the format required for publication in their respective journals. I collected all the data that is presented here as well as wrote the manuscripts. Dr. Bruce advised all the projects and provided the funding. The work described in Chapter 2 was published in the *Journal of the American Society for Mass Spectrometry* (Nathan K. Kaiser, Gordon A. Anderson, and James E. Bruce, J. Am. Soc. Mass Spectrom. **2005,** *16*, 463-470.). In this work, Gordon offered valuable advice on the data processing.

Chapter 3 contains the work published in the journal of *Analytical Chemistry* (Nathan K. Kaiser and James E. Bruce, *Anal. Chem*. **2005,** *77*, 5973-5981).

The research work in chapter 4 was published in the *International Journal of Mass Spectrometry* (Nathan K. Kaiser and James E. Bruce, *Int. J. Mass Spectrom.* **2007,** 265, 271-280.).

The research work contained in chapter 5 has been submitted for publication to the *Journal of the American Society for Mass Spectrometry* (Nathan K. Kaiser, Brian N.

Webb, Chad R. Weisbrod, and James E. Bruce.) Chad and Brian help perform the SIMION calculations.

Chapter 6 was written in the format required for publication in the journal of *Rapid Communications in Mass Spectrometry* (Nathan K. Kaiser, Gunnar E. Skulason, Chad R. Weisbrod, David C. Prior, Michael Buschbach, Gordon A. Anderson, and James E. Bruce.) Gunnar built the RF generators, excitation amplifier, and was crucial in developing and trouble shooting the instrument. Chad designed the ICR cell used for image current detection. Buschbach wrote the RIPT computer program. David Prior helped build the RF generators and offered sound advice on construction of the RIPT ion guide. Gordon offered advice on the RIPT ion guide construction.

Chapter 7 describes the in-house designed FTICR mass spectrometer. Si Wu and Kai Zhang helped in the instrument design and construction. In particular, help with the development of the ion source region. Gunnar helped troubleshoot the instrument and made valuable suggestions as well as provided most of the electronics support.

References

1. Lawrence, E. O., Livingston, M. S., The production of high-speed light ions without the use of high voltages, *Physical Review*. **1932,** *40*, 19-35.

2. Hipple, J. A., Sommer, H., Thomas, H. A., *Physcial Reviews*. **1949,** *76*, 1877.

3. Moylan, C. R., Brauman, J. I., Gas phase acid-base chemistry, *Annu Rev Phys Chem*. **1983,** *34*, 187-215.

4. Baldeschwieler, J. D., Benz, H., Llewellyn, P. M., Ion-molecule reactions in an ion-cyclotron-resonance mass spectrometer, *Advances in Mass Spectrometry*. **1968,** *4*, 113-120.

5. Anders, L. R., Beauchamp, J. L., Dunbar, R. C., Baldeschwieler, J. D., Ion-cyclotron double resonance, *J Chem Phys*. **1966,** *45*, 1062-1063.

6. Cooley, J. W., Tukey, J. W., *Math Comp.* **1975,** *19*, 9.

7. Low, M. J. D., Freeman, S. K., Measurements of infrared spectra of gas-liquid chromatography fractions using multiple-scan interference spectrometry, *Analytical Chemistry*. **1967,** *39*, 194-198.

8. Ernst, R. R., Anderson, W. A., Application of Fourier transform spectroscopy to magnetic resonance, *Review of Scientific Instruments*. **1966,** *37*, 93-102.

9. Bloom, M., Riggin, M., Theory of ion cyclotron resonance, *Can J Phys*. **1974,** *52*, 436-455.

10. Comisarow, M. B., Marshall, A. G., Fourier transform ion cyclotron resonance spectroscopy, *Chemical Physics Letters*. **1974,** *25*, 282-283.

11. Comisarow, M. B., Marshall, A. G., Frequency-sweep Fourier transform ion cyclotron resonance spectroscopy, *Chemical Physics Letters*. **1974,** *26*, 489-490.

12. Marshall, A. G., Milestones in Fourier transform ion cyclotron resonance mass spectrometry technique development, *International Journal of Mass Spectrometry*. **2000,** *200*, 331-356.

13. Purcell, J. M., Hendrickson, C. L., Rodgers, R. P., Marshall, A. G., Atmospheric Pressure Photoionization Proton Transfer for Complex Organic Mixtures Investigated by Fourier Transform Ion Cyclotron Resonance Mass Spectrometry, *Journal of the American Society for Mass Spectrometry*. **2007,** *18*, 1682-1689.

14. Shi, S. D. H., Hendrickson, C. L., Marshall, A. G., Counting individual sulfur atoms in a protein by ultrahigh-resolution Fourier transform ion cyclotron resonance mass spectrometry: experimental resolution of isotopic fine structure in proteins, *Proceedings of the National Academy of Sciences of the United States of America*. **1998,** *95*, 11532-11537.

15. Kim, S., Rodgers, R. P., Marshall, A. G., Truly "exact" mass: Elemental composition can be determined uniquely from molecular mass measurement at .apprx.0.1mDa accuracy for molecules up to .apprx.500Da, *International Journal of Mass Spectrometry*. **2006,** *251*, 260-265.

16. Muddiman, D. C., Oberg, A. L., Statistical Evaluation of Internal and External Mass Calibration Laws Utilized in Fourier Transform Ion Cyclotron Resonance Mass Spectrometry, *Analytical Chemistry*. **2005,** *77*, 2406-2414.

17. Easterling, M. L., Mize, T. H., Amster, I. J., Routine part-per-million mass accuracy for high-mass ions: space-charge effects in MALDI FT-ICR, *Analytical Chemistry*. **1999,** *71*, 624-632.

18. Limbach, P. A., Grosshans, P. B., Marshall, A. G., Experimental determination of the number of trapped ions, detection limit, and dynamic range in Fourier transform ion cyclotron resonance mass spectrometry, *Analytical Chemistry*. **1993,** *65*, 135-140.

19. Guan, S., Marshall, A. G., Ion traps for Fourier transform ion cyclotron resonance mass spectrometry: principles and design of geometric and electric configurations, *International Journal of Mass Spectrometry and Ion Processes*. **1995,** *146/147*, 261-296.

20. Grosshans, P. B., Marshall, A. G., Theory of ion cyclotron resonance mass spectrometry: resonant excitation and radial ejection in orthorhombic and cylindrical ion traps, *International Journal of Mass Spectrometry and Ion Processes*. **1990,** *100*, 347-379.

21. Smith, R. D., Cheng, X., Bruce, J. E., Hofstadler, S. A., Anderson, G. A., Trapping, detection and reaction of very large single molecular ions by mass spectrometry, *Nature (London, United Kingdom)*. **1994,** *369*, 137-139.

22. Marshall, A. G., Roe, D. C., Theory of Fourier transform ion cyclotron resonance mass spectroscopy: response to frequency-sweep excitation, *J Chem Phys*. **1980,** *73*, 1581-1590.

23. Alan G. Marshall, Verdun, F. R., Fourier Transforms in NMR, optical, and mass spectrometry: a user's handbook, **1990.**

24. Marshall, A. G., Hendrickson, C. L., Jackson, G. S., Fourier transform ion cyclotron resonance mass spectrometry: a primer, *Mass Spectrometry Reviews*. **1998,** *17*, 1-35.

25. Jackson, G. S., Canterbury, J. D., Guan, S., Marshall, A. G., Linearity and quadrupolarity of tetragonal and cylindrical Penning traps of arbitrary length-to-width ratio, *Journal of the American Society for Mass Spectrometry*. **1997,** *8*, 283-293.

26. Marshall, A. G., Ricca, T. L., Wang, T.-C. L., Tailored excitation for trapped ion mass spectrometry, *U.S.* **1988,** 23 pp.

27. Marshall, A. G., Wang, T. C. L., Ricca, T. L., Tailored excitation for Fourier transform ion cyclotron mass spectrometry, *Journal of the American Chemical Society*. **1985,** *107*, 7893-7897.

28. Guan, S., Marshall, A. G., Stored waveform inverse Fourier transform (SWIFT) ion excitation in trapped-ion mass spectrometry: theory and applications, *International Journal of Mass Spectrometry and Ion Processes*. **1996,** *157/158*, 5-37.

29. Frahm, J. L., Velez, C. M. C., Muddiman, D. C., Understanding the influence of post-excite radius and axial confinement on quantitative proteomic measurements using Fourier transform ion cyclotron resonance mass spectrometry, *Rapid Communications in Mass Spectrometry*. **2007,** *21*, 1196-1204.

30. Gorshkov, M. V., Marshall, A. G., Analysis and elimination of systematic errors originating from Coulomb mutual interaction and image charge in Fourier transform ion cyclotron resonance precise mass difference measurements, *Journal of the American Society for Mass Spectrometry*. **1993,** *4*, 855-868.

31. Ledford, E. B., Jr., Rempel, D. L., Gross, M. L., Space charge effects in Fourier transform mass spectrometry. I. Electrons, *International Journal of Mass Spectrometry and Ion Processes*. **1984,** *55*, 143-154.

32. Ledford, E. B., Jr., Rempel, D. L., Gross, M. L., Space charge effects in Fourier transform mass spectrometry. Mass calibration, *Anal Chem*. **1984,** *56*, 2744-2748.

33. Francl, T. J., Fukuda, E. K., McIver, R. T., Jr., A diffusion model for nonreactive ion loss in pulsed ion cyclotron resonance experiments, *International Journal of Mass Spectrometry and Ion Physics*. **1983,** *50*, 151-167.

34. Shi, S. D. H., Drader, J. J., Freitas, M. A., Hendrickson, C. L., Marshall, A. G., Comparison and interconversion of the two most common frequency-to-mass calibration functions for fourier transform ion cyclotron resonance mass

spectrometry, *International Journal of Mass Spectrometry*. **2000,** *195/196*, 591-598.

35. Zhang, L. K., Rempel, D. L., Gross, M. L., Accurate Mass Measurements by Fourier Transform Mass Spectrometry, *Mass Spectrometry Reviews*. **2005,** *24*, 286-309.

36. Jeffries, J. B., Barlow, S. E., Dunn, G. H., Theory of space-charge shift of ion cyclotron resonance frequencies, *International Journal of Mass Spectrometry and Ion Processes*. **1983,** *54*, 169-187.

37. Belov, M. E., Zhang, R., Strittmatter, E. F., Prior, D. C., Tang, K., Smith, R. D., Automated gain control and internal calibration with external ion accumulation capillary liquid chromatography-electrospray ionization-Fourier transform ion cyclotron resonance, *Analytical Chemistry*. **2003,** *75*, 4195-4205.

38. Syka, J. E. P., Marto, J. A., Bai, D. L., Horning, S., Senko, M. W., Schwartz, J. C., Ueberheide, B., Garcia, B., Busby, S., Muratore, T., Shabanowitz, J., Hunt, D. F., Novel linear quadrupole ion trap/FT mass spectrometer: performance characterization and use in the comparative analysis of histone H3 post-translational modifications, *Journal of Proteome Research*. **2004,** *3*, 621-626.

39. Hannis, J. C., Muddiman, D. C., A dual electrospray ionization source combined with hexapole accumulation to achieve high mass accuracy of biopolymers in Fourier transform ion cyclotron resonance mass spectrometry, *Journal of the American Society for Mass Spectrometry*. **2000,** *11*, 876-883.

40. Kruppa, G., Schnier, P. D., Tabei, K., Van Orden, S., Siegel, M. M., Multiple ion isolation applications in FT-ICR MS: exact-mass MSn internal calibration and purification/interrogation of protein-drug complexes, *Anal Chem*. **2002,** *74*, 3877-3886.

41. Solouki, T., Gillig, K. J., Russell, D. H., Mass measurement accuracy of matrix-assisted laser desorbed biomolecules: a Fourier-transform ion cyclotron resonance mass spectrometry study, *Rapid Communications in Mass Spectrometry*. **1994,** *8*, 26-31.

42. Yanofsky, C. M., Bell, A. W., Lesimple, S., Morales, F., Lam, T. T., Blakney, G. T., Marshall, A. G., Carrillo, B., Lekpor, K., Boismenu, D., Kearney, R. E., Multicomponent Internal Recalibration of an LC-FTICR-MS Analysis Employing a Partially Characterized Complex Peptide Mixture: Systematic and Random Errors, *Analytical Chemistry*. **2005,** *77*, 7246-7254.

43. Burton, R. D., Matuszak, K. P., Watson, C. H., Eyler, J. R., Exact mass measurements using a 7 tesla fourier transform ion cyclotron resonance mass

spectrometer in a good laboratory practices-regulated environment, *Journal of the American Society for Mass Spectrometry*. **1999,** *10*, 1291-1297.

44. Taylor, P. K., Amster, I. J., Space charge effects on mass accuracy for multiply charged ions in ESI-FTICR, *International Journal of Mass Spectrometry*. **2003,** *222*, 351-361.

45. Bruce, J. E., Anderson, G. A., Brands, M. D., Pasa-Tolic, L., Smith, R. D., Obtaining more accurate Fourier transform ion cyclotron resonance mass measurements without internal standards using multiply charged ions, *Journal of the American Society for Mass Spectrometry*. **2000,** *11*, 416-421.

46. Kaiser, N. K., Anderson, G. A., Bruce, J. E., Improved mass accuracy for tandem mass spectrometry, *Journal of the American Society for Mass Spectrometry*. **2005,** *16*, 463-470.

47. Masselon, C., Tolmachev, A. V., Anderson, G. A., Harkewicz, R., Smith, R. D., Mass measurement errors caused by "local" frequency perturbations in FTICR mass spectrometry, *Journal of the American Society for Mass Spectrometry*. **2002,** *13*, 99-106.

48. Wong Richard, L., Amster, I. J., Sub part-per-million mass accuracy by using stepwise-external calibration in fourier transform ion cyclotron resonance mass spectrometry, *J Am Soc Mass Spectrom* ***2006,*** *17*, 1681-1691.

49. Tolmachev, A. V., Monroe, M. E., Jaitly, N., Petyuk, V. A., Adkins, J. N., Smith, R. D., Mass Measurement Accuracy in Analyses of Highly Complex Mixtures Based Upon Multidimensional Recalibration, *Analytical Chemistry*. **2006,** *78*, 8374-8385.

50. Williams, D. K., Jr., Muddiman, D. C., Parts-Per-Billion Mass Measurement Accuracy Achieved through the Combination of Multiple Linear Regression and Automatic Gain Control in a Fourier Transform Ion Cyclotron Resonance Mass Spectrometer, *Analytical Chemistry*. **2007,** *79*, 5058-5063.

51. Naito, Y., Inoue, M., Peak confluence phenomenon in Fourier transform ion cyclotron resonance mass spectrometry, *Journal of the Mass Spectrometry Society of Japan*. **1994,** *42*, 1-9.

52. Stults, J. T., Minimizing peak coalescence: high-resolution separation of isotope peaks in partially deamidated peptides by matrix-assisted laser desorption/ionization Fourier transform ion cyclotron resonance mass spectrometry, *Analytical Chemistry*. **1997,** *69*, 1815-1819.

53. Pasa-Tolic, L., Huang, Y., Guan, S., Kim, H. S., Marshall, A. G., Ultrahigh-resolution matrix-assisted laser desorption/ionization Fourier transform ion

cyclotron resonance mass spectra of peptides, *Journal of Mass Spectrometry*. **1995,** *30*, 825-833.

54. Solouki, T., Emmett, M. R., Guan, S., Marshall, A. G., Detection, number, and sequence location of sulfur-containing amino acids and disulfide bridges in peptides by ultrahigh-resolution MALDI FTICR mass spectrometry, *Anal Chem:**1997.** 69*, 1163-1168.

55. Beu, S. C., Senko, M. W., Quinn, J. P., Wampler, F. M., III, McLafferty, F. W., Fourier-transform electrospray instrumentation for tandem high-resolution mass spectrometry of large molecules, *Journal of the American Society for Mass Spectrometry*. **1993,** *4*, 557-565.

56. Guan, S., Wahl, M. C., Marshall, A. G., Elimination of frequency drift from Fourier transform ion cyclotron resonance mass spectra by digital quadrature heterodyning: ultrahigh mass resolving power for laser-desorbed molecules, *Anal Chem*. **1993,** *65*, 3647-3653.

57. Bruce, J. E., Anderson, G. A., Hofstadler, S. A., Winger, B. E., Smith, R. D., Time-base modulation for the correction of cyclotron frequency shifts observed in long-lived transients from Fourier-transform ion-cyclotron-resonance mass spectrometry of electrosprayed biopolymers, *Rapid Communications in Mass Spectrometry*. **1993,** *7*, 700-703.

58. Anderson, J. S., Vartanian, H., Laude, D. A., Evolution of trapped ion cells in Fourier transform ion cyclotron resonance mass spectrometry, *TrAC, Trends in Analytical Chemistry*. **1994,** *13*, 234-239.

59. Van der Hart, W. J., Van de Guchte, W. J., Excitation of the z-motion of ions in a cubic ICR cell, *International Journal of Mass Spectrometry and Ion Processes*. **1988,** *82*, 17-31.

60. Van de Guchte, W. J., Van der Hart, W. J., Excitation of the z motion of ions in cubic and elongated ion cyclotron resonance cells, *International Journal of Mass Spectrometry and Ion Processes*. **1990,** *95*, 317-326.

61. Beu, S. C., Laude, D. A., Jr., Elimination of axial ejection during excitation with a capacitively coupled open trapped-ion cell for Fourier transform ion cyclotron resonance mass spectrometry, *Analytical Chemistry*. **1992,** *64*, 177-180.

62. Caravatti, P., Allemann, M., The infinity cell: a new trapped-ion cell with radiofrequency covered trapping electrodes for Fourier transform ion cyclotron resonance mass spectrometry, *Organic Mass Spectrometry*. **1991,** *26*, 514-518.

63. Wang, M., Marshall, A. G., A "screened" electrostatic ion trap for enhanced mass resolution, mass accuracy, reproducibility, and upper mass limit in Fourier-

transform ion cyclotron resonance mass spectrometry, *Analytical Chemistry*. **1989,** *61*, 1288-1293.

64. Hanson, C. D., Castro, M. E., Kerley, E. L., Russell, D. H., Field-corrected ion cell for ion cyclotron resonance, *Analytical Chemistry*. **1990,** *62*, 520-526.

65. Marto, J. A., Marshall, A. G., Schweikhard, L., A two-electrode ion trap for Fourier transform ion cyclotron resonance mass spectrometry, *International Journal of Mass Spectrometry and Ion Processes*. **1994,** *137*, 9-30.

66. Rempel, D. L., Ledford, E. B., Jr., Huang, S. K., Gross, M. L., Parametric mode operation of a hyperbolic Penning trap for Fourier transform mass spectrometry, *Analytical Chemistry*. **1987,** *59*, 2527-2532.

67. Vartanian, V. H., Hadjarab, F., Laude, D. A., Open cell analog of the screened trapped-ion cell using compensation electrodes for Fourier transform ion cyclotron resonance mass spectrometry, *International Journal of Mass Spectrometry and Ion Processes*. **1995,** *151*, 175-187.

68. Mitchell, D. W., Theory of trapped ion motion in the non-quadrupolar electrostatic potential of a cubic ion cyclotron resonance cell, *International Journal of Mass Spectrometry and Ion Processes*. **1995,** *142*, 1-22.

69. Brown, L. S., Gabrielse, G., Geonium theory: physics of a single electron or ion in a Penning trap, *Reviews of Modern Physics*. **1986,** *58*, 233-311.

70. Holliman, C. L., Rempel, D. L., Gross, M. L., A mechanism for poor high mass performance in Fourier transform mass spectrometry, *Journal of the American Society for Mass Spectrometry*. **1992,** *3*, 460-463.

71. Solouki, T., Gillig, K. J., Russell, D. H., Detection of High-Mass Biomolecules in Fourier Transform Ion Cyclotron Resonance Mass Spectrometry: Theoretical and Experimental Investigations, *Analytical Chemistry*. **1994,** *66*, 1583-1587.

72. Guan, S., Kim, H. S., Marshall, A. G., Wahl, M. C., Wood, T. D., Xiang, X., Shrink-wrapping an ion cloud for high-performance Fourier transform ion cyclotron resonance mass spectrometry, *Chemical Reviews*. **1994,** *94*, 2161-2182.

73. Guan, S., Gorshkov, M. V., Marshall, A. G., Circularly polarized quadrature excitation for Fourier-transform ion cyclotron resonance mass spectrometry, *Chemical Physics Letters*. **1992,** *198*, 143-148.

74. Bollen, G., Moore, R. B., Savard, G., Stolzenberg, H., The accuracy of heavy-ion mass measurements using time of flight-ion cyclotron resonance in a Penning trap, *J Appl Phys*. **1990,** *68*, 4355-4374.

75. Speir, J. P., Gorman, G. S., Pitsenberger, C. C., Turner, C. A., Wang, P. P., Amster, I. J., Remeasurement of ions using quadrupolar excitation Fourier transform ion cyclotron resonance spectrometry, *Analytical Chemistry*. **1993,** *65*, 1746-1752.

76. O'Connor, P. B., Speir, J. P., Wood, T. D., Chorush, R. A., Guan, Z., McLafferty, F. W., Broadband quadrupolar axialization of large multiply charged ions to enhance measurement and minimize conformational restrictions, *Journal of Mass Spectrometry*. **1996,** *31*, 555-559.

77. Williams, E. R., Henry, K. D., McLafferty, F. W., Multiple remeasurement of ions in Fourier-transform mass spectrometry, *Journal of the American Chemical Society*. **1990,** *112*, 6157-6162.

78. Solouki, T., Pasa-Tolic, L., Jackson, G. S., Guan, S., Marshall, A. G., High-Resolution Multistage MS, MS2, and MS3 Matrix-Assisted Laser Desorption/Ionization FT-ICR Mass Spectra of Peptides from a Single Laser Shot, *Analytical Chemistry*. **1996,** *68*, 3718-3725.

79. Solouki, T., Marto, J. A., White, F. M., Guan, S., Marshall, A. G., Attomole Biomolecule Mass Analysis by Matrix-Assisted Laser Desorption/Ionization Fourier Transform Ion Cyclotron Resonance, *Analytical Chemistry*. **1995,** *67*, 4139-4144.

80. Gabrielse, G., Haarsma, L., Rolston, S. L., Open-endcap Penning traps for high precision experiments, *International Journal of Mass Spectrometry and Ion Processes*. **1989,** *88*, 319-332.

81. Beu, S. C., Laude, D. A., Jr., Open trapped ion cell geometries for Fourier transform ion cyclotron resonance mass spectrometry, *International Journal of Mass Spectrometry and Ion Processes*. **1992,** *112*, 215-230.

82. Malek, R., Wanczek, K. P., Nested ion traps and their effects on ion storage and excitation, *Advances in Mass Spectrometry*. **1998,** *14*, B025210/025211-B025210/025210.

83. Vartanian, V. H., Laude, D. A., Optimization of a fixed-volume open geometry trapped ion cell for Fourier transform ion cyclotron mass spectrometry, *International Journal of Mass Spectrometry and Ion Processes*. **1995,** *141*, 189-200.

84. Bruce, J. E., Anderson, G. A., Lin, C.-Y., Gorshkov, M., Rockwood, A. L., Smith, R. D., A novel high-performance Fourier transform ion cyclotron resonance cell for improved biopolymer characterization, *Journal of Mass Spectrometry*. **2000,** *35*, 85-94.

85. Quint, W., Kaiser, R., Hall, D., Gabrielse, G., (Anti)hydrogen recombination studies in a nested Penning trap, *Hyperfine Interact*. **1993,** *76*, 181-188.

86. Jackson, G. S., White, F. M., Guan, S., Marshall, A. G., Matrix-shimmed ion cyclotron resonance ion trap simultaneously optimized for excitation, detection, quadrupolar axialization, and trapping, *Journal of the American Society for Mass Spectrometry*. **1999,** *10*, 759-769.

87. Bruce, J. E., Cheng, X., Bakhtiar, R., Wu, Q., Hofstadler, S. A., Anderson, G. A., Smith, R. D., Trapping, Detection, and Mass Measurement of Individual Ions in a Fourier Transform Ion Cyclotron Resonance Mass Spectrometer, *Journal of the American Chemical Society*. **1994,** *116*, 7839-7847.

88. Bruce, J. E., Anderson, G. A., Udseth, H. R., Smith, R. D., Large Molecule Characterization Based upon Individual Ion Detection with Electrospray Ionization-FTICR Mass Spectrometry, *Analytical Chemistry*. **1998,** *70*, 519-525.

89. Hendrickson, C. L., Beu, S. C., Laude, D. A., Jr., Two-dimensional Coulomb-induced frequency modulation in Fourier transform ion cyclotron resonance: a mechanism for line broadening at high mass and for large ion populations, *Journal of the American Society for Mass Spectrometry*. **1993,** *4*, 909-916.

90. Peurrung, A. J., Kouzes, R. T., Long-term coherence of the cyclotron mode in a trapped ion cloud, *Physical Review. E. Statistical Physics, Plasmas, Fluids, and Related Interdisciplinary Topics*. **1994,** *49*, 4362-4368.

91. Mitchell, D. W., Smith, R. D., Cyclotron motion of two Coulombically interacting ion clouds with implications to Fourier-transform ion cyclotron resonance mass spectrometry, *Physical Review. E. Statistical Physics, Plasmas, Fluids, and Related Interdisciplinary Topics*. **1995,** *52*, 4366-4386.

92. Laukien, F. H., The effects of residual spatial magnetic field gradients on Fourier transform ion cyclotron resonance spectra, *International Journal of Mass Spectrometry and Ion Processes*. **1986,** *73*, 81-107.

93. Hartmann, H., Chung, K. M., Baykut, G., Wanczek, K. P., Dependence of ion cyclotron frequency on electric field inhomogeneity, *J Chem Phys*. **1983,** *78*, 424-431.

94. Chen, S. P., Comisarow, M. B., Simple physical models for Coulomb-induced frequency shifts and Coulomb-induced inhomogeneous broadening for like and unlike ions in Fourier transform ion cyclotron resonance mass spectrometry, *Rapid Communications in Mass Spectrometry*. **1991,** *5*, 450-455.

95. Mitchell, D. W., Smith, R. D., Prediction of a space charge induced upper molecular mass limit towards achieving unit mass resolution in Fourier transform

ion cyclotron resonance mass spectrometry, *Journal of Mass Spectrometry*. **1996,** *31*, 771-790.

96. Nikolaev, E. N., Miluchihin, N., Inoue, M., Evolution of an ion cloud in a Fourier transform ion cyclotron resonance mass spectrometer during signal detection: its influence on spectral line shape and position, *International Journal of Mass Spectrometry and Ion Processes*. **1995,** *148*, 145-157.

97. Nikolaev, E. N., 54th ASMS Conference on Mass Spectrometry and Allied Topics, Seattle, WA, **2006**.

98. Mitchell, D. W., Realistic simulation of the ion cyclotron resonance mass spectrometer using a distributed three-dimensional particle-in-cell code, *Journal of the American Society for Mass Spectrometry*. **1999,** *10*, 136-152.

CHAPTER 2

Improved Mass Accuracy for Tandem Mass Spectrometry

Abstract

With the emergence of top-down proteomics the ability to achieve high mass measurement accuracy on tandem MS/MS data will be beneficial for protein identification and characterization. Fourier Transform Ion Cyclotron Resonance Mass Spectrometers (FT-ICR MS) are the ideal instruments to perform these experiments with their ability to provide high resolution and mass accuracy. A major limitation to mass measurement accuracy in FT-ICR instruments arises from the occurrence of space charge effects. These space charge effects shift the cyclotron frequency of the ions, which compromises the mass measurement accuracy. While several methods have been developed that correct for these space charge effects, they have limitations when applied to MS/MS experiments. It has already been shown that additional information inherent in electrospray spectra can be used for improved mass measurement accuracy with the use of a computer algorithm called DeCAL (Deconvolution of Coulombic Affected Linearity). This paper highlights a new application of the strategy for improved mass accuracy in tandem mass analysis. The results show a significant improvement in mass measurement accuracy on complex electron capture dissociation spectra of proteins. We also demonstrate how the improvement in mass accuracy can increase the confidence in

protein identification from the fragment masses of proteins acquired in MS/MS experiments.

Introduction

FT-ICR MS [1] (Fourier Transform Ion Cyclotron Resonance Mass Spectrometry) is a unique technique with its ability to provide simultaneous high resolution, sensitivity, and accurate mass measurements. However, the mass accuracy of the FT-ICR is known to be compromised by the influence of space charge effects [2-4], which arise from the Coulombic interaction of trapped ions in the ICR cell. The measured quantity in FT-ICR MS is ion cyclotron frequency. Space charge effects resultant from ion-ion repulsion can produce a systematic shift in the observed cyclotron frequencies. If unaccounted for, these shifts in cyclotron frequency severely degrade mass measurement accuracy. Ion cyclotron frequency and *m/z* are related by equation (1), and perturbations in the observed cyclotron frequency will correspond to a shift in the *m/z* value. The relationship between *m/z*, charge state, and frequency is

$$(m/z)_n = \frac{M + n(M_c)}{n} = \frac{kB}{f_n} \quad (1)$$

where $(m/z)_n$ is the observed mass-to-charge ratio, n is the number of charges, M is the molecular weight of the analyte being measured, M_c is the mass of the charge carrier, k is a proportionality constant relating *m/z* to the magnetic field B, and f_n is the cyclotron frequency. The magnitude of the frequency shift depends on the changes in the total ion population in the ICR cell during experimental conditions, as compared to the total ion

population present during calibration [4]. The frequency shift is constant to a first order approximation across the entire spectrum, in that all ions are shifted by the same amount in frequency space. With a larger number of charge states with increased intensity, possible higher-order non-linear frequency shifts can occur. The systematic shift in ion cyclotron frequency can be expressed by equation (2) where f is the expected cyclotron frequency and Δf is the frequency shift that is resultant from the imposed space charge effects.

$$m/z = \frac{kB}{\left(f + \Delta f\right)} \tag{2}$$

A number of different calibration functions that convert the ion cyclotron frequency to *m/z* have been developed [3, 5].

Space charge effects limit the mass accuracy and have spurred an active area of research to correct for and reduce this phenomenon. There have been a few methods developed to correct for space charge effects to obtain more accurate mass measurements, while others have reduced the presence of space charge effects by controlling the number of ions that are trapped in the ICR cell [6, 7]. Burton *et al.* [8] developed a method based on the addition of an internal standard after the initial calibration. Since the frequency shift is constant across the entire spectrum, the added standard will encounter the same shift in frequency space as all the other trapped ions. The frequency shift of the standard can be determined by the difference in observed and expected mass of the added standard. This frequency shift is then applied to all ions present in the ICR cell to obtain improved mass accuracy. Another method developed by Easterling *et al.* [4] shows that space charge effects can be corrected with a calibration

expression that relates the trapped ion population in the ICR cell during calibration to the trapped ion population during the experiment, through a shift in frequency. A third method called Deconvolution of Coulombic Affect Linearity (DeCAL) developed by Bruce *et al*. [9] corrects for space charge effects in spectra that contain multiply charged ions. This method relies on a computer algorithm that aligns the deconvoluted isotopic distributions of multiple charge states of the same molecular species. Improved mass accuracy was demonstrated by iteratively shifting the entire frequency-domain spectra prior to deconvolution. This is done without knowing any other parameters, such as exact molecular weight, ion abundances, or the identity of the species.

Mass accuracy is a critical feature in the emerging field of proteomics. Proteomics can be defined as the effort to establish identity, structure, and function of all proteins present in the organism, and how these can change in time, space, and other conditions. A newer approach to proteome analysis with mass spectrometry called "top-down proteomics" [10-12], aims to combine protein identification with protein characterization, and locate post-translational modifications (PTMs) present on the proteins. PTMs are important to biological systems because they can change the structure and regulate the functionality of proteins. To determine sequence and PTM sites, proteins have traditionally been proteolytically digested prior to mass spectral analysis. However, some of these PTMs are labile and dissociate easily from the parent ion when performing tandem MS/MS techniques such as CAD (collisionally activated dissociation) or IRMPD (infrared multiphoton dissociation). These methods can potentially lose information on some PTM sites. A unique new dissociation method pioneered by McLafferty *et al.* called Electron Capture Dissociation (ECD) [13, 14] gives

a larger number of fragments and sequence coverage than the previously mentioned fragmentation techniques, while preserving labile PTMs intact on the fragment ions [15-18]. This technique offers the capability to locate PTMs from the intact protein without first having to digest the protein. Currently ECD is only compatible with the FT-ICR mass spectrometer [19]. Although Electron Transfer Dissociation (ETD) reported recently by Hunt *et al.* [20], enables similar fragmentation pathways to be observed with other types of mass spectrometers, FT-ICR instrumentation uniquely allows simultaneous high resolution, mass accuracy, and sensitivity for complex spectral interpretation. The advantage that high mass accuracy offers to proteomics is its ability to identify and unambiguously confirm protein identification through the production of sequence tag information, and peptide or fragment masses when dealing with the top-down approach.

When analyzing proteins through the bottom up approach it is possible to identify a protein based only on a few peptide masses, when these masses are searched against a database. The number of peptide masses required for positive identification of a protein is decreased as the mass accuracy increases [21-23]. It has been shown that with adequate mass accuracy and additional constraints, it is possible to identify a protein with just one peptide mass [23]. There have been a number of different search tools designed to deal with this type of bottom up analysis of proteins. The same idea applies when dealing with MS/MS fragments of whole proteins instead of peptides; as the mass accuracy of the measurement increases, the number of fragment masses needed to identify a protein is decreased. High mass accuracy will prove to be advantageous when doing chromatographic runs of whole proteins which are heavily modified or when there are multiple proteins present. Since the mass accuracy in ICR technology can be limited

by space charge effects, a method to correct for space charge effects in tandem MS/MS experiments to obtain high mass accuracy is needed. Furthermore, the number of ions entering the mass spectrometer during a chromatographic run can vary greatly which will lead to mass errors associated with space charge effects since the number of ions entering the ICR cell is not constant. There have been many research efforts designed to circumvent this problem and obtain high mass accuracy in tandem MS/MS ICR experiments [24-28]. Efforts have also been made to control the number of ions entering the ICR cell; the development of automated gain control limits the need to correct for space charge effects by routinely allowing the same total ion population to enter the ICR cell [6, 7, 29]. However, during ECD and top-down experiments it is desirable to obtain a large parent ion population in the ICR cell. This is because of the lower efficiency of the dissociation process and the large number of possible fragmentation pathways that result in an increased production of lower intensity fragment ions. If a smaller population of precursor ions is used for dissociation, the fragment ions that form to a lesser degree are lost in the noise and not detected. Also, the parent ion population is often not the same as the total ion population after dissociation because of the charge reduction processes that can take place during ECD. Thus, controlling the ion population by limiting the number of ions in the ICR cell can be problematic when doing ECD experiments. Finally, correction of space charge effects with an internal calibrant for MS/MS experiments adds additional complexity to the experiments, such as the need to inject the calibrant species along with the MS/MS fragment ions into the ICR cell. In dissociation spectra such as those resultant from ECD, there are a large number of peaks with a wide range of charge states. This makes the detected time-domain signal more

complex due to the amount of constructive and destructive interferences [30, 31]. The complexity affects the peak intensities in such a way that the summation of the peak intensities may no longer reflect the total ion intensity in the ICR cell [32]. During MS/MS experiments there are a wide range of fragment masses that are formed. The calibration procedure works best when it is possible to accurately determine the exact ion intensity and works best for high mass species when the *m/z* of the calibrant is matched to the analyte [32]. DeCAL only requires that multiple charge states of the same molecular species be present in the spectrum; therefore it will only work with multiply charged ions. During MS/MS experiments there is usually only one charge state that is selected for dissociation. However, for highly charged ions, these species often dissociate in such a way that there are multiple charge states of the same molecular fragment produced. When intact protein ions are analyzed by electrospray and ECD they dissociate to produce many charge state pairs, thus allowing the opportunity for space charge effect correction with DeCAL. The advantage that DeCAL provides is that everything that is needed to correct for space charge effects is inherent in the spectrum. The correction is done through post processing and can be done without any further manipulation of the ion population or previous knowledge of the species being analyzed.

Experimental

Ubiquitin (MW_{avg} = 8565Da) and horse myoglobin (MW_{avg} = 16952Da) were dissolved in a solution of 49:49:2 by volume of water, methanol, and acetic acid and diluted to 10uM. Electrospray was used as the ionization source. The voltage on the capillary was

set between 2,050V and 2,350V. A syringe pump used to introduce the solutions was set between 15-25uL/hr. A Bruker Daltonics Apex-Q 7T FT-ICR mass spectrometer was used to acquire the mass spectral data using Xmass as the data acquisition software program. The instrument was externally calibrated using ubiquitin a few days prior to the collection of data presented here. However, careful adjustments of trapped ion population sizes present during data acquisition to match those that were present during calibration was not performed. Therefore, the observed uncorrected error is not what one might expect from a high performance mass analyzer operated under carefully controlled conditions. The ions enter the instrument through a glass capillary and then pass through a hexapole followed by a quadrupole then a second hexapole. The quadrupole was used to select the specific *m/z* ions of interest to be fragmented (11+ for ubiquitin, 16+ for myoglobin). These ions were accumulated between 1-2 seconds in the second hexapole to acquire sufficient ion population for ECD. The ions were then transported to the ICR cell using electrostatic focusing. The ions were trapped in the ICR cell using a low energy sidekick potential to keep the ions close to the central *z*-axis of the cell. Electron capture dissociation was performed using a heated cathode dispenser located outside the ICR cell to obtain the MS/MS data. The cathode dispenser was heated with 1.6 to 1.8A and held at approximately 5 to 6V. The electron injection time was set at 1.0-3.0ms, the potential on the solid cathode dispenser was set at -7.5 to -15V. The spectra were obtained by signal averaging 65 scans. All data sets acquired were 512k points. Data were interpreted with aid of the computer program ICR-2LS [33]. The calibration function that was used to convert ion cyclotron frequency to *m/z* values is written as a

variation of Equation 2 and represented by Equation 3, where *A* and *B* are calibration constants, and *f* is the measured cyclotron frequency.

$$m/z = \frac{A}{(f - B)} \tag{3}$$

The data sets were apodized using the Welch apodization function and zero-filled twice before Fourier transformation to the frequency domain. The DeCAL program used to correct for the frequency shift in the tandem MS/MS data is a module written within ICR-2LS. The monoisotopic masses of the fragment ions from the spectra were entered into the web based software and database tool called ProSight PTM, designed by Kelleher et. al. [34] to specifically deal with the characteristics of the top-down proteomics approach. To compare the effects of identification of a protein using fragment masses from ECD data, monoisotopic masses of the fragment ions with and without the use of DeCAL were entered into the ProSight PTM program.

Results and Discussion

When two charge states of the same molecular species are deconvoluted and overlaid, optimum overlap occurs when the observed frequency shift is equal to the shift resultant from space charge effects. Here our assumption is that the frequency shift is a constant value across the entire spectrum, which seems to be true at least to a first order approximation. However, DeCAL or derivatives of this approach can also account for more complex non-linear shifts. This requires that sufficient charge states exist in the spectrum to allow functional characterization of non-linear shifts. A constant shift in frequency space causes different *m/z* values to be shifted to slightly different degrees in

the mass domain causing the two deconvoluted isotopic distributions of the same molecular species to not overlap exactly as would be expected. The two isotopic distributions are expected to overlap exactly when deconvoluted because they have the same molecular composition. DeCAL shifts the original frequency-domain spectrum in an iterative fashion in frequency-space until the resultant two deconvoluted isotopic distributions overlap in the mass-domain. Importantly, when the two isotopic distributions converge, they do so in alignment with the theoretical isotopic distribution as can be seen in Figure 1. In this figure, the theoretical isotopic distribution of ubiquitin is shown, along with deconvolved isotopic distributions resultant from the 8+ and 7+ charge states of ubiquitin. Initially, the two isotopic distributions do not overlap extremely well. As the two isotopic distributions are shifted in frequency space they begin to merge together and do so in good agreement with the theoretical isotopic distribution. The error between the deconvoluted isotopic distributions is minimized at the same time that the alignment with the theoretical distribution (which is not normally known, but shown here for illustrative purpose) becomes optimal. When the two deconvoluted isotopic distributions overlap, the shift in frequency is equal to the frequency shift due to the space charge effects. DeCAL acts as a correction process for space charge effects resultant from Coulombic interactions. However, it should be noted that this correction process will be ineffective if the instrument is initially poorly calibrated.

ECD was performed on the 11+ charge state of ubiquitin (Figure 2), and the resulting fragment ion peaks within 100ppm error range were identified using ProSight PTM. The average mass error in the spectrum without correction for space charge effects

was 53ppm. While better than data from some MS/MS instruments, these results do not match the performance in mass accuracy that is expected from a FT-ICR instrument. It should also be noted that much better performance could have been obtained through careful calibration and matching of total ion populations. This example is used to show the utility of DeCAL to correct space charge effects when the ion populations are not matched. In the absence of sophisticated "automated gain control" type experiments, this mismatch of ion population sizes is very likely in LC/MS or LC/MS/MS experiments. Fortunately, space charge effects result in a systematic error in which a constant offset is applied to all frequencies in the spectrum. Plotting the error in ppm of the identified peaks in the spectrum vs. *m/z* as seen in Figure 3, gives a visual indication of the systematic error that occurs. As the *m/z* value increases, the error also increases in a linear fashion. This increase in error as the *m/z* increases is expected based on the inverse relationship between *m/z* and cyclotron frequency as seen in Equation 1. As the *m/z* value increases, the frequency decreases. Thus, for a constant frequency offset, the higher *m/z* (lower frequency) will exhibit a larger relative shift in frequency and be shifted to a greater extent in the mass-domain than the lower *m/z* (higher frequency) ions. DeCAL was then applied to the same set of acquired data to correct space charge effects. No knowledge of the ion identity or ion abundance was used. A plot of resultant error in ppm of the identified fragment ions vs. *m/z* is shown in Figure 4. This figure shows substantial improvement in error and the feasibility of correction for this type of systematic error in MS/MS spectra. The plotted error points no longer have a linear trend of increasing error, which shows that DeCAL has virtually removed the systematic error. After applying DeCAL to the data, the average error in ppm decreased to less than 2ppm

which is greater than a 30 fold improvement. Thus, DeCAL has the capability of correcting space charge effects in tandem MS/MS experiments used for top-down proteomics.

During the experiment, the 11+ charge state of ubiquitin was isolated using the mass selective quadrupole. These ions were then dissociated inside the ICR cell by ECD to give an array of charge states that ranged from 11+ to 1+. When the ions dissociated, a large number of isotopic distributions resulted, some of which were the same molecular fragment but with different charge states. This production of charge state pairs is common with dissociation of highly charged precursor ions, and is advantageous since DeCAL relies on charge state pairs to perform its calculations for correction. Within the ubiquitin spectrum, the program was able to locate eleven charge state pairs, and these charge state pairs were used to perform DeCAL. The induced frequency shift for the data set was determined to be 6.03Hz.

The application of DeCAL to MS/MS data is useful for the top-down proteomic approach. The increased mass accuracy is useful when analyzing fragment masses to determine the identity and possible PTM sites. The data collected from the ECD spectrum of the 16+ charge state of horse myoglobin (Figure 5) was used in the database search to determine how the mass accuracy effects the ability to identify the protein based on the fragment masses. ECD produces primarily *c* and *z*• fragments when the parent ion dissociates, so the search was performed looking for these fragments. Without the correction of space charge effects, 50 monoisotopic masses were selected corresponding to the most intense isotopic distributions in the spectrum, and were entered into ProSight PTM. When setting the parameter for fragment mass tolerance to 25ppm, there were 28

proteins that were identified as possible matches, none of which were myoglobin. After performing DeCAL and running the search at 5ppm myoglobin is readily identified with a P-score of 8.1×10^{-48}. This P-score gives the probability of a match being a random event, so the lower the P-score the higher the confidence of the search [35]. The average error for the identified fragment ion peaks in the myoglobin raw data was 58.8ppm. Figure 6 shows this substantial error. The error associated with the spectrum is not too surprising since the FT-ICR instrument was calibrated using ubiquitin, with a different set of parameters and different ion abundances in the ICR cell, a few days prior to obtaining the mass spectrum of myoglobin. Figure 7 shows how the error in ppm changes after the application of DeCAL on the same set of data. DeCAL indicated a frequency shift of 6.07 Hz and the average error dropped to 5.5ppm, which is over a factor of 10 improvement. By statically removing the two outliers, which can be seen in Figure 7, the average error drops to 1.7ppm which gives about another factor of 3 improvement.

The advantage that DeCAL offers when applied to MS/MS data for this type of analysis is to increase the confidence of obtaining positive protein identification. Ubiquitin was used to test how the probability of a random match is effect by mass accuracy. The top 50 most intense fragment masses from the spectrum were selected and entered into the database. The mass tolerance parameter in ProSight PTM was varied with and without the application of DeCAL (Table 1). Without DeCAL, ubiquitin was not selected as a probable match until the mass tolerance parameter of the search increased to 35ppm. At this tolerance, even though ubiquitin was selected as a probable match, it did not receive the lowest P-score of the proteins selected as a probable match.

The probability of a match did not become significant until the mass tolerance was increased to 50ppm, which is also close to the average error of the assigned isotopic peaks (53ppm) in the data shown in Figure 3. The probability that the identified protein was not a random event reached a maximum at $1.2x10^{-18}$, at which the mass tolerance was set at 65ppm. With the use of DeCAL, ubiquitin was detected with confidence within a mass tolerance of 5ppm, with the probability of it being a random event being $9.8x10^{-43}$. Table 1 shows the impact of database searching with and without the application of DeCAL. In Table 1, the P-scores are lower with the application of DeCAL until the mass tolerance is set to 65ppm, at which the two columns have equal P-scores. The reason is that at 65ppm the same number of fragment ions have been assigned to ubiquitin for both cases. As the mass tolerance is allowed to increase to 100ppm the P-score without DeCAL becomes less (more significant) than the P-score with DeCAL. The reason for this observation is that there are more peaks assigned to ubiquitin within that mass tolerance. As seen in Figure 3 there is a cluster of identified peaks that fall below the trend line formed due to the systematic error. These peaks are the result of the misassigned monoisotopic peaks in the ECD spectrum. All of the misassigned fragment ions were highly charged and of relatively low abundance so that the monoisotopic peak was not visible in the spectrum. These peaks were actually assigned to the correct fragment. However, since the algorithm misidentified the monoisotopic peaks, the error values from these fragments do not follow the observed trend. When the frequency shift is corrected, these peaks are shifted out of the 100ppm error window and are not seen in Figure 4. These possible misassigned peaks are taken into account when determining the P-score, which artificially causes the P-score of the uncorrected data to be better than it

should be. With the use of DeCAL these possible misassigned peaks are outside of the search tolerance. The application of DeCAL allows the mass tolerance to be minimized, reducing the number of possible misassigned peaks that could possibly lead to incorrect protein identification, thus allowing greater confidence in identification of the intact protein. DeCAL will be even more useful when identifying a protein with unknown modifications, where many of the fragment masses will have modifications associated with them. DeCAL should also prove useful when multiple proteins are present, as might be expected with chromatographic separation of large numbers of proteins. The P-score is based on the mass tolerance window, the number of identified fragments, and the number of masses being searched. Therefore, with multiple proteins present, many of the fragment masses will come from different proteins and the more masses searched that do not fit within the mass tolerance will lead to a higher the P-score. With the application of DeCAL, the mass tolerance range can be decreased which will lead to a decrease in the P-score and a more confident identification can be assigned. Increasing the mass accuracy will also help to find sites of PTM with higher confidence.

Conclusions

The high mass measurement accuracy in FT-ICR MS can be severely limited by space charge effects. These space charge effects present in tandem MS/MS experiments can be corrected with the application of DeCAL when total ion populations are not well matched with those encountered during calibration. This can be especially problematic in ECD experiments as normally these experiments are carried out with maximum trap

capacity of the precursor, and result in variable amounts of product ions. However, ECD spectra often contain a number of charge state pairs that can be used for correction. The application of DeCAL results in an average error for tandem MS/MS data in the low ppm range, even when trapped ion populations are not carefully controlled. This improvement in mass accuracy allows one to accurately identify proteins based on accurate fragment masses. Without the use of DeCAL, our database search did not correctly identify myoglobin protein when the search mass tolerance was set at 25ppm or better. With DeCAL application, we were able to identify proteins unambiguously with the mass tolerance set to much tighter constraints. These tighter search constraints yield much greater confidence in the search results. Additionally, the higher mass accuracy possible with DeCAL will be beneficial when analyzing complex protein mixtures. Finally, increased mass measurement accuracy will also likely allow more accurate determination of posttranslational sites from top-down proteomic studies.

Acknowledgements

This research was supported by the National Science Foundation, Instrument Development for Biological Research Program, Grant No. DBI-0352451, and the Murdock Charitable Trust. The authors also thank Dr. Gary Kruppa for his assistance with initial ECD experiments.

References

1. Marshall, A.G., C.L. Hendrickson, and G.S. Jackson, *Fourier transform ion cyclotron resonance mass spectrometry: a primer.* Mass Spectrometry Reviews, 1998. **17**(1): p. 1-35.

2. Ledford, E.B., Jr., D.L. Rempel, and M.L. Gross, *Space charge effects in Fourier transform mass spectrometry. I. Electrons.* International Journal of Mass Spectrometry and Ion Processes, 1984. **55**(2): p. 143-54.

3. Ledford, E.B., Jr., D.L. Rempel, and M.L. Gross, *Space charge effects in Fourier transform mass spectrometry. Mass calibration.* Anal Chem, 1984. **56**(14): p. 2744-8.

4. Easterling, M.L., T.H. Mize, and I.J. Amster, *Routine part-per-million mass accuracy for high-mass ions: space-charge effects in MALDI FT-ICR.* Analytical Chemistry, 1999. **71**(3): p. 624-632.

5. Francl, T.J., R.L. Hunter, and R.T. McIver, Jr., *Zoom transform for mass measurement accuracy in Fourier transform mass spectrometry.* Analytical Chemistry, 1983. **55**(13): p. 2094-6.

6. Belov, M.E., R. Zhang, E.F. Strittmatter, D.C. Prior, K. Tang, and R.D. Smith, *Automated gain control and internal calibration with external ion accumulation capillary liquid chromatography-electrospray ionization-Fourier transform ion cyclotron resonance.* Analytical Chemistry, 2003. **75**(16): p. 4195-4205.

7. Belov, M.E., V.S. Rakov, E.N. Nikolaev, M.B. Goshe, G.A. Anderson, and R.D. Smith, *Initial implementation of external accumulation liquid chromatography/electrospray ionization Fourier transform ion cyclotron resonance with automated gain control.* Rapid Communications in Mass Spectrometry, 2003. **17**(7): p. 627-636.

8. Burton, R.D., K.P. Matuszak, C.H. Watson, and J.R. Eyler, *Exact mass measurements using a 7 tesla fourier transform ion cyclotron resonance mass spectrometer in a good laboratory practices-regulated environment.* Journal of the American Society for Mass Spectrometry, 1999. **10**(12): p. 1291-1297.

9. Bruce, J.E., G.A. Anderson, M.D. Brands, L. Pasa-Tolic, and R.D. Smith, *Obtaining more accurate Fourier transform ion cyclotron resonance mass measurements without internal standards using multiply charged ions.* Journal of the American Society for Mass Spectrometry, 2000. **11**(5): p. 416-421.

10. Ge, Y., B.G. Lawhorn, M. ElNaggar, E. Strauss, J.H. Park, T.P. Begley, and F.W. McLafferty, *Top down characterization of larger proteins (45 kDa) by electron capture dissociation mass spectrometry.* J Am Chem Soc, 2002. **124**(4): p. 672-8.

11. Reid, G.E. and S.A. McLuckey, *'Top down' protein characterization via tandem mass spectrometry.* J Mass Spectrom, 2002. **37**(7): p. 663-75.

12. Sze, S.K., Y. Ge, H. Oh, and F.W. McLafferty, *Top-down mass spectrometry of a 29-kDa protein for characterization of any posttranslational modification to within one residue.* Proc Natl Acad Sci U S A, 2002. **99**(4): p. 1774-9.

13. Zubarev, R.A., N.L. Kelleher, and F.W. McLafferty, *Electron Capture Dissociation of Multiply Charged Protein Cations. A Nonergodic Process.* Journal of the American Chemical Society, 1998. **120**(13): p. 3265-3266.

14. McLafferty, F.W., D.M. Horn, K. Breuker, Y. Ge, M.A. Lewis, B. Cerda, R.A. Zubarev, and B.K. Carpenter, *Electron capture dissociation of gaseous multiply charged ions by Fourier-transform ion cyclotron resonance.* Journal of the American Society for Mass Spectrometry, 2001. **12**(3): p. 245-249.

15. Kelleher, N.L., R.A. Zubarev, K. Bush, B. Furie, B.C. Furie, F.W. McLafferty, and C.T. Walsh, *Localization of Labile Posttranslational Modifications by Electron Capture Dissociation: The Case of g-Carboxyglutamic Acid.* Analytical Chemistry, 1999. **71**(19): p. 4250-4253.

16. Hakansson, K., H.J. Cooper, M.R. Emmett, C.E. Costello, A.G. Marshall, and C.L. Nilsson, *Electron capture dissociation and infrared multiphoton dissociation MS/MS of an N-glycosylated tryptic peptide to yield complementary sequence information.* Analytical Chemistry, 2001. **73**(18): p. 4530-4536.

17. Mirgorodskaya, E., P. Roepstorff, and R.A. Zubarev, *Localization of O-glycosylation sites in peptides by electron capture dissociation in a Fourier Transform mass spectrometer.* Analytical Chemistry, 1999. **71**(20): p. 4431-4436.

18. Shi, S.D.H., M.E. Hemling, S.A. Carr, D.M. Horn, I. Lindh, and F.W. McLafferty, *Phosphopeptide/phosphoprotein mapping by electron capture dissociation mass spectrometry.* Analytical Chemistry, 2001. **73**(1): p. 19-22.

19. Zubarev, R.A., *Reactions of polypeptide ions with electrons in the gas phase.* Mass Spectrometry Reviews, 2003. **22**(1): p. 57-77.

20. Syka, J.E., J.J. Coon, M.J. Schroeder, J. Shabanowitz, and D.F. Hunt, *Peptide and protein sequence analysis by electron transfer dissociation mass spectrometry.* Proc Natl Acad Sci U S A, 2004. **101**(26): p. 9528-33.

21. Takach, E.J., W.M. Hines, D.H. Patterson, P. Juhasz, A.M. Falick, M.L. Vestal, and S.A. Martin, *Accurate Mass measurements using MALDI-TOF with delayed extraction.* Journal of Protein Chemistry, 1997. **16**(5): p. 363-369.

22. Clauser, K.R., P. Baker, and A.L. Burlingame, *Role of Accurate Mass Measurement (+-10 ppm) in Protein Identification Strategies Employing MS or MS/MS and Database Searching.* Analytical Chemistry, 1999. **71**(14): p. 2871-2882.

23. Goodlett, D.R., J.E. Bruce, G.A. Anderson, B. Rist, L. Pasa-Tolic, O. Fiehn, R.D. Smith, and R. Aebersold, *Protein Identification with a Single Accurate Mass of a Cysteine-Containing Peptide and Constrained Database Searching.* Analytical Chemistry, 2000. **72**(6): p. 1112-1118.

24. Masselon, C., G.A. Anderson, R. Harkewicz, J.E. Bruce, L. Pasa-Tolic, and R.D. Smith, *Accurate mass multiplexed tandem mass spectrometry for high-throughput polypeptide identification from mixtures.* Analytical chemistry, 2000 Apr 15. **72**(8): p. 1918-24.

25. Kruppa, G., P.D. Schnier, K. Tabei, S. Van Orden, and M.M. Siegel, *Multiple ion isolation applications in FT-ICR MS: exact-mass MSn internal calibration and purification/interrogation of protein-drug complexes.* Anal Chem, 2002. **74**(15): p. 3877-86.

26. Hannis, J.C. and D.C. Muddiman, *A dual electrospray ionization source combined with hexapole accumulation to achieve high mass accuracy of biopolymers in Fourier transform ion cyclotron resonance mass spectrometry.* Journal of the American Society for Mass Spectrometry, 2000. **11**(10): p. 876-883.

27. Brock, A., D.M. Horn, E.C. Peters, C.M. Shaw, C. Ericson, Q.T. Phung, and A.R. Salomon, *An Automated Matrix-Assisted Laser Desorption/Ionization Quadrupole Fourier Transform Ion Cyclotron Resonance Mass Spectrometer for "Bottom-Up" Proteomics.* Analytical Chemistry, 2003. **75**(14): p. 3419-3428.

28. Chan, T.W.D., L. Duan, and T.P.E. Sze, *Accurate Mass Measurements for Peptide and Protein Mixtures by Using Matrix-Assisted Laser Desorption/Ionization Fourier Transform Mass Spectrometry.* Analytical Chemistry, 2002. **74**(20): p. 5282-5289.

29. Michael Senko, Vladimir Zabrouskov, Oliver Lange, Andreas Wieghaus, and S. Horning, LC/MS with External Calibration Mass Accuracies Approaching 100 ppb. In Proceedings of the 52nd ASMS Conference on Mass Spectrometry and Allied Topics, Nashville, TN, May 23-27, 2004.

30. Easterling, M.L., I.J. Amster, G.J. van Rooij, and R.M.A. Heeren, *Isotope beating effects in the analysis of polymer distributions by Fourier transform mass spectrometry.* Journal of the American Society for Mass Spectrometry, 1999. **10**(11): p. 1074-1082.

31. Hofstadler, S.A., J.E. Bruce, A.L. Rockwood, G.A. Anderson, B.E. Winger, and R.D. Smith, *Isotopic beat patterns in Fourier transform ion cyclotron resonance mass spectrometry: implications for high resolution mass measurements of large biopolymers.* International Journal of Mass Spectrometry and Ion Processes, 1994. **132**(1-2): p. 109-27.

32. Taylor, P.K. and I.J. Amster, *Space charge effects on mass accuracy for multiply charged ions in ESI-FTICR.* International Journal of Mass Spectrometry, 2003. **222**(1-3): p. 351-361.

33. Anderson, G.A., J.E. Bruce, and Eds, ICR-2LS1995, Pacific Northwest National Laboratory: Richland, WA,1995.

34. Taylor, G.K., Y.-B. Kim, A.J. Forbes, F. Meng, R. McCarthy, and N.L. Kelleher, *Web and database software for identification of intact proteins using "top down" mass spectrometry.* Analytical Chemistry, 2003. **75**(16): p. 4081-4086.

35. Meng, F., B.J. Cargile, L.M. Miller, A.J. Forbes, J.R. Johnson, and N.L. Kelleher, *Informatics and multiplexing of intact protein identification in bacteria and the archaea.* Nat Biotechnol, 2001. **19**(10): p. 952-7.

Figure 1

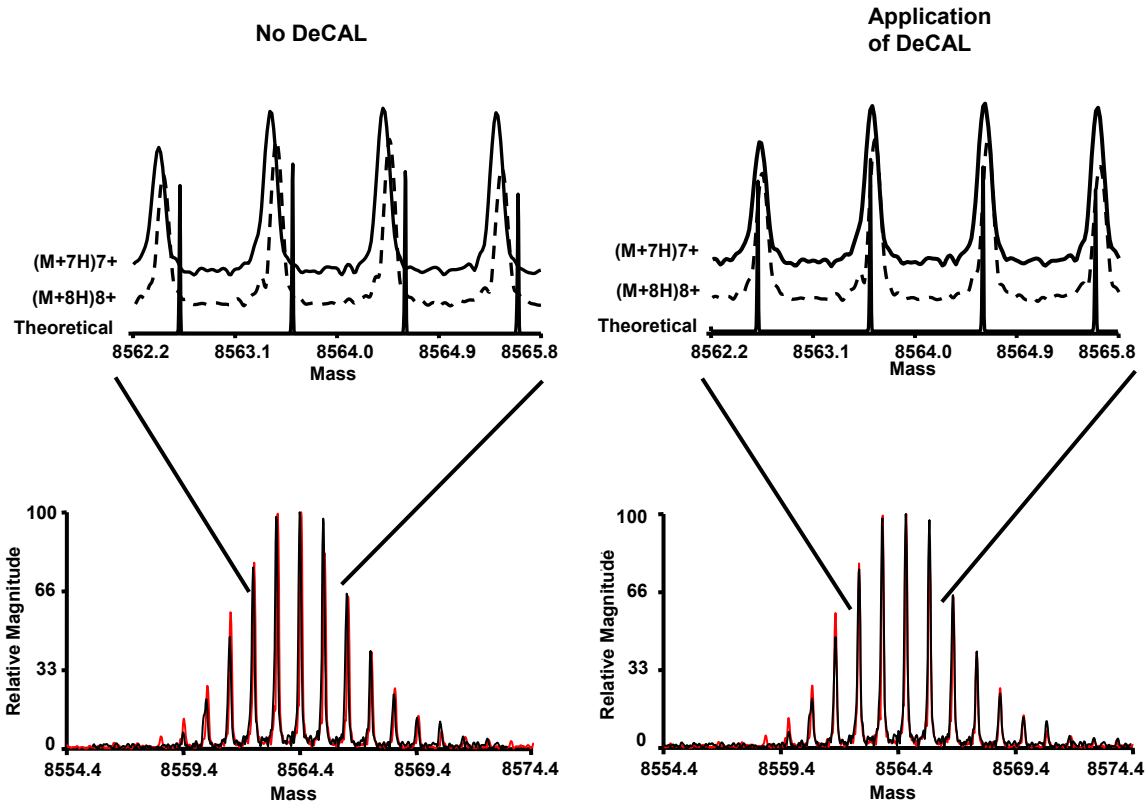

Figure 1. The deconvoluted isotopic distributions of the 8+ and 7+ charge states of ubiquitin are overlaid. The spectrum on the left is with no correction of frequency. The expanded region reveals that the two isotopic distributions do not exactly overlap. The theoretical isotopic distribution is also displayed. The spectrum on the right is after the application of DeCAL. Here the isotopic distributions overlap much better, and as the isotopic distributions converge they do so in good agreement with the theoretical isotopic distribution.

Figure 2

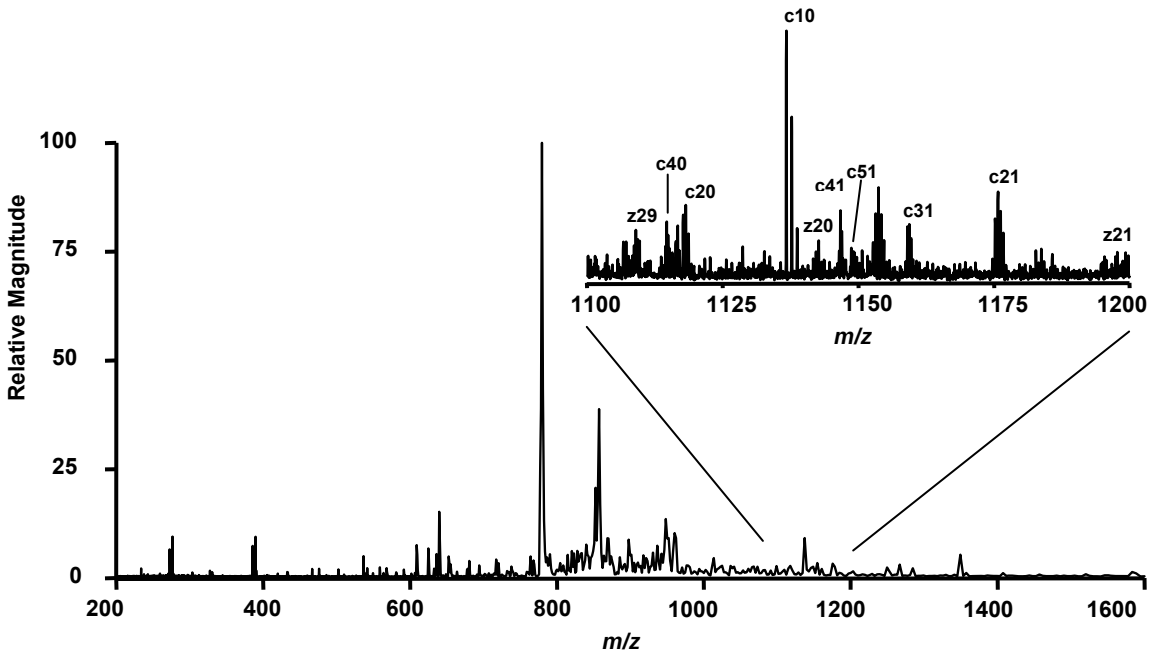

Figure 2. The ECD spectrum of ubiquitin 11+. The inset shows identification of several *c* and *z* ions.

Figure 3.

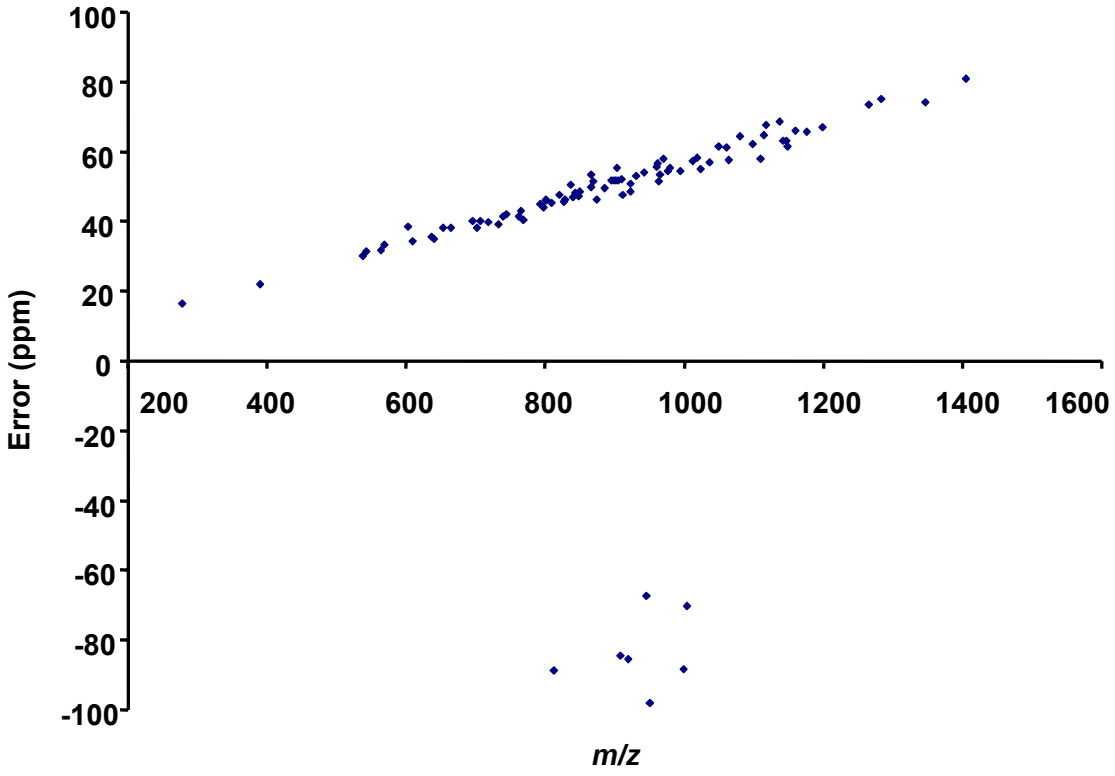

Figure 3. A visual representation of the error associated with the identified isotopic distributions of ubiquitin fragment ions following ECD of the ubiquitin 11+ ions. The graph shows a systematic increase in error with increasing *m/z*. The average error in the spectra was 53.1ppm. Peaks that have misassigned monoisotopic peaks are located in a cluster toward the bottom of the graph.

Figure 4

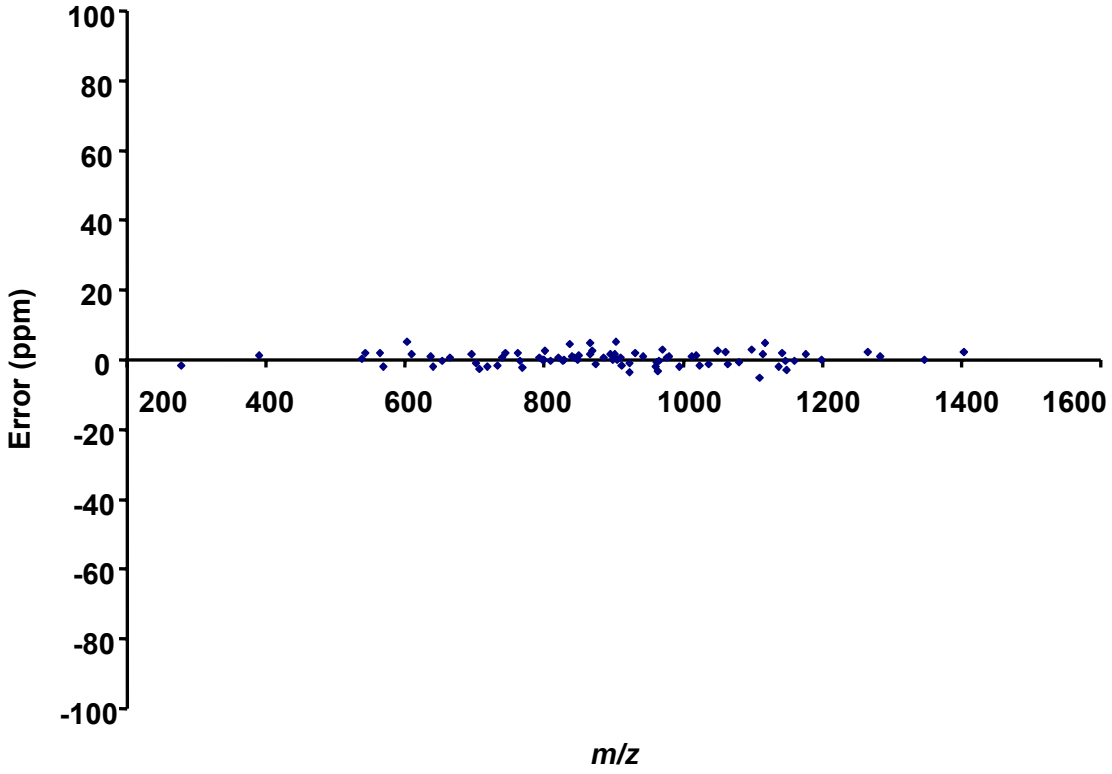

Figure 4. The error associated with the identified isotopic distributions of the fragment ions produced from ECD of the ubiquitin 11+ ions following the application of DeCAL. The graph shows the correction of the systematic error produced by space charge effects. The average error in the fragment ion spectra after DeCAL application was 1.59ppm. The cluster of misassigned peaks seen in Figure 3 are now shifted out of the 100ppm search window.

Figure 5

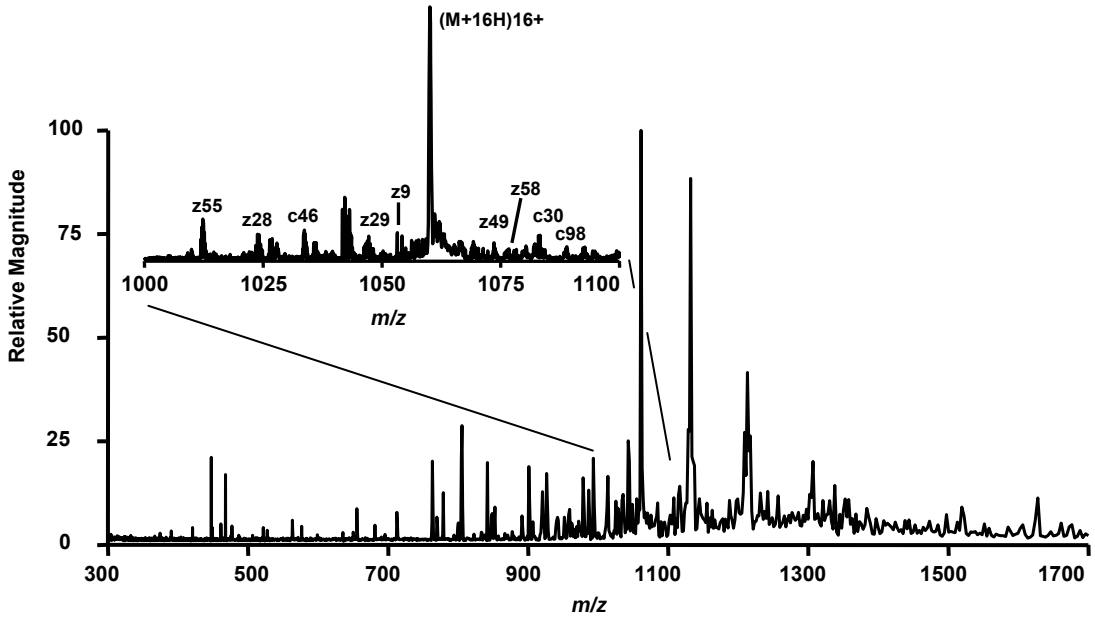

Figure 5. ECD-FTICR mass spectrum of myoglobin 16+. The inset shows the identification of several c and z ions.

Figure 6

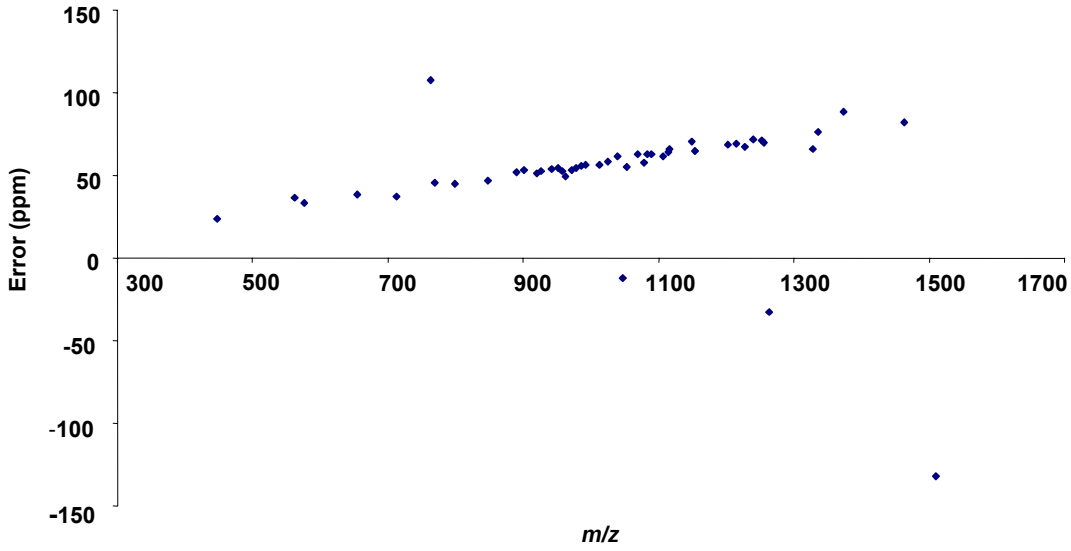

Figure 6. The error associated with the identified isotopic distributions of the fragment ions produced from ECD of the myoglobin 16+ ion. The average error of the identified peaks in the spectra was 58.9ppm.

Figure 7

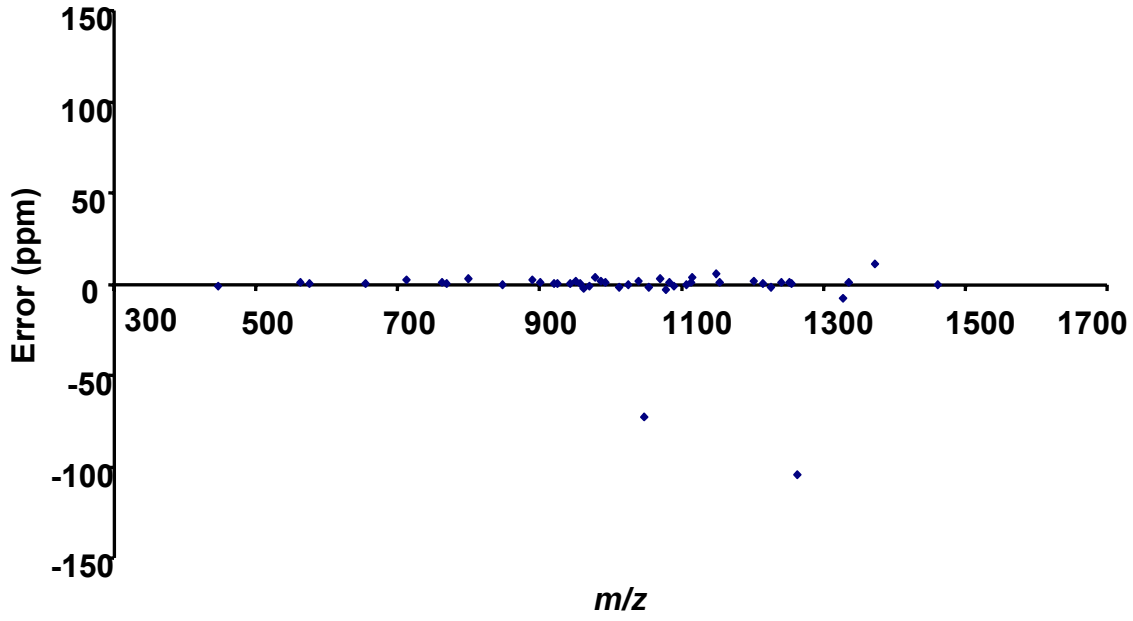

Figure 7. The error associated with the identified isotopic distributions of the fragment ions produced from ECD on the myoglobin 16+ ion following the application of DeCAL. The application of DeCAL shows a dramatic effect on the distribution and average error in the spectra. The average error in the spectra decreased to 5.5ppm.

Table 1

Allowed Mass Tolerance in ppm	Without DeCAL		P-score With DeCAL	
	Fragments Identified	P-score	Fragments Identified	P-score
5	0	----	22	9.84E-43
10	0	----	22	3.80E-36
25	0	----	22	1.71E-27
35	3	35.92	22	2.40E-24
50	15	2.19E-11	22	4.84E-21
65	22	1.22E-18	22	1.22E-18
85	23	1.90E-17	22	3.27E-16
100	24	4.16E-17	22	9.22E-15

Table 1. The top 50 most intense fragment masses from the ubiquitin ECD spectra of the 11+ ions were entered into ProSight PTM. The intact protein mass range was set at 8500 +/- 2000 Da while the mass tolerance of the fragment masses was varied. The use of DeCAL shows a substantial improvement in the P-Score and in the ability to identify a protein from its fragment masses.

CHAPTER 3

Observation of Increased Ion Cyclotron Resonance Signal Duration through Electric Field Perturbation

Abstract

Ion motion in Fourier Transform Ion Cyclotron Resonance Mass Spectrometry (FTICR-MS) is complex and the subject of ongoing theoretical and experimental studies. Two predominant pathways for the loss of ICR signals are thought to include damping of cyclotron motion, where ions lose kinetic energy and radially damp toward the center of the ICR cell, and de-phasing of ion coherence, where ions of like cyclotron frequency become distributed out of phase at similar cyclotron radii. Both mechanisms result in the loss of induced ion image current in FTICR-MS measurements and are normally inseparable during time-domain signal analysis. For conventional ICR measurements which take advantage of ion ensembles, maximization of the ion population size and density can produce the desired effect of increasing phase coherence of ions during cyclotron motion. However, this approach also presents the risk of coalescence of ion packets of similar frequencies. In general, ICR researchers in the past have lacked the tools necessary to distinguish or independently control de-phasing and damping

mechanisms for ICR signal loss. Nonetheless, the ability to impart greater phase coherence of ions in ICR measurements will allow significant advances in FTICR-MS research by improving the current understanding of ICR signal loss contributions of de-phasing and damping of ion ensembles, increasing overall time-domain signal length, and possibly, resulting in more routine ultrahigh resolution measurements. The results presented here demonstrate the ability to employ a high density electron beam to perturb electric fields within the ICR cell during detection of cyclotron motion, in an approach we call Electron-Promoted Ion Coherence (EPIC). As such, EPIC reduces ICR signal degradation through loss of phase coherence and much longer time-domain signals can be obtained. Our results demonstrate that time-domain signals can be extended by more than a factor of 4 with the implementation of EPIC, compared to conventional experiments with otherwise identical conditions. The application of EPIC has also been observed to reduce the appearance of peak coalescence. These capabilities are not yet fully optimized nor fully understood in terms of the complex physics that underlie the enhancement. However, the enhanced time-domain signals can result in improved resolution in frequency-domain signals and as such, this result is important for more efficient utilization of FTICR-MS. High resolution and accurate mass analysis are prime motivating factors in the application of advanced FTICR technology. We believe the approach presented here and derivatives from it may have significant benefit in future applications of advanced FTICR technology.

Introduction

Fourier Transform Ion Cyclotron Resonance (FTICR) mass spectrometry[1] is unique in its ability to measure the mass-to-charge ratios (***m/z***) of many different charged species simultaneously while providing high resolution and mass measurement accuracy. The high performance capabilities associated with FTICR mass spectrometry arise from the extended time period in which ion detection takes place, and allows for unambiguous charge state determination of large multiply charged ions, accurate mass analysis of complex peptide mixtures, and interpretation of complex MS/MS spectra[2-10]. The ICR experiment starts by first trapping the ions in the ICR cell with an axial magnetic field and an electrostatic potential well. Ions of the same ***m/z*** are excited together and form a coherent ion cloud that has a single measurable cyclotron frequency. Excited ion clouds must remain coherent in cyclotron motion for an extended period of time to allow multiple period measurements. As the ion clouds traverse their cyclotron orbits, they induce oscillating current in the detection circuitry with oscillation frequencies that result from the summation of all ion cyclotron frequencies. This detection process allows for simultaneous high resolution and mass measurement accuracy, as is detailed in many excellent review articles and books [11-13]. Other types of mass spectrometers besides FTICR mass spectrometers have also utilized this non-destructive detection technique[14, 15]. Detection of ICR signals for extended periods of time allows multiple measurements of each ***m/z*** species, and provides the foundation for the high performance capabilities of FTICR-MS. In principle, the longer time period that ion signals are detected, the greater the possible resolution and mass measurement accuracy. Furthermore, the achievable

sensitivity of FTICR-MS is also related to the length of the detectable sinusoidal signal. However, in practice, acquisition of long time-domain signals does not guarantee high performance measurements with FTICR-MS.

Several factors can affect higher performance measurements with FTICR-MS. Although resolution, mass accuracy, and sensitivity can all be increased with improved time-domain signal length, Coulombic interactions and inhomogeneities in the axial electrostatic trapping potentials can cause variations in the observed cyclotron frequency with time and space within the ICR cell. In a three-dimensional quadrupolar potential field, the ion cyclotron frequency is independent of the positions of the ion clouds in the ICR cell [16]. However in most ICR cell designs, this ideal three-dimensional quadrupolar potential is not achieved and the resulting non-quadrupolar trapping potentials may contribute to frequency drifts[17, 18]. There have been many different trap geometries designed to minimize electric field inhomogeneity and achieve improved quadrupolar trapping potentials, while also maintaining high excitation and detection efficiencies [16, 19-21]. Also, the space charge potential arising from Coulombic interactions among ion clouds may vary with time. For example, as the ion clouds relax back toward the center of the ICR cell through collisional damping, their Coulombic interactions increase due to the higher ion density experienced at smaller cyclotron radii. This increase in ion density may cause the observed cyclotron frequency to decrease, as discussed by Guan et al [17]. Therefore, conditions can arise within the ICR cell that decrease instrument performance and prevent extended periods of ion signal detection. To exploit the high performance capabilities of FTICR-MS in more routine fashion, these conditions must be minimized.

Two primary processes are currently thought to limit ions from being detected for extended periods of time. The combination of collisional damping [22] and de-phasing of the ion packet cause the detected ICR signal to decay over time. Collisional damping is resultant from collisions between the ions and residual neutral gas molecules present in the ICR cell during detection of cyclotron motion. The coherent ion packet loses kinetic energy through these collisions. To maintain constant cyclotron frequency, the lower kinetic energy of the ions results in a smaller cyclotron orbit. As such, the ions become further away from the detection plates and the observed signal is decreased. Ion/neutral collisions are the primary reason that ICR measurements are normally carried out under ultra-low pressure conditions. There are two limiting forms of collisional damping, ion-induced dipole (Langevin) collision model, leading to an equation of ion motion damping term that is linear in velocity resulting in a Lorentzian frequency-domain line shape, and a hard-sphere collisional model, that produces a quadratic damping term[22]. The other primary mechanism for loss of ICR signal is de-phasing. This process happens when the ion cloud losses its phase coherence and ions of the same ***m/z*** value become distributed at varying cyclotron phase angles instead of remaining as a coherent ion packet. A number of different processes have been identified that contribute to ion cloud de-phasing. For example, ion cloud density, magnetic field strength, Coulombic interaction with other ion clouds, total cloud charge, and ion velocity are all parameters that have an effect on de-phasing [23]. As described by Peurrung and Kouzes, imposed shear effects disrupt the ion phase coherence and cause the ion cloud to be distributed at various cyclotron phase angles. These authors list possible sources of shear to include magnetic-field inhomogeneities, image charge effects, passive space charge at the trap center and non-

harmonic or asymmetric components of the trapping potential well[23]. Also, some ions present in the ICR cell may have sufficient energy to follow a trajectory that is different from that of the bulk ion cloud. For example, ions with velocities significantly different from that of the ion cloud are able to separate from the majority of ions which leads to a loss of detected ICR signal. As a result, the reduction of charge in the ion packet decreases coherence and induces a smaller image charge on the detection plates. Currently, there is no convenient way to determine the contribution of each signal loss mechanism to the observed signal decay; however, differentiation between damping and de-phasing of cyclotron motion can be obtained through observation of multiple harmonics[24-27]. Normally, the observed decay in the time-domain signal is considered to be some combination of collisional damping and de-phasing.

Efforts have been made to minimize damping and de-phasing of ion cyclotron motion [7, 28, 29,10]. There are also examples in which ion de-phasing has been completely eliminated, such as demonstrated with single or individual ion measurements [30-35]. In those experiments, a single ion carried enough charge that it produced a detectable image current. Single ion measurements are unique in that there is no need for phase coherence between ions, since only one ion of a specific ***m/z*** is present. In those cases, the only signal loss mechanism other than through reaction, is through collisional damping. This earlier work [36] demonstrated a significant improvement in time-domain signal length compared to the conventional ion ensemble detection scheme. In single ion experiments, measurements were conducted with species of the same molecular weight and under similar vacuum conditions. Thus, increased time-domain signals could be attributed to the removal of de-phasing mechanisms. However, most ions do not carry enough total

charge to be detected as single ions. In most conventional detection methods, an ensemble of ions is needed to supply enough charge to induce a detectable image current. Ions of the exact same ***m/z*** are excited in-phase with each other. These ions form a stable ion packet and their collective charge induces a measurable image current for detection. These ion packets seem to be more stable as the number of charges in the ion packets increase. Ion cloud stability is important since it prevents de-phasing, however it can also be limited by a number of factors. Peurrung and Kouzes [23] presented an explanation for the underlying foundation of long term ion cloud stability. Nikoleav et al. have recently presented numerical simulations with a higher degree of accuracy and give a more revealing model of the complex ion motion in the ICR cell[37]. Peurrung and Kouzes pointed out that the ion cloud undergoes an additional rotational motion separate from cyclotron and magnetron motion. The ion cloud generates its own electric field and in the presence of a magnetic field the ion cloud rotates about its own center. Ion cloud rotation counterbalances shear factors mentioned above that can tear the ion cloud apart. Ion cloud rotation is thought to be the primary basis which makes the duration of long time-domain signals possible for an ensemble of ions. This ion cloud spin rotation increases cloud stability as a function of higher charge density. However, the number of ions that can form an ion cloud and still retain the resolving power necessary to separate closely spaced peaks is limited by phase-locking or ion cloud coalescence. Mitchell and Smith [38] reported that this coalescence phenomenon occurs when ion clouds have similar cyclotron frequencies and large Coulombic charges. As the Coulombic charge in the ion clouds increase, there is an increased likelihood that ion clouds with similar, but not identical cyclotron frequencies will begin to rotate around each other. These separate ion

clouds can phase-lock and continue on a cyclotron orbit at a mutual cyclotron frequency and will appear as one peak in the mass spectrum. Thus, mitigation of ion cloud de-phasing through increased ion cloud density requires careful control to avoid conditions that promote phase-locking or coalescence [29]. These two opposing constraints, namely, the ability to trap enough ions to promote single ***m/z*** ion cloud stability during detection while keeping the ion population small enough to avoid coalescence represent real, fundamental limitations of FTICR-MS performance.

Increased time-domain signal length can provide improved resolution and mass measurement accuracy, and as such, increased routine time-domain signal acquisition length is a goal of many studies to advance FTICR-MS technology. However, ion motion in the ICR cell is still not completely understood and improved comprehension of ion motion could result from methods that de-couple collisional damping and de-phasing signal loss mechanisms. The primary motivation of the present manuscript is to report the observation of experimental effects that serve to reduce ion cloud de-phasing mechanisms. We call the observed effect, Electron-Promoted Ion Coherence, or EPIC, since, with the application of a high density electron beam during detection, we observed significant improvement in the length of detected coherent cyclotron motion. Electron beams have been previously introduced into the ICR detection cell for a number of different reasons such as ionization, dissociation[39], ion transfer[40], and ion trapping (EBIT)[41]. However, to the best of our knowledge this is the first time that the electron beam has been used to modulate electric fields during detection of during detection of cyclotron motion. To the best of our ability to determine, the effects described below appear to result in decreased ion cloud de-phasing and result in significantly improved

time-domain signal length. Also to the best of our knowledge, this capability represents an entirely new tool that can be used to improve FTICR-MS performance as well as help distinguish the two primary signal loss mechanisms. For example, this de-coupling could enable a better understanding of ion motion and phase coherence which ultimately enables improved detection techniques that enhance resolution, mass measurement accuracy, and sensitivity.

Experimental

Ubiquitin (MW_{avg} = 8,565Da), Bradykinin (MW_{avg} = 1,060Da), and Substance P (MW_{avg} = 1348Da) obtained from Sigma Aldrich were dissolved and diluted to 10uM concentration with a solution of 49:49:2 by volume of water, methanol, and acetic acid. The experiments were performed with a Bruker Daltonics Apex-Q 7-T FTICR mass spectrometer. The instrument has a mass selective quadrupole which allows for mass-selective accumulation of a specific ***m/z*** species. Electrospray was used as the ionization source in which the voltage on the capillary was set between -1,800V and -2,000V. A syringe pump was used to introduce solutions at a rate of 15-25uL/hr. Ions were trapped in the ICR cell using sidekick [42]. In select experiments, argon was pulsed into the ICR cell to cool the ions followed by a 2 to 4 second delay for pump down time before excitation of ion cyclotron motion. Experiments that utilized argon cooling gas are indicated below. In all experiments, the ion-gauge reached a minimum value of 5 X 10^{-10} Torr before the ions were excited. The projected pressure in the cell may be up to an order of magnitude higher. Electron-Promoted Ion Coherence, or EPIC experiments

were performed by supplying a high density beam of electrons through the center of the ICR cell during the detection event. The electron beam was produced using a hollow cathode emitter[43] normally used for Electron Capture Dissociation (ECD) experiments [39, 44, 45]. The cathode emitter is located outside the ICR cell and is positioned along the central axis of the ICR cell. The outer diameter of the cathode is 7.6 mm and has an inner diameter of 3.5mm and was heated by passing a current of 1.5 Amps through it using an external power supply. The pulse sequence of the experiment was modified so that the electron beam was initiated after the cyclotron excitation event and before the detection event. The electrons were pulsed into the ICR cell with conditions similar to those used with ECD, except that the timing of the pulse sequence is different from normal ECD experiments. The electron emitter was continually heated throughout all phases of the experiment. The bias applied to the emitter was set at 0.0V for no electron beam, and between -0.1V and -1.3V to stimulate emission of electrons. This high density beam of electrons was continuously produced during the entire length of the detection event. In EPIC experiments, the electron beam was turned on only after ions reached their excited cyclotron orbits and was turned off after the termination of the detection event. Experiments were performed in narrow-band detection mode for ultra-high resolution and acquisition of longer attainable time-domain signals. Isolation of specific charge states was performed prior to the ions entering the ICR cell with the mass-selective quadrupole. Xmass (version 7.0.6) was used as the data acquisition software. All data sets were collected as single scans. Control, or normal time-domain signals shown for comparison were obtained by applying 0.0V bias to the emitter; during the subsequent EPIC experiment, a voltage bias of -0.1V to -1.3V was applied to the emitter

to produce the high density electron beam. No other parameters were changed between experiments. ICR-2LS [46] was used for data processing. The substance P data set was apodized (Welch) and zero-filled once before obtaining the mass spectrum. The measurements of cyclotron frequency drift with time were obtained using the "Sweep" [18] program, written as a module within ICR-2LS.

Results and Discussion

A high density, low energy electron beam produced along the central axis outside the ICR cell during detection of ion cyclotron motion was found to significantly increase the length of the observed time-domain signal. Though the dispenser cathode used to create the electron beam was installed to produce electrons for ECD, no fragmentation resultant from the electron beam was observed during EPIC experiments. The ion cloud and electron beam likely have no overlap during detection, since the ion cloud is at a larger cyclotron orbit as its motion is being detected. The calculated post excitation ICR orbital radius was ~1.8cm, determined through single frequency excitation experiments. Furthermore, if the electron beam and the excited ion cloud were to intersect during detection, the resultant ECD fragment ions, if formed, would likely be distributed out of phase with each other at similar radii, and little or no observable signal would have been detected. With the present EPIC approach, the electron beam is only turned on after the ions have been promoted to their excited cyclotron radius. As mentioned above, this process is different than what normally occurs for ECD in which the electrons are pulsed into the ICR cell with the sole purpose of interacting with the parent ions to cause

fragmentation. It should be noted that ECD experiments performed with application of electron beams of similar density and duration result in complete loss of all observed ion signals. For ECD experiments, the electron pulse is initiated for a short time period, fragmentation takes place, and the resulting ions are excited and detected.

We originally investigated the use of the electron beam on ion cyclotron motion in an attempt to learn about electrostatic field effects on ion cyclotron frequencies. Previous publications reported the observation and correction of cyclotron frequencies drifts during signal acquisition [17, 18]. Since many of these efforts ascribe measured cyclotron frequency shifts to electrostatic field effects on cyclotron motion, we anticipated the high density electron beam produced from the ECD dispenser cathode would prove to be a useful tool to investigate these affects.

However, a very striking and unexpected result was observed from the initial experiments, which was a substantial increase in time-domain transient length. The initial observation of increased time-domain transient length with the electron beam was carried out using bradykinin with conditions that were not optimized for long-time domain signal acquisition. Bradykinin ions were trapped in the ICR cell using sidekick, which is thought to cause the ions to have slight magnetron motion and to be slightly more spatially distributed in the ICR cell [42]. Also, no collision gas was added for ion cooling and compression of trapped ions before excitation. The initial observed result is illustrated in **Figure 1**, which shows both the traditional time-domain signal and the initial EPIC results along with their corresponding mass spectra. As mentioned above, the initial non-EPIC results shown here were acquired without prior optimization of conditions that enable long time-domain signal acquisition and thus, are not

representative of what one might expect in terms of longer time-domain transient performance from this type of instrument. However, initial application of EPIC resulted in improvement in the observed time-domain signal length, even for these non-ideal conditions. The striking feature here of significant interest to us was the unexpected increase in time-domain signal length.

The observation of increased signal duration during the electron beam application was surprising to us for several reasons. First, ICR signal detection was not precluded from noise or disrupted ion phase coherence caused by pulsing the dispenser cathode during detection. One might expect that, given the small signals resultant from ion motion, and the extreme high sensitivity of the detection circuitry normally used with FTICR-MS, that signal detection might be much more difficult with the electron beam turned on. Secondly, one might consider that changes in the electrostatic field inside the ICR cell might disrupt all coherent ion motion due to the previous discussion of cloud stability and electrostatic field-induced shear effects. These data suggest, at least under a range of conditions that were investigated, that this is not the case. In fact, the ICR signal appears more stable with EPIC conditions.

We believe that this observation of increased time-domain signal length has significance, and our initial results warranted further investigation. Therefore, the next experiments were performed to see if we could obtain a similar increase in ICR signal duration under conditions that were more amenable to longer time-domain signals with conventional or non-EPIC experiments. The conditions in the ICR cell were slightly modified from those applied for the experiments discussed above by pulsing argon gas into the ICR cell to cool the ions and reduce axial oscillation after trapping, but prior to

cyclotron excitation. This approach is similar to those used in most labs to acquire longer time-domain signals, since reduction of axial motion results in a more compact ion cloud and the opportunity to work at lower trapping potentials which seem more suitable to longer time-domain signal detection. **Figure 2a** shows the resultant time-domain signal from the narrow-band detection of ubiquitin $(M+7H)^{7+}$. All parameters in the experiment were carefully adjusted and controlled to maximize the observed time-domain signal length. This resulted in detectable signal for approximately 25 seconds, and this result represents the best we could achieve with the normal detection method on that particular day. The subsequent time-domain signal was acquired immediately following, with the exact same experimental parameters as was used in Figure 2a with the exception of the application of the electron beam, and the results are shown in **Figure 2b**. With EPIC, the length of the observed time-domain signal increased to over 70 seconds. This observation was very exciting, since it demonstrated that significantly improved ion signal duration could be achieved with EPIC, even when carefully optimized conditions were implemented prior to EPIC. We were still able to observe the same significant improvement in time-domain signal length as we observed without careful tuning and cooling of axial motion. With the application of EPIC, the time-duration that signal could be detected was enhanced by approximately a factor of 3.

As mentioned above, ICR signal loss is a convoluted combination of collisional damping and de-phasing. Collisional damping occurs when the ion packet collides with neutral molecules in the ICR cell. Therefore, with higher pressure in the ICR cell, we would expect to see shorter time-domain signals. In our experiments, the pressure in the ICR cell during signal acquisition was the same to the best of our ability to measure it.

Since the only difference was the application of the electron beam, one might consider the effects of the electron beam on the effective pressure in the ICR cell. Pressure changes associated with the activation of the electron beam are likely small, if any, based on the lack of any measured changes observed with the ion gauge. In addition, any negative change in pressure, as would be needed to ascribe the observed increase in performance with EPIC to changes in collisional damping rates seem highly unlikely, given the low energy of the electrons and the low base pressure measured on the system. That is, any possible "pumping" resultant from electrons interacting with neutrals, producing ions that are effectively able to escape the trap, and thus result in lower in-cell pressures, is unlikely due to the fact that the electron energies are well below the ionization energies of any possible neutral species that could be present in the cell. Instead, it seems more likely that if any change to the pressure were to occur as a result of the electron beam, it would likely be a shift to a higher pressure resulting from the heating associated with the production of electrons from the dispenser cathode. This too, is likely a very small contribution to the observations. Therefore, decay of signal amplitude resultant from collisional damping of the ion packet is expected to be approximately the same in both experiments. The calculated collision frequency between the ions and residual neutral molecules was ~2 collisions per second, based on the approximate cell pressure of $5x10^{-9}$ Torr and an excitation radius of 1.8cm. Thus, we suspect that electrostatic field effects and ion cloud coherence are much more likely the root of the observed enhancement in time-domain signal length and that application of a steady stream of electrons through the ICR cell reduces electrostatic factors that promote ion cloud de-phasing.

As pointed out in several previous theoretical treatments of ion motion, the number of ions can significantly impact the stability of ion clouds and the length of detectable ICR signals. This factor was considered in these investigations as well. The number of ions that make up the ion clouds in each experiment from Figures 2a and 2b was held constant to the best of our ability. Since the number of ions can be significantly altered with ionization, ion accumulation, injection, trapping and excitation conditions, all parameters were held constant between EPIC and non-EPIC experiments. Furthermore, one thing to note in comparison of Figures 2a and 2b is that the initial amplitudes of the two time-domain signals are approximately the same. The initial amplitude is a function of the total charge in the ion packet and the radius to which the ions clouds are accelerated. The initial amplitudes of the time-domain signals shown in Figure 2 are the same within expected experimental error, indicating that the number of ions present in each experiment is very nearly the same. Besides the application of the electron beam, no modification was performed to any other parameter in the experiment. As the number of ions in the ICR cell was decreased by reducing the ion accumulation time, the length of the detected transient signal also decreased with and without the application of EPIC. However, the same relative improvement in transient signal length was observed with the application of EPIC, even with reduced ion population sizes. This suggests that the effects of EPIC can not be entirely ascribed to reduction of the number of trapped ions present during detection.

As mentioned previously, the initial motivation behind the application of the electron beam during detection was to investigate possible perturbations in the electrostatic fields and subsequent frequency shifts that may arise. **Figure 3** illustrates

the effect that the electron beam can have on the measured cyclotron frequency shift, compared to that observed with non-EPIC experiments using different isotope peaks of bradykinin $(M+2H)^{2+}$. This figure illustrates how the ion cyclotron frequency of the ion packet is shifting with time as it spins on its excited cyclotron orbit. With the traditional detection technique, it is common to see the frequency shift to a lower value with time [17, 47]. However, with the EPIC-produced signals, we observe the frequency shift to a higher value with time. One possible explanation for this observation is that when the electron beam is turned on, changes in the electrostatic field potentials inside the ICR cell are observed. The addition of the electron beam produces a radially inward-directed force on the positive ions, and would thus be expected to shift the ICR frequency higher, lower *m/z*, even at time zero during detection as observed in figure 3. This figure shows the frequency shift with time to be much more prominent with the EPIC produced spectra. In the resultant mass spectra of bradykinin (data not shown) the peaks produced from the EPIC signal are thus broader due to the cyclotron frequency drifting with time. However, this is not always the case; with careful optimization of the detection parameters it is possible to nearly eliminate any frequency shift with time. **Figure 4** shows the frequency shift with time of the different isotope peaks of substance P $(M+2H)^{2+}$. Here the frequency shifts with the non-EPIC results are greater and slope to a lower frequency with time with EPIC. The frequency with EPIC produced signal is relatively constant, in which the standard deviation of the detected frequency for the monoisotopic peak is 0.119 Hz over the 10 second detection period, while the standard deviation for non-EPIC result is 1.4 Hz. This results in higher resolving power in the mass spectra which are shown in **Figure 5**. In this figure, the observed resolving power (FWHM) increased from

~250,000 to ~850,000 with the application of EPIC. Data was only collected over a 10 second detection period. The non-EPIC signal decayed below the noise within that time frame (~8 sec), while the EPIC signal was still ~15 times the noise level in the time-domain signal**.** It should be noted that even though the frequency drift was eliminated which improved the resolving power in the previous example no fine structure was observed. However, we are able resolve two closely spaced peaks with the application of EPIC**.** **Figure 6** shows an example of the ability to observe fine structure in the Bradykinin $(M+2H)^{2+}$ peak that is 2 Da above the monoisotopic mass with EPIC utilization. This peak is composed of both ^{15}N and ^{13}C substitutions and in this figure, the ^{15}N and ^{13}C peaks are resolved. The mass difference between ^{15}N and ^{13}C is 6.4 mDa and requires a resolving power of 165,000 to observe separation. The resolving power increased from ~90,000 to ~250,000 with application of EPIC and fine structure is observed in the spectrum.

It is likely that increasing the potential applied to the heated cathode increases the number of electrons traversing the ICR cell. It should be noted that applying a potential to the cathode surface, in the absence of any cathode heating current, resulted in no observed change in time-domain signal duration as compared with non-EPIC results. Thus, cathode surface voltage itself is not directly contributing to the observed effects of EPIC. The number of electrons that enter the ICR cell is controlled by the cathode heating current and the bias voltage applied to the dispenser cathode. As the applied voltage increases, the number of electrons being sent through the ICR cell increases.

Application of EPIC is likely to result in alteration of the trapping electrostatic field potentials. Due to the high electron densities experienced, EPIC likely modifies

potential fields in a similar manner as a solid electrode placed through the center of the ICR cell. Solouki et al. [48] previously implemented a Kingdon trap[49] to be used with ICR detection which utilized a solid copper wire electrode placed on the central axis of the ICR cell to act as an ion guide and facilitate ion transfer from the source cell to the analyzer cell. The presence of this wire caused perturbations in electrostatic field lines of the trapping potentials. It is likely that there are similar shifts in the electrostatic field lines when there is a high density electron beam present in the ICR cell, as encountered during EPIC experiments. The electron beam will produce a negative potential region through the center of the ICR cell**.** Gillig et. al.[50] described the theoretical ion motion within this particular ICR cell design. When a negative potential is placed through the center of the ICR cell, the radial electric field is directed inwards for some volume of the ICR cell. Thus, the magnetron motion within this region will relax back toward the central axis of the ICR cell with time, with the presence of collisional damping. Potentially, EPIC experiments will present many advantages inherent in the cell design presented by Solouki et al., but also allow flexibility in the time in which the "electrode" is present within the cell. However, the similarity of the axial electron beam to the actual Kingdon trap will depend on the extent to which the electron beam density is constant along the z-axis of the ICR cell.

Another important point to consider is that increased time-domain signals are a prerequisite for high performance, but do not always translate into improved resolving power. The time-domain signals in Figure 2a and 2b resulted in mass spectra of approximately equal resolving power despite the much longer EPIC-produce result. However under some conditions, it is possible to produce spectra of improved resolving

power and sensitivity with EPIC. **Figure 7** shows the time-domain signal produced with the ubiquitin 7^+ charge state. Figure 7a shows the non-EPIC control results, while Figure 7b illustrates the EPIC results. With the application of EPIC, the time-domain signal increases from ~8 seconds to ~40 seconds which is approximately a factor of 5 improvement. **Figure 8** provides an overlay of the Fourier transformed time-domain signals of Figures 7a and 7b. The higher-magnitude, isotopic envelope of ubiquitin 7^+ observed with higher resolving power is the EPIC result, and the lower-magnitude, lower performance spectrum is the result of the non-EPIC experiment. Figure 8 demonstrates that both longer time-domain signals and improved spectral resolving power are possible with EPIC. In the analysis of data in Figure 8, it was also noticed that as the two spectra are overlaid the position of the isotopic distributions do not match up exactly. This in not surprising since the instrument was not calibrated with the electron beam turned on. The radial electric field is resultant from the applied trapping potentials and drives magnetron motion. The effect of turning on the electron beam changes the radial electric field, and thus also changes the magnetron motion. Any change to parameters associated with the ICR cell will cause changes in the calibration of the instrument. In order to maintain the expected high mass measurement accuracy achievable with FTICR-MS, the calibration of the instrument needs to be performed with the electron beam turned on. Therefore, the mass measurement accuracy should not be compromised with the use of the electron beam.

The application of EPIC has also been observed to affect the phenomenon known as peak coalescence. Coalescence limits the number of ions that can be effectively contained and detected in FTICR experiments. **Figure 9a** depicts the time-domain

signals for the 2^+ charge state of bradykinin in which closely spaced ***m/z*** species coalesce after a short time period. The resulting mass spectra show a small peak just to the right of the monoisotopic which is the result of peak coalescence. This was determined by segmenting the time-domain signal into two different regions. **Figure 9b** shows the first segment which contains the first 1.15 seconds of the time-domain signal. This part of the signal contains information of different isotopes of bradykinin. **Figure 9c** shows the second segment which contains the information from 1.25 to 16 seconds. The mass spectrum that results from this time-domain segment contains only a single ***m/z*** peak, and no isotopic information. The appearance of this peak happens at the same time that all the isotopic peaks disappear. This collapse of isotopic peaks into a single peak is known as coalescence and serves as a limitation to FTICR performance. **Figure 10** shows the EPIC produced time-domain signal and the resulting mass spectra under otherwise identical experimental conditions as those in Figure 8. With the application of EPIC, the coalescence is no longer observed. This observation was repeatable, as we were able to turn the electron beam on and off and see the appearance and disappearance of the peak coalescence. Under normal conditions, coalescence was observed with bradykinin $(M+2H)^{2+}$, however, with the application of EPIC, peak coalescence was mitigated.

Conclusions

Factors which promote de-phasing and degrade ion cloud phase coherence during detection can be substantially reduced by producing a high density beam of electrons through the center of the ICR cell. The improved ion cloud stability can be observed by

the increased length of the time-domain signal. The application of EPIC produces time-domain signals that are on average, 3 to 5 times longer than non-EPIC results. Though resolution and mass accuracy are typically a function of time-domain signal length, the improved time-domain data sets taken with EPIC do not necessarily lead to improved resolution. However, under some of the experimental conditions we investigated, it is possible to obtain an increase in both resolution and sensitivity with EPIC. We demonstrate a factor of 3 improvement in resolution with the application of EPIC.

An additional interesting feature of the EPIC results is the observed effect that the electron beam has on the cyclotron frequency shift. The application of EPIC seems to cause the frequencies to shift to a higher value with time. Also, the application of EPIC can prevent closely spaced peaks from coalescing. The mechanisms underlying the electron beam effects on ion cloud motion that result in longer observed time-domain signals are not fully understood at present. However, this observation of increased time-domain signal is significant and should provide greater insight into ion motion and the effects caused by perturbations in the electric field within the ICR cell. Finally it is likely that the application of EPIC, or a derivative of it, can be implemented in the future to exploit the unique enhancements that it provides.

Acknowledgements

This research was supported by the National Science Foundation, Instrument Development for Biological Research Program, grant no. DBI-0352451, the Murdock Charitable Trust, and the National Institutes of Health Biotechnology Training Grant. The

authors would also like to thank Gordon Anderson for the data analysis tools (ICR-2LS) and Harold R. Udseth, Gökhan Baykut and Eugene Nikolaev for helpful discussions.

References

(1) Comisarow, M. B.; Marshall, A. G. *Chemical Physics Letters* **1974**, *25*, 282-283.

(2) Masselon, C.; Anderson, G. A.; Harkewicz, R.; Bruce, J. E.; Pasa-Tolic, L.; Smith, R. D. *Analytical Chemistry* **2000**, *72*, 1918-1924.

(3) He, F.; Emmett, M. R.; Hakansson, K.; Hendrickson, C. L.; Marshall, A. G. *J Proteome Res* **2004**, *3*, 61-67.

(4) Bossio, R. E.; Marshall, A. G. *Anal Chem* **2002**, *74*, 1674-1679.

(5) Kelleher, N. L.; Lin, H. Y.; Valaskovic, G. A.; Aaserud, D. J.; Fridriksson, E. K.; McLafferty, F. W. *Journal of the American Chemical Society* **1999**, *121*, 806-812.

(6) Reid, G. E.; McLuckey, S. A. *J Mass Spectrom* **2002**, *37*, 663-675.

(7) Wigger, M.; Eyler, J. R.; Benner, S. A.; Li, W.; Marshall, A. G. *J Am Soc Mass Spectrom* **2002**, *13*, 1162-1169.

(8) Little, D. P.; Speir, J. P.; Senko, M. W.; O'Connor, P. B.; McLafferty, F. W. *Anal Chem* **1994**, *66*, 2809-2815.

(9) Lipton, M. S.; Pasa-Tolic, L.; Anderson, G. A.; Anderson, D. J.; Auberry, D. L.; Battista, J. R.; Daly, M. J.; Fredrickson, J.; Hixson, K. K.; Kostandarithes, H.; Masselon, C.; Markillie, L. M.; Moore, R. J.; Romine, M. F.; Shen, Y.; Stritmatter, E.; Tolic, N.; Udseth, H. R.; Venkateswaran, A.; Wong, K. K.; Zhao, R.; Smith, R. D. *Proc Natl Acad Sci U S A* **2002**, *99*, 11049-11054.

(10) Shi, S. D. H.; Hendrickson, C. L.; Marshall, A. G. *Proceedings of the National Academy of Sciences of the United States of America* **1998**, *95*, 11532-11537.

(11) Marshall, A. G.; Hendrickson, C. L.; Jackson, G. S. *Mass Spectrometry Reviews* **1998**, *17*, 1-35.

(12) Marshall, A. G.; Hendrickson, C. L. *International Journal of Mass Spectrometry* **2002**, *215*, 59-75.

(13) Alan G. Marshall; Verdun, F. R. *Fourier Transforms in NMR, optical, and mass spectrometry: a user's handbook*; Elsevier Science Publishers: New York, 1990.

(14) Benner, W. H. *Analytical Chemistry* **1997**, *69*, 4162-4168.

(15) Makarov, A. *Analytical Chemistry* **2000**, *72*, 1156-1162.

(16) Guan, S.; Marshall, A. G. *International Journal of Mass Spectrometry and Ion Processes* **1995**, *146/147*, 261-296.

(17) Guan, S.; Wahl, M. C.; Marshall, A. G. *Anal Chem* **1993**, *65*, 3647-3653.

(18) Bruce, J. E.; Anderson, G. A.; Hofstadler, S. A.; Winger, B. E.; Smith, R. D. *Rapid Communications in Mass Spectrometry* **1993**, *7*, 700-703.

(19) Ostrander, C. M.; Arkin, C. R.; Laude, D. *Journal of the American Society for Mass Spectrometry* **2001**, *12*, 30-37.

(20) Guan, S.; Marshall, A. G. *Review of Scientific Instruments* **1995**, *66*, 63-66.

(21) Bruce, J. E.; Anderson, G. A.; Lin, C.-Y.; Gorshkov, M.; Rockwood, A. L.; Smith, R. D. *Journal of Mass Spectrometry* **2000**, *35*, 85-94.

(22) Guan, S.; Li, G.-Z.; Marshall, A. G. *International Journal of Mass Spectrometry and Ion Processes* **1997**, *167/168*, 185-193.

(23) Peurrung, A. J.; Kouzes, R. T. *Physical Review. E. Statistical Physics, Plasmas, Fluids, and Related Interdisciplinary Topics* **1994**, *49*, 4362-4368.

(24) Pan, Y. P.; Ridge, D. P.; Wronka, J.; Rockwood, A. L. *Rapid Communications in Mass Spectrometry* **1987**, *1*, 121.

(25) Pan, Y. P.; Ridge, D. P.; Rockwood, A. L. *International Journal of Mass Spectrometry and Ion Processes* **1988**, *84*, 144.

(26) Nikolaev, E. N.; Gorshkov, M. V.; Mordehai, A. V.; Talrose, V. L. *Rapid Communications in Mass Spectrometry* **1990**, *4*, 144.

(27) Grosshans, P. B.; Marshall, A. G. *International Journal of Mass Spectrometry and Ion Processes* **1991**, *107*, 49-81.

(28) Gordon, E. F.; Muddiman, D. C. *Journal of Mass Spectrometry* **2001**, *36*, 195-203.

(29) Stults, J. T. *Analytical Chemistry* **1997**, *69*, 1815-1819.

(30) DiFilippo, F.; Natarajan, V.; Bradley, M.; Palmer, F.; Pritchard, D. E. *Physica Scripta, T* **1995**, *T59*, 144-154.

(31) Bruce, J. E.; Cheng, X.; Bakhtiar, R.; Wu, Q.; Hofstadler, S. A.; Anderson, G. A.; Smith, R. D. *Journal of the American Chemical Society* **1994**, *116*, 7839-7847.

(32) Smith, R. D.; Cheng, X.; Bruce, J. E.; Hofstadler, S. A.; Anderson, G. A. *Nature (London, United Kingdom)* **1994**, *369*, 137-139.

(33) Cheng, X.; Camp, D. G., 2nd; Wu, Q.; Bakhtiar, R.; Springer, D. L.; Morris, B. J.; Bruce, J. E.; Anderson, G. A.; Edmonds, C. G.; Smith, R. D. *Nucleic Acids Res* **1996**, *24*, 2183-2189.

(34) Cheng, X.; Bakhtiar, R.; Van Orden, S.; Smith, R. D. *Anal Chem* **1994**, *66*, 2084-2087.

(35) Chen, R.; Cheng, X.; Mitchell, D. W.; Hofstadler, S. A.; Wu, Q.; Rockwood, A. L.; Sherman, M. G.; Smith, R. D. *Analytical Chemistry* **1995**, *67*, 1159-1163.

(36) Bruce, J. E.; Anderson, G. A.; Udseth, H. R.; Smith, R. D. *Analytical Chemistry* **1998**, *70*, 519-525.

(37) Nikolaev, E. N.; Popov, A. M.; Heeren, R. M. A.; Sharova, M. S.; Pozdneev, A. V.; Chingin, K. S.; Taban, I. M., 53rd ASMS Conference, San Antonio, TX, June 5-9 2005.

(38) Mitchell, D. W.; Smith, R. D. *Physical Review. E. Statistical Physics, Plasmas, Fluids, and Related Interdisciplinary Topics* **1995**, *52*, 4366-4386.

(39) Zubarev, R. A.; Kelleher, N. L.; McLafferty, F. W. *Journal of the American Chemical Society* **1998**, *120*, 3265-3266.

(40) Hendrickson, C. L.; Hadjarab, F.; Laude, D. A., Jr. *International Journal of Mass Spectrometry and Ion Processes* **1995**, *141*, 161-170.

(41) Beiersdorfer, P.; Becker, S.; Beck, B.; Elliott, S.; Widmann, K.; Schweikhard, L. *Nuclear Instruments & Methods in Physics Research, Section B: Beam Interactions with Materials and Atoms* **1995**, *98*, 558-561.

(42) Caravatti, P.; Allemann, M. *Organic Mass Spectrometry* **1991**, *26*, 514-518.

(43) Tsybin, Y. O.; Witt, M.; Baykut, G.; Kjeldsen, F.; Hakansson, P. *Rapid Communications in Mass Spectrometry* **2003**, *17*, 1759-1768.

(44) Zubarev, R. A. *Mass Spectrometry Reviews* **2003**, *22*, 57-77.

(45) Sze, S. K.; Ge, Y.; Oh, H.; McLafferty, F. W. *Proc Natl Acad Sci U S A* **2002**, *99*, 1774-1779.

(46) Anderson, G. A., Bruce J.E., Smith R.D., 2.18 ed.: Richland, WA, 1996.

(47) Guan, S.; Wahl, M. C.; Wood, T. D.; Marshall, A. G. *Anal Chem* **1993**, *65*, 1753-1757.

(48) Solouki, T.; Gillig, K. J.; Russell, D. H. *Analytical Chemistry* **1994**, *66*, 1583-1587.

(49) Kingdon, K. H. *Physical Review* **1923**, *21*, 408-418.

(50) Gillig, K. J.; Bluhm, B. K.; Russell, D. H. *International Journal of Mass Spectrometry and Ion Processes* **1996**, *157/158*, 129-147.

Figure 1

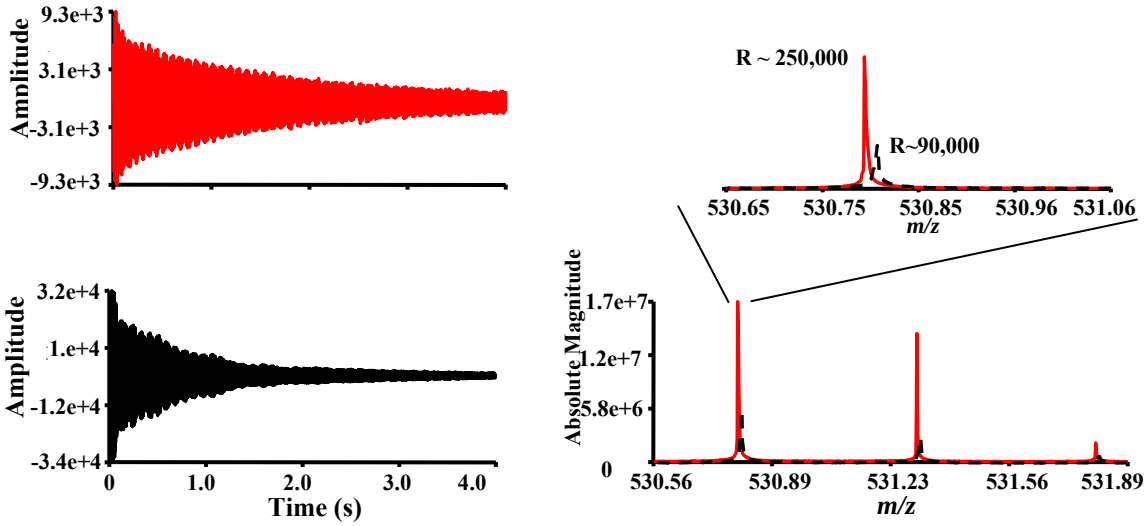

Figure 1. Our initial observation of EPIC is shown with successive time-domain signals of bradykinin $(M+2H)^{2+}$. a) with no modification to the detection scheme. b) EPIC time-domain signal. The EPIC results extend well past the collected 4 seconds. The resultant mass spectra obtained from the time-domain signal are also shown.

Figure 2

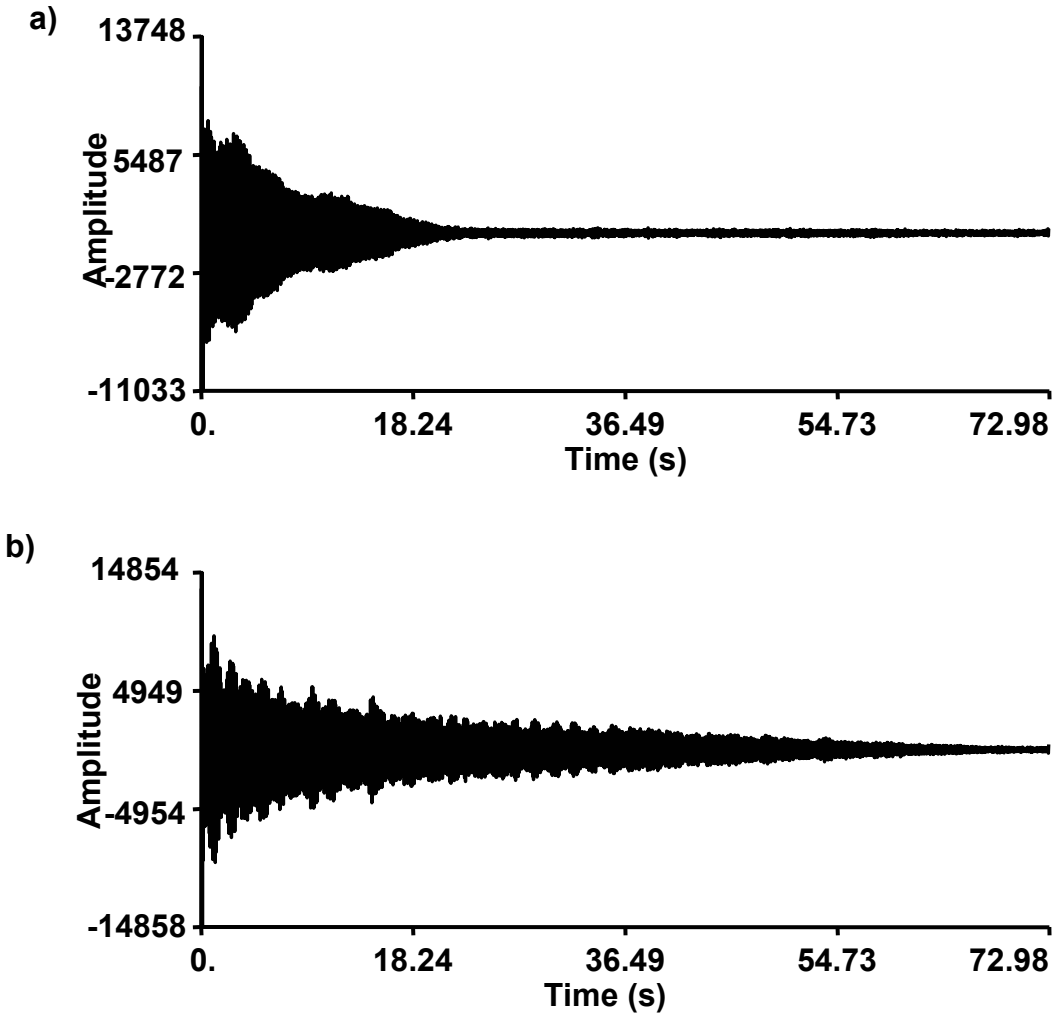

Figure 2. Successive time-domain signals for the ubiquitin $(M+7H)^{7+}$ a) with the no modification to the detection scheme there is signal duration for approximately 25 seconds. b) With the EPIC experiment there is signal duration for over 70 seconds. There is approximately a factor of 3 improvement with the application of EPIC

Figure 3

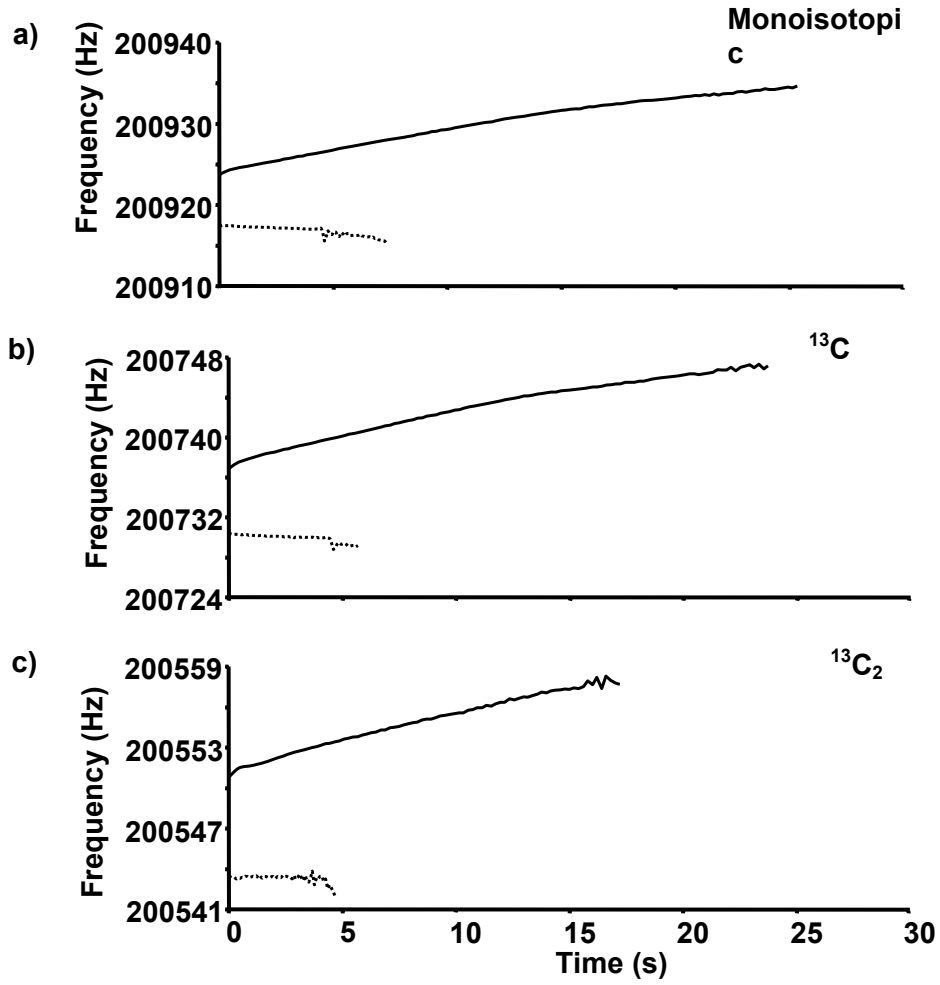

Figure 3. Bradykinin $(M+2H)^{2+}$ was used to show that the frequency shift in time changes direction with the application of EPIC. The non-modified detection technique (dotted line) slopes to a lower frequency with time, while the EPIC produced signal (solid line) shifts to a higher frequency with time. a) the frequency change for the monoisotopic ***m/z*** species. b) the frequency shift for the $^{13}C_1$ isotope peak. c) the frequency shift for the $^{13}C_2$ isotope peak. The higher magnitude peaks are detected for a longer period of time, when comparing the monoisotopic peak in part a to the $^{13}C_2$ isotope peak in part c.

Figure 4

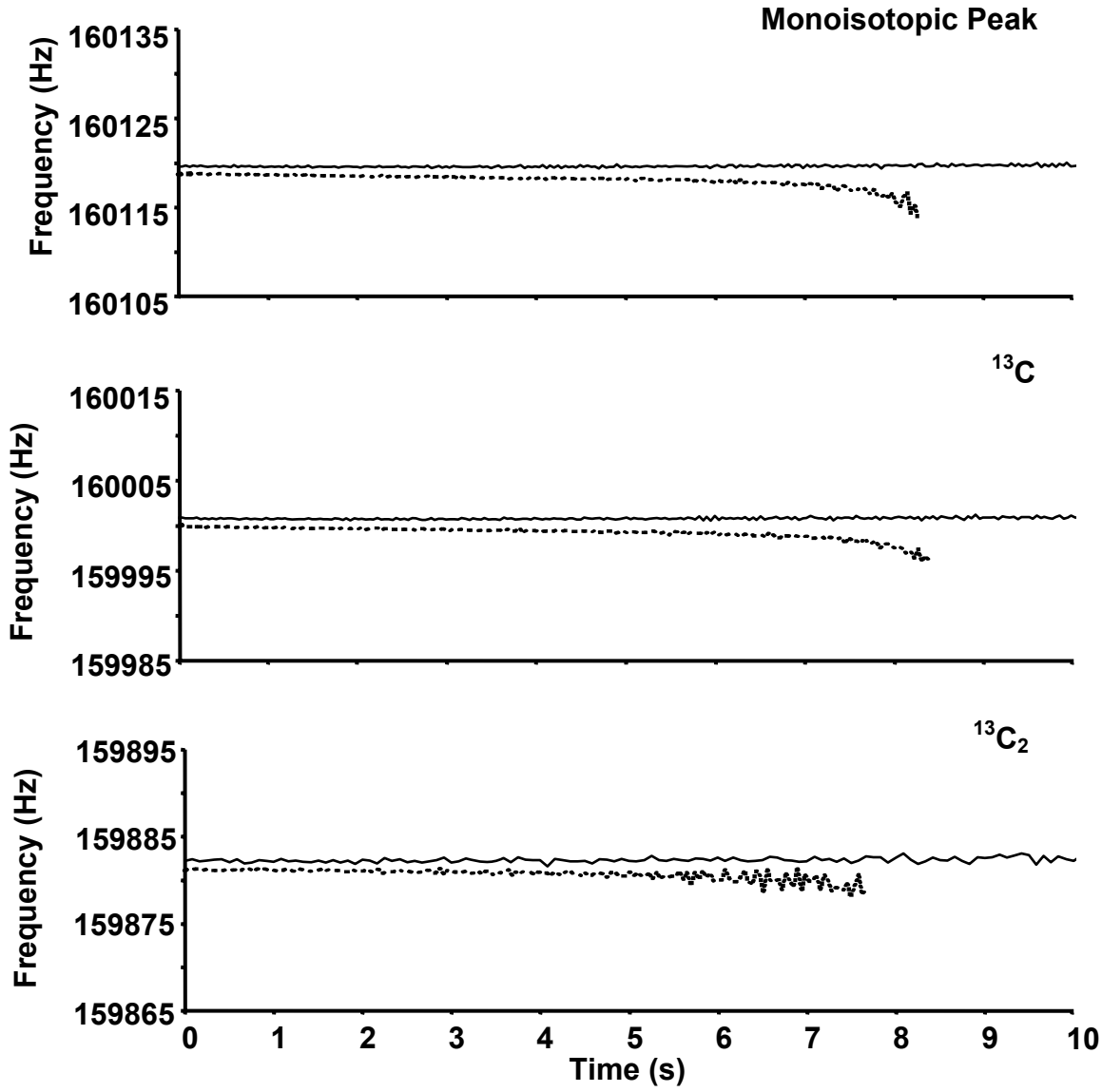

Figure 4. Plots the shift in frequency for the different isotope peaks for substance P $(M+2H)^{2+}$. The solid line is the result of the EPIC experiment. The dotted line is the non-EPIC result. The EPIC results produce less drift in frequency and yield a higher resolution mass spectrum.

Figure 5

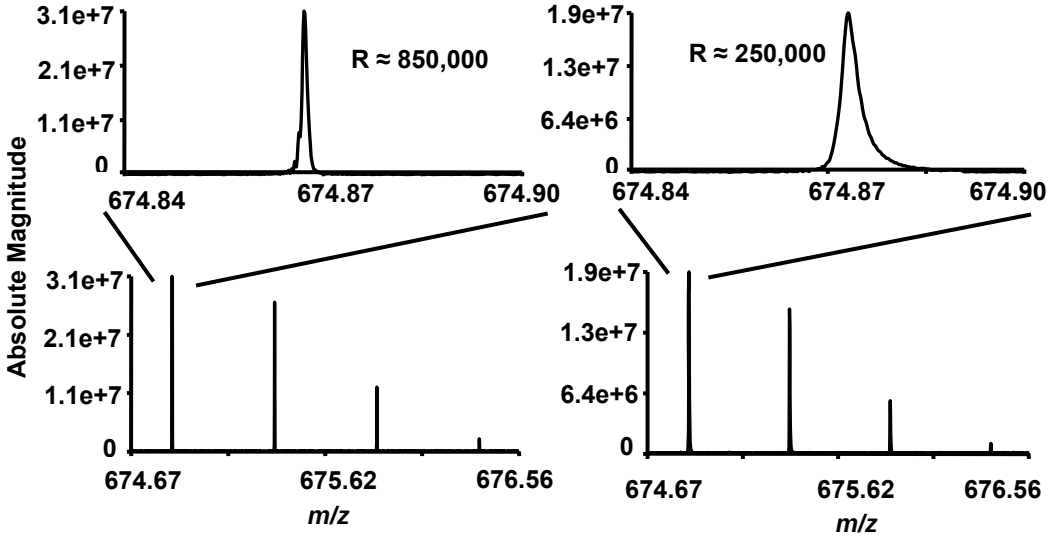

Figure 5. Mass spectrum of the substance P $(M+2H)^{2+}$ without EPIC (right) and with EPIC (left). The inset spectra illustrate the observed monoisotopic peak and demonstrate a factor of 3 improvement in resolving power with the application of EPIC.

Figure 6

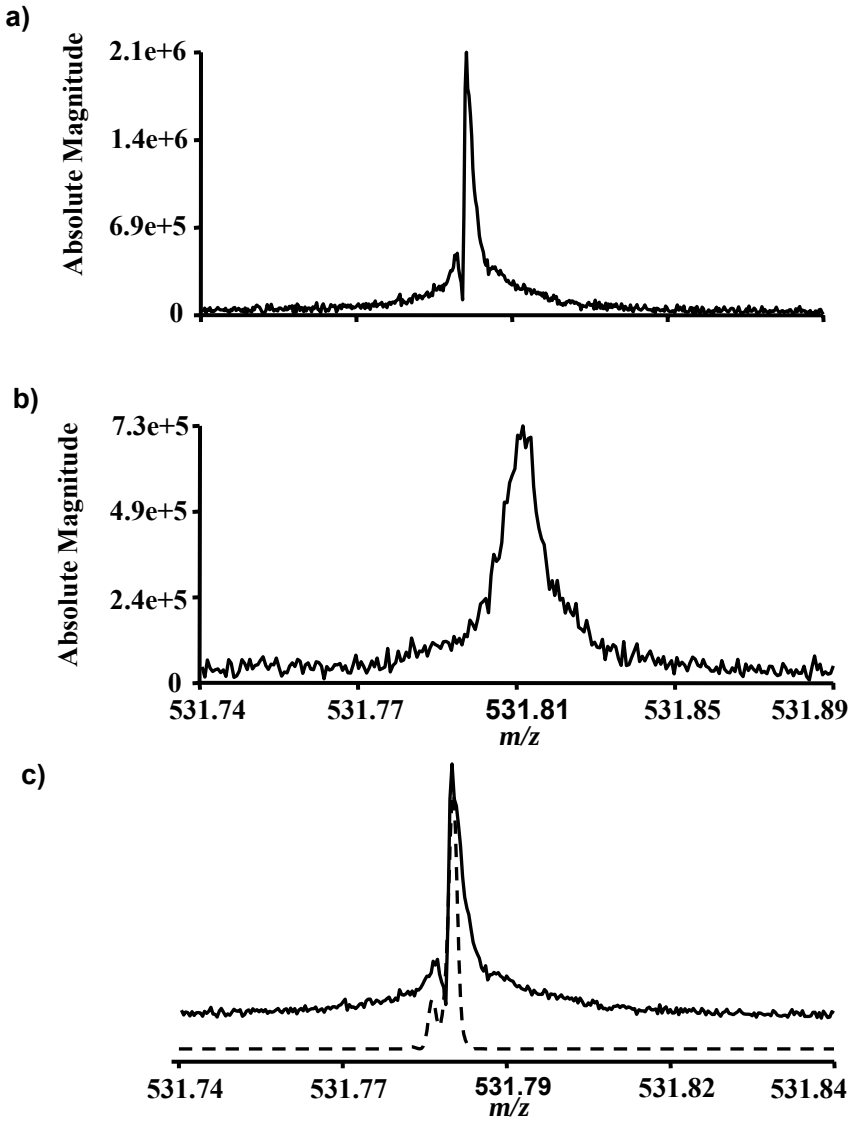

Figure 6. Mass spectra of the M+2 isotope peak of Bradykinin $(M+2H)^{2+}$ ions. a) EPIC mass spectrum. The split in the peak results from the mass difference of ^{15}N and ^{13}C. b) Mass spectrum from non-EPIC experiment. Here no fine structure is observed. c) An overlay of the EPIC data (top-solid line) and the theoretical fine structure (bottom-dotted line).

Figure 7

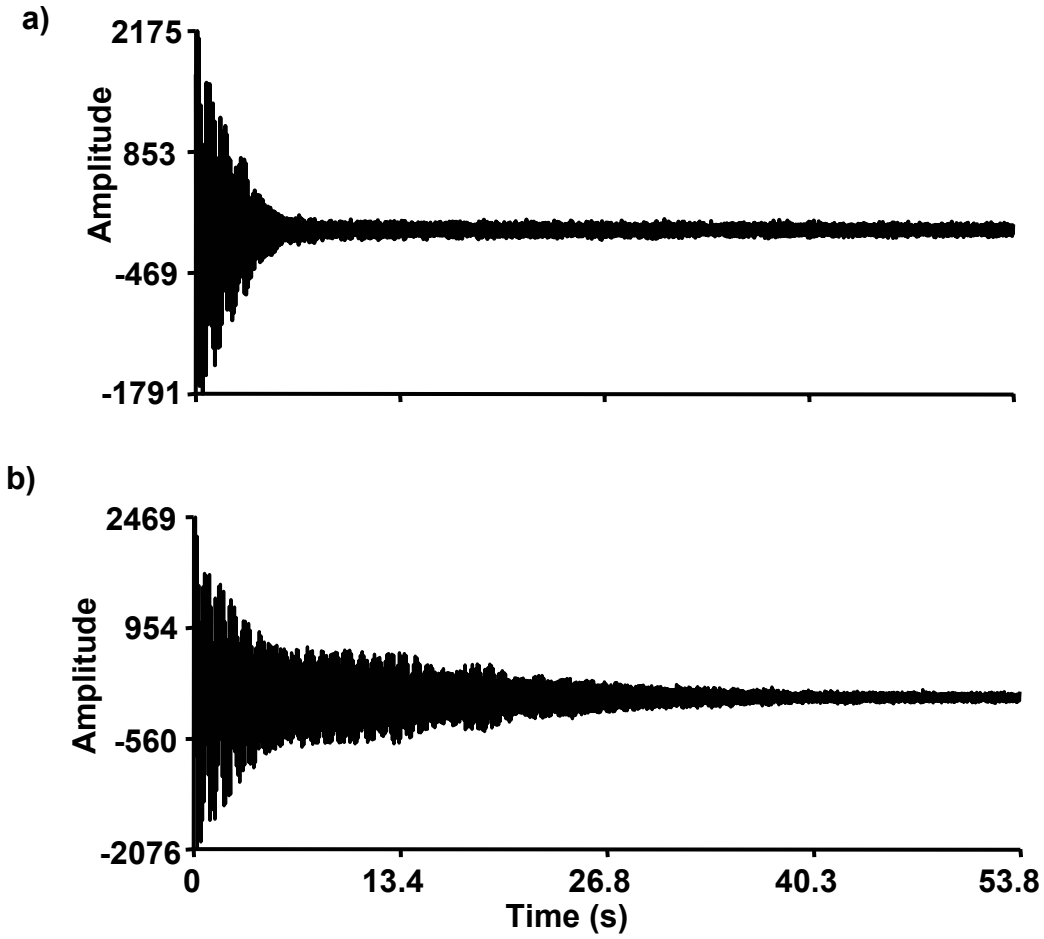

Figure 7. Successive time-domain signals for ubiquitin $(M+6H)^{6+}$. a) Time-domain signal for the non-modified detection technique. b) EPIC-produced time-domain signal. The length of the detected ion signal increased by an approximate factor of 5 with the application of EPIC.

Figure 8

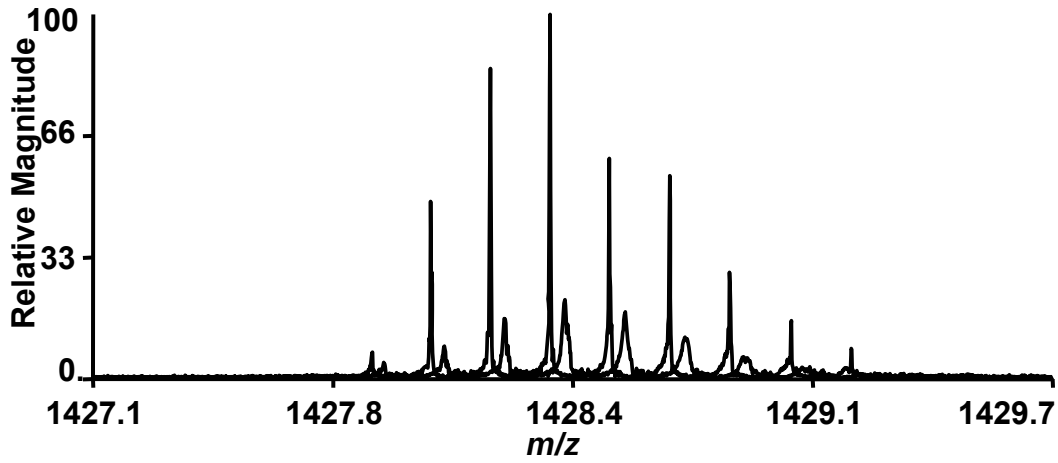

Figure 8. The mass spectra from the time-domain signals from Figures 7a and 7b. The two spectra are overlaid to show the increased resolution and sensitivity with the EPIC results.

Figure 9

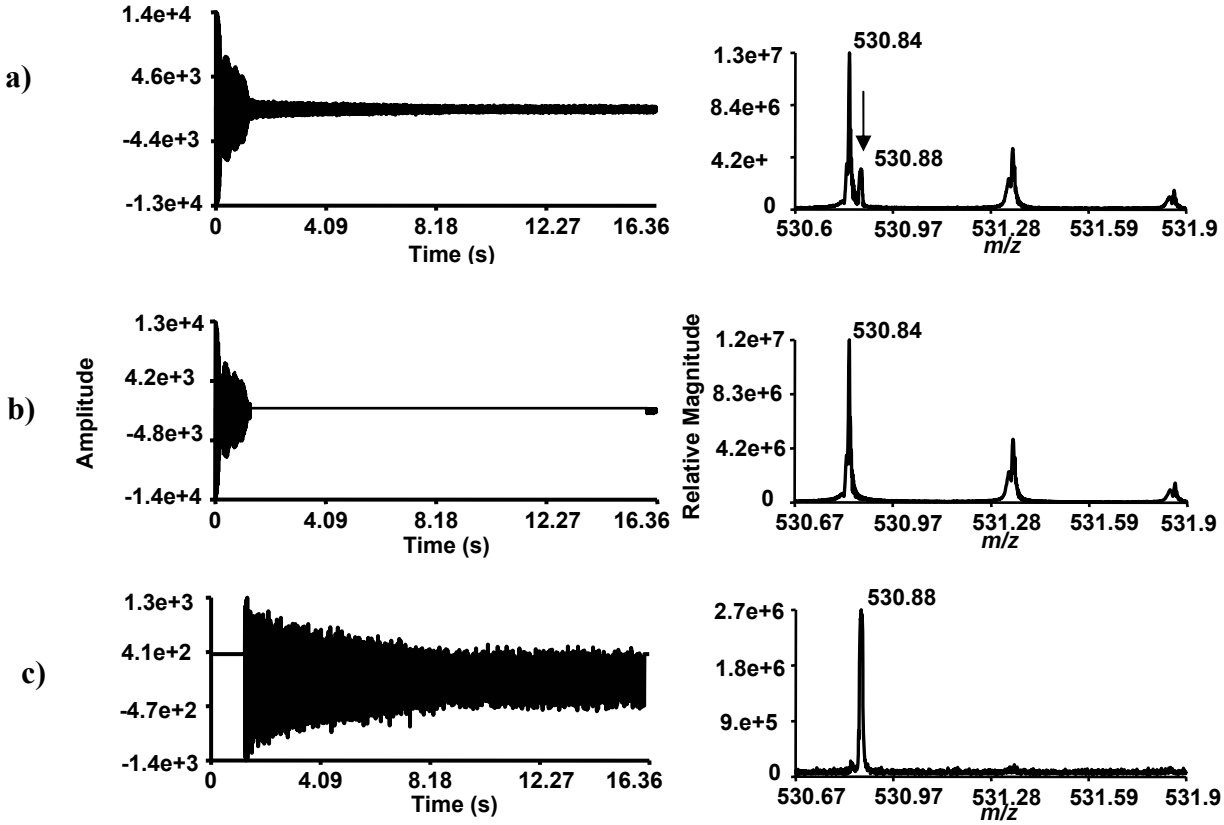

Figure 9. Peak coalescence a) The full time-domain signal and the resultant mass spectrum of bradykinin $(M+2H)^{2+}$. The small peak to the right of the monoisotopic peak is the coalesced signal (marked by an arrow). b) The first part of the time-domain signal is conserved and all other data points are set to zero. The Fourier transform of the truncated time-domain signal yields a mass spectrum with an isotopic distribution of bradykinin 2^{+} as would be expected. c) The second part of the time-domain signal is conserved, while all data points in the first part are set to zero. The resultant mass spectrum yields a single peak which is caused from the coalescence of the different isotope peaks of bradykinin 2^{+}.

Figure 10

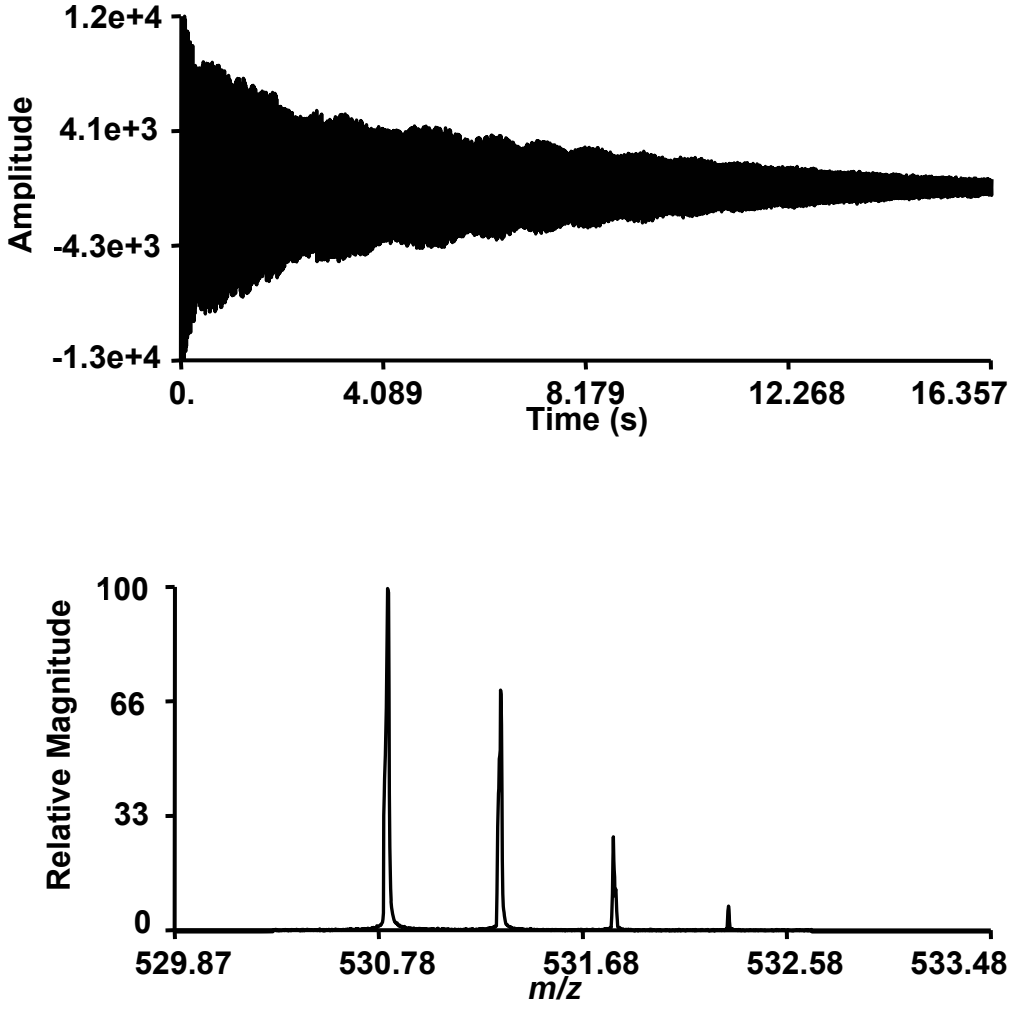

Figure 10. The time-domain signal and the resultant mass spectrum after application of EPIC under the same conditions that yielded peak coalescence shown in figure 9. With EPIC, peak coalescence is eliminated.

CHAPTER 4

Reduction of Ion Magnetron Motion and Space Charge Using Radial Electric Field Modulation

Abstract

Ions of the same *m*/*z* must remain in phase with each other during the detection time period used for FTICR-MS signal acquisition for optimal performance. The loss of coherence of the ion cloud during detection leads to faster rates of signal decay which results in a decrease in the achievable resolution and mass measurement accuracy with FTICR-MS technology. As the ions spin on their excited cyclotron orbit, many factors contribute to de-phasing of ion motion; such as the presence of radial electric fields and the Coulombic interaction of ion clouds of different mass-to-charge ratios. With the application of Electron Promoted Ion Coherence or EPIC, signal duration can be increased. Since FTICR-MS achieves high performance through measurement of frequency, the ability to observe ions over a longer time period increases the performance of FTICR-MS. Radial electric fields are an unavoidable consequence of applied trapping potentials to confine ion motion parallel to the magnetic field in the ICR cell; however, the presence of radial electric fields also induces magnetron motion. With EPIC it is possible to control the shape of the radial electric fields that the ions experience by changing the number of electrons that are sent through the center of the ICR cell. Furthermore, the electric field shape produced with EPIC can be altered to decrease space

charge contributions by increasing the length of the ion oscillation path along the axis of the ICR cell and decrease radial electric fields effects, which alter detected ion frequencies. Here we report theoretical and experimental results to evaluate and describe the impact of EPIC on the performance of FTICR-MS.

Introduction

Fourier transform ion cyclotron resonance mass spectrometry FTICR-MS [1] has become an important analytical tool, especially in the analysis of complex mixtures. The capability to provide high resolution, mass measurement accuracy, and sensitivity is important in the area of proteomics [2]. The basis for which FTICR mass spectrometers can offer such high performance is their ability to detect ions for an extended period of time. The mass-to-charge ratio (*m*/*z)* of an ion is determined by measuring the frequency of its excited cyclotron motion in the ICR cell. The longer that the frequency is detected the more accurately the frequency can be determined and the higher the performance of the instrument. The ions are trapped in the detection cell by the Lorentz force (*x*-*y* dimension) and by an electric potential applied to trapping electrodes (*z* dimension). The application of an electrostatic field retains ions in the homogenous region of the magnetic field. However, this electrostatic field also induces magnetron motion and lead to deviations in the observed cyclotron frequency. Magnetron motion changes the observed ion frequency, limits the critical mass that can be stored [3], and causes ion loss and reduced sensitivity. Ideally, the application of trapping potentials will create a three

dimensional axial quadrupolar electrostatic potential, which will result in ion frequency being independent of ion position inside the ICR cell [4].

The stability of an excited ion cloud is critical for detection of image current for an extended period of time [5]. There are many factors which contribute to ion cloud coherence such ion cloud density [6] and applied trapping potentials [7]. Control of the total ion population trapped in the ICR cell is very critical for the performance of the instrument [8, 9]. A trapped population with too few ions leads to a reduction in the signal-to-noise ratio and less stable ion clouds. However, if too many ions are trapped the Coulombic interaction of ion clouds with different mass-to-charge ratios disrupts ion cloud stability, causes ion cloud coalescence for closely spaced m/z species [10], and induce space charge effects. An increase in space charge conditions effectively reduces the observed cyclotron frequency. Due to the presence of quadrupolar trapping fields parallel to the magnetic field, the space charge in the ICR cell is not constant throughout an experiment and results in observed frequency shifts with time [11, 12]. Ions which are excited to a large cyclotron orbit can travel a longer distance in the z-dimension than if they were located close to the central axis of the cell. As ions traverse their excited cyclotron orbit, they encounter collisions with residual gas molecules, and damp back toward the center of the ICR cell (collisional damping). This causes the ion cyclotron radius to decrease and the ions are funneled back toward the central axis of the ICR cell, where the ions also have a shorter path length in the z-dimension. Furthermore, the radial spatial distribution of the ions is decreased with decreased cyclotron radius. The increase in space charge causes the observed cyclotron frequency to shift to lower frequency with

time as the ions damp back toward the center of the ICR cell, which causes the *m*/*z* value of the ions to increase to a larger value with time [12].

There has been considerable attention devoted to ICR cell design to improve the performance of FTICR mass spectrometers [13-16]. There are three different types of electrical field shapes that are critical for optimal ICR analysis, including uniform RF electric field for excitation, azimuthal quadrupolar RF electric field for ion axialization, and three-dimensional axial quadrupolar electric field for ion axial confinement [17]. There is usually a compromise between these different electrical field shapes for most ICR cell designs. Solouki et al. [18] suspended a copper wire through the center of the ICR to form electric field potentials that simulate a Kingdon trap [19] which was later described by Gillig et al. [20]. Electrons sent through the center of the ICR cell have previously been used for electron impact ionization, to trap ions in the cell [21] and to perform electron capture dissociation (ECD) [22, 23]. The application of an electron beam through the center of the ICR cell during detection has brought interesting results. Easterling and Amster [24] reported that with the presence of a low energy electron beam during detection the transient signals lasted much longer. However, they also reported a current dependent mass shift which in extreme cases approached 10-12 *m*/*z* units. An earlier paper from our group demonstrated that proper tuning of a low energy electron beam, which we call Electron Promoted Ion Coherence or EPIC [25], not only enhanced the time of signal duration but could eliminate frequency shifts and allow acquisition of higher quality spectra. Nikolaev et al. has produced the most accurate computer simulations of ICR motion to date [26], has modeled the effect of an electron beam

through the center of the ICR cell, and has shown an increase in ICR signal duration is possible with this configuration [27].

This paper aims to further describe the unique characteristics of EPIC and the basis for an improvement in instrument performance. Here we report that EPIC is a method capable of reducing both conditions. We present a comparison between theoretical predictions and experimental results of how EPIC affects the electric field shape in the ICR cell. We investigate how the numbers of electrons affect the trapping electric field shape. We also determine how perturbations in the trapping fields affect the mass measurement accuracy.

Experimental

Electrospray was used as the ionization method. Electrospray solutions consisted of 49/49/2 by volume of water/methanol/acetic acid. All samples (substance p, bradykinin, melittin, and BSA digest) of 10uM were infused by direct injection with a syringe pump at a rate of 0.4 uL/min. All standard proteins and peptides were purchased from Sigma (St. Louis, MO) and used without further purification. Sequencing grade modified trypsin was purchased from Promega (Madison, WI). A Bruker Daltonics 7T Apex-Q FTICR mass spectrometer (Billerica, MA) was used to acquire the mass spectral data using Xmass version 7.0.6 as the data acquisition software program. Ion accumulation took place in the hexapole ion guide that is external to the magnetic field prior to injection into the ICR cell. Typically the ion accumulation time was set between 0.5–1.0 s, but was held constant for all EPIC and non-EPIC comparison spectra. Ions

were trapped in an infinity cell [28] using the sidekick technique [29]. The conventional detection technique was modified to perform EPIC experiments. After the ions had been excited to a large cyclotron orbit using a broadband frequency sweep excitation waveform, the electron beam was initiated allowing electrons to traverse the cell. The electron beam was produced with a hollow heated cathode, 3.5 mm I.D, 7.6 mm O.D. The outer diameter of the electron beam entering the ICR cell was determined by a lens which has an I.D. of 6 mm placed between the heated cathode and the back trap plate. The cathode was heated with approximately 1.50 A, the lens was held at ground, and a voltage bias of 0.0 to -1.5 V was placed on the heated cathode to produce an electron beam through the central axis of the ICR cell. At all other times when the cathode was heated there was an applied voltage bias of +10 V. The numbers of electrons that are emitted is determined by the heating current and the applied bias potential. The number of electrons entering the ICR cell is controlled by changing the bias potential since a change in the heating current takes a much longer time to stabilize.

ICR signal was analyzed with ICR-2LS [30]. The time-dependence of the detected frequency was obtained with the sweep [11] module within ICR-2LS, which Fourier transforms consecutive segments of the transient signals. Each segment of the transient signal was Welch apodized, zero-filled 3 times, and Fourier transformed to obtain a frequency-domain spectrum and allow determination of ion frequency at various points along the transient signal. The number of data points in each segment of the recorded time-domain signal was dependent upon the total data set size; typically parameters for a 128k data set consisted of a segment size of 16,384 points with an advancement of 8,192 points.

The resolution and mass accuracy for the broadband experiments were limited by the size of the data sets that could be recorded with the conventional Bruker hardware and software. For extended broadband signal acquisition experiments, the broadband spectra of BSA digest were digitized with a PCI-6111 National Instruments board (Austin, TX) and recorded on PC with 512 MB of RAM. The data sets collected were 4 MB at a sample rate of 600,000 Hz. BSA digest spectra were collected after a pulsed gas event to cool the ions followed by a 7 second delay to allow time for the cooling gas to be pumped away.

Simion 7.0 software (SIMION 7.0 3D, version 7.0, D.A. Dahl, Idaho National Engineering Laboratory, Idaho Falls, ID) was used to produce the equipotential field lines, to provide an approximation of the shape of the electric field and the effects of an electron beam through the center of the ICR cell. Electron current was measured on the lens with a current amplifier (Keithley, model 428, Cleveland, OH), with the cathode heated with 1.5 A and various applied voltages.

Results and Discussion

The unperturbed cyclotron frequency is dependent only on the m/z of the ion and the strength of the magnetic field. However, the application of trapping potentials to trap ions in the z-axis induces deviations in the observed cyclotron frequency. The magnitude of these deviations depends on the magnitude of the applied trapping potential. The application of an electron beam through the center of the ICR cell during detection has been shown to increase the resolution and the signal-to-noise ratio of FTICR-MS [25].

However, if experimental conditions such as total ion abundance, trap plate potentials, and number of electrons are not carefully controlled, an increase in performance is not observed and can result in large observed frequency shifts. The presence of an electron beam through the center of the ICR cell results in a negative charge along the central axis. This negative charge dramatically alters the shape of the electric field used to confine the ions to a finite space, thus altering the space charge conditions within the cell. Therefore, changes in the measured frequency should be expected. The electric field lines produced with a closed cylindrical cell are shown in **Figure 1a**. The segmented trapping electrodes in the Infinity cell are used to flatten out the excite potential across the entire cell. Each trapping electrode has the same applied trapping potential with varying RF amplitude applied during the excite. Thus, the shape of the electric field lines produced from the segmented trapping electrodes will be very similar to those generated with a solid trapping electrode. The exact modeling of an electron beam and the affect it will have on the shape of the electric field is not easily solved. However, the presence of electrons will produce a negative potential along the axis of cell. For simplification of modeling efforts, a solid electrode that was biased at a negative potential was used to represent the electron beam. Therefore, the electrode represents a first approximation of the negative potential produced by the electrons and the resulting change in field shape, which is shown in **Figure 1b**. The electrons produced in the magnetic field will follow the magnetic field lines, thus electrons created on the axis of the ICR cell will remain in a beam on axis through the cell. Any electrons that do scatter in the cell will hit the positive trapping electrodes, thus the negative charge will be kept localized along the *z*-axis of the cell. For the ICR cell with an electron beam through the center, the

equipotential contour lines for a given potential do not penetrate as far into the middle of the cell as the unmodified cell (cell with no electron beam). Therefore, ions with the same cyclotron radius and z-axis kinetic energy should exhibit a larger range of *z*-axis motion. **Figure 1c** shows how the electric field lines are affected by an increase in the number of electrons through the center of the ICR cell. As the potential applied to the central electrode becomes more negative, the electric field lines become closer to the trap plates and the inflection point (point at which radial electric field changes from inward- to outward-directed) is located further from the central axis.

With no electron beam, the electric fields in the cylindrical cell should approximate a three dimensional axial quadrupolar electrostatic potential. This is important since in this case, cyclotron frequency is independent of cyclotron radius. However, **Figure 2a** illustrates the measured cyclotron frequency at different applied excitation voltages and shows that there is a very strong dependence of observed frequency with cyclotron radius. At higher excitation voltage and larger cyclotron radius, the observed change in frequency can be attributed to alterations in space charge effects at different excited cyclotron radii. Cyclotron radius can affect space charge conditions in two different ways. First, since the trapping potentials approximate a quadrupolar electric field, the *z*-axis oscillation path length decreases as the cyclotron radius gets smaller. Therefore, at smaller cyclotron radii the ions are confined closer axially. Second, at large cyclotron radii, ions with different mass-to-charge ratios will have a greater spatial distribution in the plane perpendicular to the magnetic field. These two effects are detrimental to high performance measurements which require long acquisition time periods, since the measured frequency will change with time. As the ions damp

back toward the center of the ICR cell (i.e., exhibit smaller cyclotron radii) the ions become confined to a smaller space increasing the ion density, and thus space charge conditions. This time-based frequency shift behavior may not be observed in all ICR applications, because either the acquisition time period is not long enough or the ions do not stay in a cohesive cloud for a sufficient period of time.

The simulated shape of the electric field lines within the ICR cell with EPIC will no longer form a three dimensional quadrupolar potential. Therefore, the magnetron frequency of an ion is no longer independent of its radial position in the ICR cell. The observed cyclotron frequency will be dependent upon the radial force exerted by the electric field and thus, the cyclotron radius that the ions exhibit as well as any changes in space charge conditions. This is demonstrated in **Figure 2a** which illustrates the observed cyclotron frequency of melittin $(M+4H)^{+4}$ at different RF excitation voltages with different cathode bias potentials. The observed cyclotron frequencies for different excitation voltages converge at larger cyclotron radii. This indicates that at larger cyclotron radii, the effect from the electron beam is diminished under the beam conditions used for these experiments. However as the initial cyclotron radius decreases, the ions become closer to the electron beam and the observed differences in cyclotron frequencies increase. This observation can be explained by the electric field shapes in Figure 1. At greater distances from the central axis, the deviation between the equipotential contour lines in **Figure 1a** and **b** are small and the observed frequencies should be similar. As the distance from the central axis becomes smaller there is a larger deviation in contour lines, which should result in larger differences in observed cyclotron frequencies, and is in agreement with experimentally observed results.

Figure 2b illustrates the measured cyclotron frequency for different numbers of trapped ions in the cell for the same experimental conditions as in **Figure 2a** with no electron beam. This is done to extrapolate the cyclotron frequency that would be observed with no space charge effects. This was determined to be ~151,659 Hz. Any change in the observed cyclotron frequency would then be attributed to a change in the magnetron frequency as shown in equation 1 were ω_c is the unperturbed cyclotron frequency, ω_+ is the reduced cyclotron frequency, and ω_- is the magnetron frequency.

$$(1) \quad \omega_+ = \omega_c - \omega_-.$$

The magnetron frequency is negative in magnitude because the outward direction of the radial fields opposes the force induced by the magnetic field, resulting in a decrease in the observed cyclotron frequency. The space charge-induced frequency shift can be accounted for by introducing an addition term to equation 1. McIver el al. [31] developed the following equation to account for space charge effect:

$$(2) \quad \omega_{obs} = \frac{qB}{m} - \frac{2aV}{a^2 B} - \frac{q\rho G_i}{\varepsilon_o B}$$

The first term in the equation describes the unperturbed cyclotron frequency, the second term describes the magnetron frequency in a perfectly quadrupolar static trapping field. While the third term represents the space charge component of the observed frequency, where q is the elementary charge, ρ the ion density, G_i the ion cloud geometry, and ε_o the permittivity of free space.

The numbers of electrons that are in the center of the ICR cell are controlled by the bias applied to the heated cathode. The more negative the bias potential the greater the electron current and the larger the negative potential through the center of the ICR cell. Increasing the bias potential will affect the electric field lines **similar to what is**

shown in Figure 1c. In **Figure 2a,** the plot of the data acquired with a cathode bias potential of -0.55 and -0.60 V shows there is an increase in frequency at low excitation voltage, but at higher excitation voltages the frequencies remain constant over a range of excited cyclotron radii. The change in spatial ion distribution perpendicular to the magnetic field is dependent only upon the excitation voltage; therefore, ions should have the same spatial distribution regardless of applied cathode bias. This would lead to an increase in space charge at smaller cyclotron radii which should result in a reduction in observed frequency. However, the reduction in the outward-directed radial field encountered when the electron beam is present in the cell leads to an increase in observed frequency. The two contributions offset each other and result in a frequency that appears more constant at various cyclotron radii. At smaller cyclotron radii the observed frequency increases indicating a larger shift in the magnetron frequency.

The ions excited and detected with the applied cathode bias potential <-0.45 exhibit an increase in frequency for all applied excite potentials, relative to non-EPIC measurements. This is likely because the ions are not excited beyond the inflection point in the equipotential contour lines shown in the SIMION calculations shown in **Figure 1b and 1c**. As the cathode bias potential increases, there is an increase in observed cyclotron frequency for a given excite potential. As the number of electrons increase, the electric field lines are pulled closer to the trap plate which expands the ion pathlength along the *z*-axis of the ICR cell and decreases the space charge conditions. Therefore, the same ion at a given excite potential within the same ion population will have a different measured cyclotron frequency at different cathode bias potential. As seen in Figure 1c

this change will be more dramatic at lower excite potentials which is also observed experimentally.

In the example shown in **Figure 1b** the electric field lines become flat at about half the cell radius, which may not be exact for the applied electron beam. However, with a negative potential through the center of the cell, the positive electric field lines will be drawn toward the center of the trapping electrode resulting in an inflection in the electric field shape. At this inflection point there is no outward-directed radial force to drive magnetron motion. At smaller radii the ion would be located on the interior of the inflection point and there would be an inward-directed radial force. The greater the number of electrons, the greater the negative potential through the center of the cell, and the further from the central axis the inflection point becomes. In comparing -0.55 and -0.60 V bias data in **Figure 2a**, both curves reach a minimum frequency as cyclotron radius is increased; however, -0.60 V bias curve reaches a minimum frequency at a larger cyclotron radius, since its expected inflection point is further from the central axis of the cell, as is shown in **Figure 1c**. The observed minimum frequency is slightly greater at -0.60 V than the minimum observed frequency for the -0.55 V bias likely due to differences in space charge conditions. There will be a greater axial distribution of the ions at larger bias potentials and greater spatial distribution at larger cyclotron radii. It should be noted that the observed frequencies at a bias potential of -0.50 V should not remain constant over a range of excite potentials because the change in spatial distribution of the ions at different excite amplitudes will alter the space charge conditions.

There are a number of advantages to exciting ions to larger cyclotron radii; there is less space charge contribution, the ions are closer to the detection plates resulting in increased signal. **Figure 2c** shows the time-domain signals acquired with the same excitation voltage at different cathode bias potentials. Without any applied bias potential the signal damps quickly and as the cathode bias potential increases the time-domain signal improves. This results in a 1.6-fold increase in the signal-to-noise ratio following comparison of spectra acquired with no electron beam to those acquired with a cathode bias of -0.60 V. For this example, the improvement in signal-to-noise ratio was limited by the size of the data set acquired, since the signal amplitude is dependent upon the magnitude of the image current and how long it is detected. However, if the post-excitation radius of the ions exceeds ~70% of the cell radius, image current interactions increase and result in a decrease in mass measurement accuracy and detected ion abundances [32-34]. The post-excitation voltage can be approximated by equation 3:

$$r_{excite} = \frac{V_{p-p}\beta_{dip}\sqrt{\frac{1}{sweep\ rate}}}{2dB_0} \qquad (3)$$

where r_{excite} is the post-excitation radius (m), $V_{p\text{-}p}$ is the amplitude of the RF voltage, β_{dip} is the dipolar constant (0.9 for Infinity Cell), the sweep rate was 3.48×10^8 Hz/s, B_0 is the magnetic field strength (7T), and d is the ICR cell diameter (m). Therefore, RF excite voltage of 300 V corresponds to ~57% of the cell radius. However, it should be noted that since the ions are trapped using the sidekick method, the ions are not located directly on axis of the ICR cell at the beginning of the excite. Therefore, the exact post-excitation radius is not known, although 50-60% of the cell radius is a reasonable approximation.

With the application of EPIC, the radial field can be made flatter at larger radii. Radial electric fields are plotted in **Figure 3** at different ICR cell radii with and without the electron beam. The radial electric fields for a closed cylindrical ICR cell were calculated with SIMION 7.0. The radial electric fields induce magnetron motion. The negative values have an outward-directed value from the central axis of the ICR cell, while the positive values have an inward directing value. Figure 3 shows that magnetron motion should not be constant as an ion oscillates along the z-axis. Generally, the larger the cyclotron radius that an ion exhibits, the larger the deviation in the radial field the ion will experience as the ions oscillate over the same distance along the z-axis. These deviations in radial electric field produce deviations in magnetron motion and may lead to de-phasing of the ion cloud. This is especially true of ion populations with a wide distribution of z-axis kinetic energies. With the application of the electron beam, it is possible to flatten out the radial field over a set radius, as is shown in the SIMION results. Therefore, as the ion oscillates along the z-axis the magnitude of the radial field remains constant.

As the ions spin on their excited cyclotron orbits they encounter collisions with residual neutral molecules in the cell. These collisions cause the cyclotron orbit to decrease with time. Since the frequency of the ion is dependent upon its radial location in the ICR cell, as the ion damps back toward the center of the ICR cell it should experience a shift in frequency. This frequency shift is based on continually decreasing radius with time and should follow the same trend in frequency change as if the ions were excited to different cyclotron radii as shown in Figure 2a. **Figure 4** illustrates the frequency of bradykinin $(M+2H)^{2+}$ over time for different excitation voltages with the

same voltage bias applied to the cathode. At larger excitation voltages there is an initial decrease in frequency with time indicting that the ions are being excited beyond the inflection point and there is an outward directed radial force (similar to as if no electron beam had been applied). With time, the ions cyclotron radii decrease and they begin to experience change in their magnetron motion at which point the observed cyclotron frequency levels off. As the ions continues to encounter collisions they may pass through the inflection point at which point they begin to feel an inward directing force from the radial fields, where the magnetron motion reverses direction and the observed frequency increases. The frequencies level out at an earlier time point in the detected signals as the excitation voltage decreases, indicating that their initial excited cyclotron radii are closer to the inflection point.

To further demonstrate the how the radial fields are affected by the application of EPIC, the frequency of bradykinin $(M+2H)^{+2}$ is monitored over the acquisition time period at different bias potentials to the cathode with the same excitation voltage. The results are shown in **Figure 5**. The bias potential applied to the cathode controls the number of electrons that are sent through the center of the ICR cell, and thus the negative charge. This shows the typical effect that the electron beam has on the observed frequency over time. With insufficient electron density at the center of the cell, the frequency will decrease with time in the same manner as if no electron beam was applied. This results from the inflection point in the radial fields being too close to the central axis. If there are too many electrons the frequency increases with time, as the ions are located at a radius which has inward directing radial fields. An important point to note is the general trend that occurs in **Figure 5**; the time point at which the observed cyclotron

frequency reaches a minimum occurs at an earlier time point with increasing voltage bias. By observing the change in frequency of the ions resultant from the direction and magnitude of the radial force acting on the ions, we can observe the rate the ions are damping back toward the center of the cell. Ideally, the electric fields would be modified to obtain long time-domain signals at larger cyclotron radius where space charge effects are minimal. This can be done by changing the number of electrons and thus, the inversion point of the radial fields and by changing the excitation voltage.

High mass measurement accuracy is a prime attribute of ICR mass spectrometers [35]. The ability to obtain accurate mass measurements is dependent on the ability to detect stable image current for an extended period of time. If the detected frequency is changing with time, it will lead to peak broadening and decrease sensitivity, resolution, and mass measurement accuracy. With the observed frequency shifts that occur with the application of EPIC, we attempted to determine if the mass measurement accuracy is affected by alterations to the radial trapping fields. The mass accuracy was tested with BSA digest peptides which would provide a wide m/z range of ions to help determine if there was an m/z dependence on observed frequency shift. Since the spectra collected in broadband were limited by the dataset size available in the conventional Bruker data acquisition hardware, the time-domain signal was simultaneously collected and digitized on a separate computer during signal acquisition. This allowed us to collect much larger datasets to determine if the frequencies of different peptides would change at different rates, thus limiting the improvement of mass measurement accuracy with EPIC. The time-domain signals were truncated at time points of 0.25, 0.50, 1.0, 2.0, 3.5, 7.0 seconds to observe if the mass measurement accuracy would deviate after extended time periods;

no further post-processing was done following truncation. Internal calibration was performed on the same 5 peptide peaks at each time interval and the mass errors for 8 other peptides were calculated. The results of the calibration at each time point are shown in **Figure 6**. There is a large increase in mass measurement accuracy within the first second, after which the mass measurement accuracy remains relatively constant. The average absolute mass measurement error for the 8 peptides measured was 0.28 ppm after 7.0 seconds. Therefore, these results show that with proper calibration, EPIC can provide high mass measurement accuracy for a diverse population of different *m*/*z* ions.

De-phasing of the excited ion cloud leads to a loss of ion signal. It is important that the stability of the ion cloud is not compromised with the application of the electron beam due to changes in the shape of the electrostatic trapping field and the radial force acting on the ions. Since the electron beam is turned on after the ions are excited, the ions will experience changes in their frequencies that may disrupt coherent motion of the ion cloud. One way of testing the stability of the ion cloud was to turn the electron beam on-off-on to see if the ion cloud stays together. **Figure 7** shows a graph of the frequencies of substance p $(M+2H)^{2+}$ at various time points for this experiment. The electron beam was turned on initially with -0.43 V bias immediately after excitation, after ~5 s the electron beam was turned off by changing the bias to 0.00 V, then at ~8 s the bias to the cathode was switched to -0.50 V. The frequency with time from the switched voltage bias experiment is compared with the frequency with time at constant bias potentials of 0.00, -0.43, and -0.50 V. The frequency in the switched voltage bias experiment matches well with the constant bias potentials. The bias potential of -0.38 V likely resulted in an inflection point in the electric field at a cell radius that is smaller than

the post-excitation cyclotron radius. This results in a continual decrease of the observed frequency with time. At -0.50 V bias the frequency is relatively flat with time meaning that the ion cloud is probably close to the inflection point in the electric field lines. In comparing the switched voltage bias to the constant -0.38 V bias we observe a slight deviation in their frequencies. This could be due to the instability of the electron beam, as we discuss below. However, the important point of **Figure 7** is that the stability of the ion cloud is not compromised by turning on and off the electron beam during a single detection event. This illustrates that the number of electrons in the ICR cell can be modulated during the course of a single acquisition without deleterious effects on ion coherence.

One note worth further consideration is the stability of the electron beam. Since the outer diameter of the cathode is larger than the hole in the lens, it is possible to measure a percentage of the electrons emitted from the cathode which hit the lens. There is a slight drift in the electron current over the course of an experiment (1-10 seconds) which may cause deviations in the frequency of the ion. **Figure 8a** shows the electron current which is collected on the lens during typical EPIC experiments at different bias potentials to the cathode. **Figure 8a** demonstrates the electron current is not entirely stable with time. **Figure 8b** shows the electron current for a single signal acquisition period taken after a number of consecutive signal acquisition periods and the electron current for a single acquisition period after a 5 min. delay between experiments. During the delay the cathode was held at +10 V. Both current measurements were taken under identical conditions. The electron current is much higher after some delay period, the exact mechanism for this phenomenon is not currently known. However, the current

fluctuations are mostly likely caused by fluctuations in the heating current. However, if multiple spectra are taken after a delay period, the current slowly decreases with each spectrum. The current typically measured on the lens at 1.5 A of heating current and -0.50 V bias on the cathode is ~3 uA. The electron current drift may limit the ability of high performance measurements since slight changes in the frequency will result in broadening of the peak and less precise determination of the exact cyclotron frequency. The variation in electron current will also make it difficult to signal average a number of high resolution spectra. It would be easier to produce a more accurate and defined negative potential along the central axis of the ICR cell with a solid electrode. The flow of electrons through the cell and unintended changes in electron flow will produce inhomogeneities in the radial electric field. However, the main advantage of the use of the electron beam is that charge is only present in the ICR cell during the detection event.

The frequency of an ion is determined by its radial location in the ICR cell as a result of the electron beam. This suggests that modulation of the electron beam could be used to eliminate frequency drift by applying a feedback loop through the bias potential to the cathode. All ions would be excited to the flat part of the electric field at larger cyclotron radii to minimize space charge effects, and the potential to the cathode could be modulated to match the flat part of the electric field with the ions radial position as their cyclotron radius damps back toward the center of the ICR cell.

Conclusions

The electric field shape can be modulated with the number of electrons present in the center of the ICR cell. Careful control of the number of electrons is needed to increase instrument performance. The application of EPIC forms an inversion point in the equipotential contours which can be determined by monitoring the frequency as a function of excited cyclotron radius. The best performance with EPIC comes when the ions are excited to a cyclotron radius close the inflection point in the radial fields. The cyclotron frequency of an ion can change with time, based on the shape of the electric field and the number of ions present within the ICR cell. The shape of the electric field potentials can be modified to reduce the time based frequency shift, and thus obtain high resolution spectra. The number of electrons being present in the ICR cell is dependent upon the heating current and the applied voltage bias; however, the number of electrons may not be constant from spectrum to spectrum and will limit the performance of this technique if not monitored.

Acknowledgements

The authors acknowledge helpful discussions with Drs. Jean Futrell and Göhkan Baykut. This material is based upon work supported by the National Science Foundation under Grant No. 0352451; Murdock Charitable Trust; Office of Science (BER), U. S. Department of Energy, Grant No. DE-FG02-04ER63924, and the National Institutes of Health Biotechnology Training Grant.

References

1. Comisarow, M. B., Marshall, A. G., Fourier transform ion cyclotron resonance spectroscopy, *Chemical Physics Letters*. **1974,** *25*, 282-283.

2. He, F., Emmett, M. R., Hakansson, K., Hendrickson, C. L., Marshall, A. G., Theoretical and experimental prospects for protein identification based solely on accurate mass measurement, *J Proteome Res*. **2004,** *3*, 61-67.

3. May, M. A., Grosshans, P. B., Marshall, A. G., Theoretical mass and energy upper limits for thermal ions in Fourier transform ion cyclotron resonance mass spectrometry, *International Journal of Mass Spectrometry and Ion Processes*. **1992,** *120*, 193-205.

4. Jackson, G. S., Canterbury, J. D., Guan, S., Marshall, A. G., Linearity and quadrupolarity of tetragonal and cylindrical Penning traps of arbitrary length-to-width ratio, *Journal of the American Society for Mass Spectrometry*. **1997,** *8*, 283-293.

5. Shi, S. D. H., Hendrickson, C. L., Marshall, A. G., Counting individual sulfur atoms in a protein by ultrahigh-resolution Fourier transform ion cyclotron resonance mass spectrometry: experimental resolution of isotopic fine structure in proteins, *Proceedings of the National Academy of Sciences of the United States of America*. **1998,** *95*, 11532-11537.

6. Peurrung, A. J., Kouzes, R. T., Long-term coherence of the cyclotron mode in a trapped ion cloud, *Physical Review. E. Statistical Physics, Plasmas, Fluids, and Related Interdisciplinary Topics*. **1994,** *49*, 4362-4368.

7. Holliman, C. L., Rempel, D. L., Gross, M. L., Detection of high mass-to-charge ions by Fourier transform mass spectrometry, *Mass Spectrometry Reviews*. **1994,** *13*, 105-132.

8. Easterling, M. L., Mize, T. H., Amster, I. J., Routine part-per-million mass accuracy for high-mass ions: space-charge effects in MALDI FT-ICR, *Analytical Chemistry*. **1999,** *71*, 624-632.

9. Ledford, E. B., Jr., Rempel, D. L., Gross, M. L., Space charge effects in Fourier transform mass spectrometry. Mass calibration, *Anal Chem*. **1984,** *56*, 2744-2748.

10. Mitchell, D. W., Smith, R. D., Cyclotron motion of two Coulombically interacting ion clouds with implications to Fourier-transform ion cyclotron resonance mass spectrometry, *Physical Review. E. Statistical Physics, Plasmas, Fluids, and Related Interdisciplinary Topics*. **1995,** *52*, 4366-4386.

11. Bruce, J. E., Anderson, G. A., Hofstadler, S. A., Winger, B. E., Smith, R. D., Time-base modulation for the correction of cyclotron frequency shifts observed in long-lived transients from Fourier-transform ion-cyclotron-resonance mass spectrometry of electrosprayed biopolymers, *Rapid Communications in Mass Spectrometry*. **1993,** *7*, 700-703.

12. Guan, S., Wahl, M. C., Marshall, A. G., Elimination of frequency drift from Fourier transform ion cyclotron resonance mass spectra by digital quadrature heterodyning: ultrahigh mass resolving power for laser-desorbed molecules, *Anal Chem*. **1993,** *65*, 3647-3653.

13. Jackson, G. S., White, F. M., Guan, S., Marshall, A. G., Matrix-shimmed ion cyclotron resonance ion trap simultaneously optimized for excitation, detection, quadrupolar axialization, and trapping, *Journal of the American Society for Mass Spectrometry*. **1999,** *10*, 759-769.

14. Bruce, J. E., Anderson, G. A., Lin, C.-Y., Gorshkov, M., Rockwood, A. L., Smith, R. D., A novel high-performance Fourier transform ion cyclotron resonance cell for improved biopolymer characterization, *Journal of Mass Spectrometry*. **2000,** *35*, 85-94.

15. Ostrander, C. M., Arkin, C. R., Laude, D., Central ring electrode for trapping and excitation/detection in Fourier transform ion cyclotron resonance mass spectrometry, *Journal of the American Society for Mass Spectrometry*. **2001,** *12*, 30-37.

16. Guan, S., Marshall, A. G., Ion traps for Fourier transform ion cyclotron resonance mass spectrometry: principles and design of geometric and electric configurations, *International Journal of Mass Spectrometry and Ion Processes*. **1995,** *146/147*, 261-296.

17. Vartanian, V. H., Anderson, J. S., Laude, D. A., Advances in trapped ion cells for Fourier transform ion cyclotron resonance mass spectrometry, *Mass Spectrometry Reviews*. **1995,** *14*, 1-19.

18. Solouki, T., Gillig, K. J., Russell, D. H., Detection of High-Mass Biomolecules in Fourier Transform Ion Cyclotron Resonance Mass Spectrometry: Theoretical and Experimental Investigations, *Analytical Chemistry*. **1994,** *66*, 1583-1587.

19. Kingdon, K. H., A method for neutralizing the electron space charge by positive ionization at very low pressures, *Physical Review*. **1923,** *21*, 408-418.

20. Gillig, K. J., Bluhm, B. K., Russell, D. H., Ion motion in a Fourier transform ion cyclotron resonance wire ion guide cell, *International Journal of Mass Spectrometry and Ion Processes*. **1996,** *157/158*, 129-147.

21. Hendrickson, C. L., Hadjarab, F., Laude, D. A., Jr., Electron beam potential depression as an ion trap in Fourier transform ion cyclotron resonance mass spectrometry, *International Journal of Mass Spectrometry and Ion Processes*. **1995,** *141*, 161-170.

22. Kruger, N. A., Zubarev, R. A., Horn, D. M., McLafferty, F. W., Electron capture dissociation of multiply charged peptide cations, *International Journal of Mass Spectrometry*. **1999,** *185/186/187*, 787-793.

23. McLafferty, F. W., Horn, D. M., Breuker, K., Ge, Y., Lewis, M. A., Cerda, B., Zubarev, R. A., Carpenter, B. K., Electron capture dissociation of gaseous multiply charged ions by Fourier-transform ion cyclotron resonance, *Journal of the American Society for Mass Spectrometry*. **2001,** *12*, 245-249.

24. Easterling, M. L., Amster, I. Jonathan, 43rd ASMS Conference on Mass Spectrometry and Allied Topics, Atlanta, GA, **1995**.

25. Kaiser, N. K., Bruce, J. E., Observation of Increased Ion Cyclotron Resonance Signal Duration through Electric Field Perturbations, *Analytical Chemistry*. **2005,** *77*, 5973-5981.

26. Nikolaev, E. N., Popov, A. M., Heeren, R. M. A., Sharova, M. S., Pozdneev, A. V., Chingin, K. S., Taban, I. M., 53rd ASMS Conference on Mass Spectrometry and Allied topics, San Antonio, TX, **2005**.

27. Nikolaev, E. N., 54th ASMS Conference on Mass Spectrometry and Allied Topics, Seattle, WA, **2006**.

28. Caravatti, P., Allemann, M., The infinity cell: a new trapped-ion cell with radiofrequency covered trapping electrodes for Fourier transform ion cyclotron resonance mass spectrometry, *Organic Mass Spectrometry*. **1991,** *26*, 514-518.

29. Caravatti, P., Method and Apparatus for The Accumulation of Ions in a Trap of an Ion Cyclotron Resonance Spectrometer, by Transferring the Kinetic Energy of the Motion Parallel to the Magnetic Field into Directions Perpendicular to the Magnetic Field., *US Patent. 4,924,089.* **1990.**

30. Anderson, G. A., Bruce J.E., Smith R.D., ICR-2LS, Richland, WA, **1996**.

31. Francl, T. J., Sherman, M. G., Hunter, R. L., Locke, M. J., Bowers, W. D., McIver, R. T., Jr., Experimental determination of the effects of space charge on ion cyclotron resonance frequencies, *International Journal of Mass Spectrometry and Ion Processes*. **1983,** *54*, 189-199.

32. Gorshkov, M. V., Marshall, A. G., Analysis and elimination of systematic errors originating from Coulomb mutual interaction and image charge in Fourier transform ion cyclotron resonance precise mass difference measurements, *Journal of the American Society for Mass Spectrometry*. **1993,** *4*, 855-868.

33. Hawkridge, A. M., Nepomuceno, A. I., Lovik, S. L., Mason, C. J., Muddiman, D. C., Effect of post-excitation radius on ion abundance, mass measurement accuracy, and isotopic distributions in Fourier transform ion cyclotron resonance mass spectrometry, *Rapid Communications in Mass Spectrometry*. **2005,** *19*, 915-918.

34. Xiang, X., Grosshans, P. B., Marshall, A. G., Image charge-induced ion cyclotron orbital frequency shift for orthorhombic and cylindrical FT-ICR ion traps, *International Journal of Mass Spectrometry and Ion Processes*. **1993,** *125*, 33-43.

35. Goodlett, D. R., Bruce, J. E., Anderson, G. A., Rist, B., Pasa-Tolic, L., Fiehn, O., Smith, R. D., Aebersold, R., Protein Identification with a Single Accurate Mass of a Cysteine-Containing Peptide and Constrained Database Searching, *Analytical Chemistry*. **2000,** *72*, 1112-1118.

Figure 1

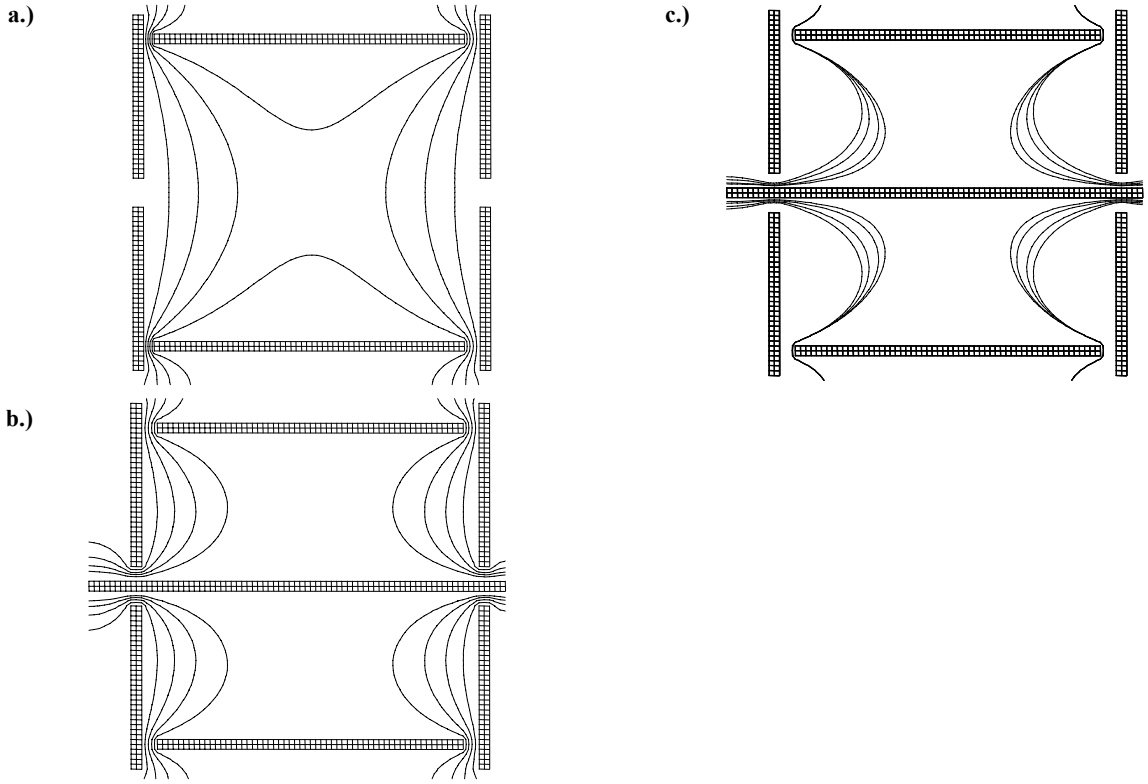

Figure 1) Simion plot of equipotential contour lines of a closed cylindrical cell with 1.0 V placed on the trapping electrodes. a) equipotential contours of 0.8, 0.6, 0.4, 0.2 V are shown b) equipotential contours of 0.8, 0.6, 0.4, 0.2 V are shown; an electrode with a -0.5 V potential is placed through the center of the closed cylindrical cell to approximate the affect the electron beam will have on the shape of the trapping potentials c) an overlay of the 0.2 V equipotential contour lines for potentials of -0.01, -0.10, -0.30, and -0.50 V applied to the central electrode.

Figure 2

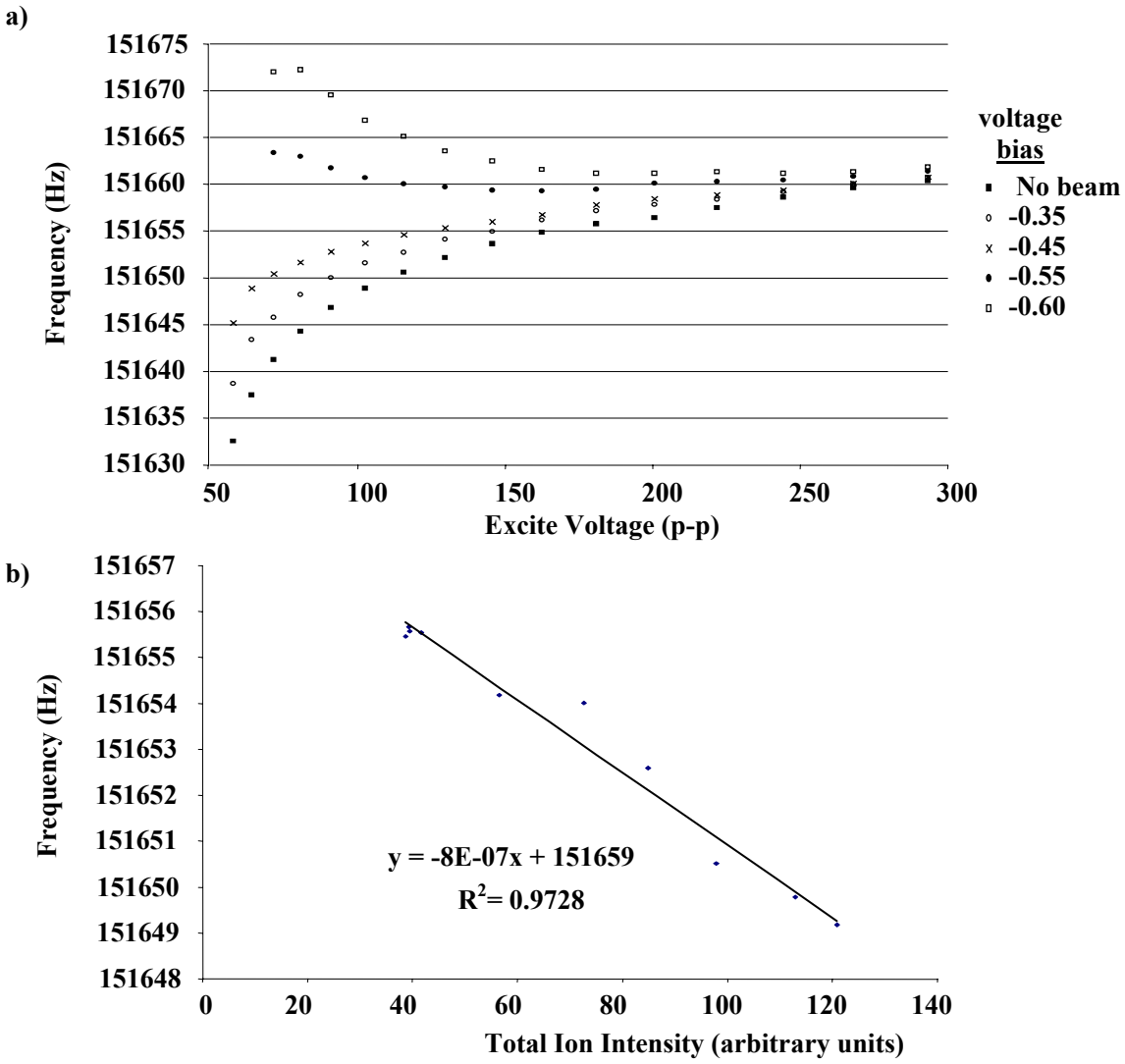

Figure 2) a) The measured cyclotron frequency of melittin $(M+4H)^{+4}$ is plotted at different RF excitation voltages. Experiments were done with different voltage biases applied on the cathode carried out to demonstrate the affect of the number of electrons have on the measured frequency. Each collected spectrum was an average of 10 signal acquisitions and the data set size was 128k. b) The total ion population in the ICR cell was varied to determine the cyclotron frequency with reduced space charge conditions.

Figure 2

c)

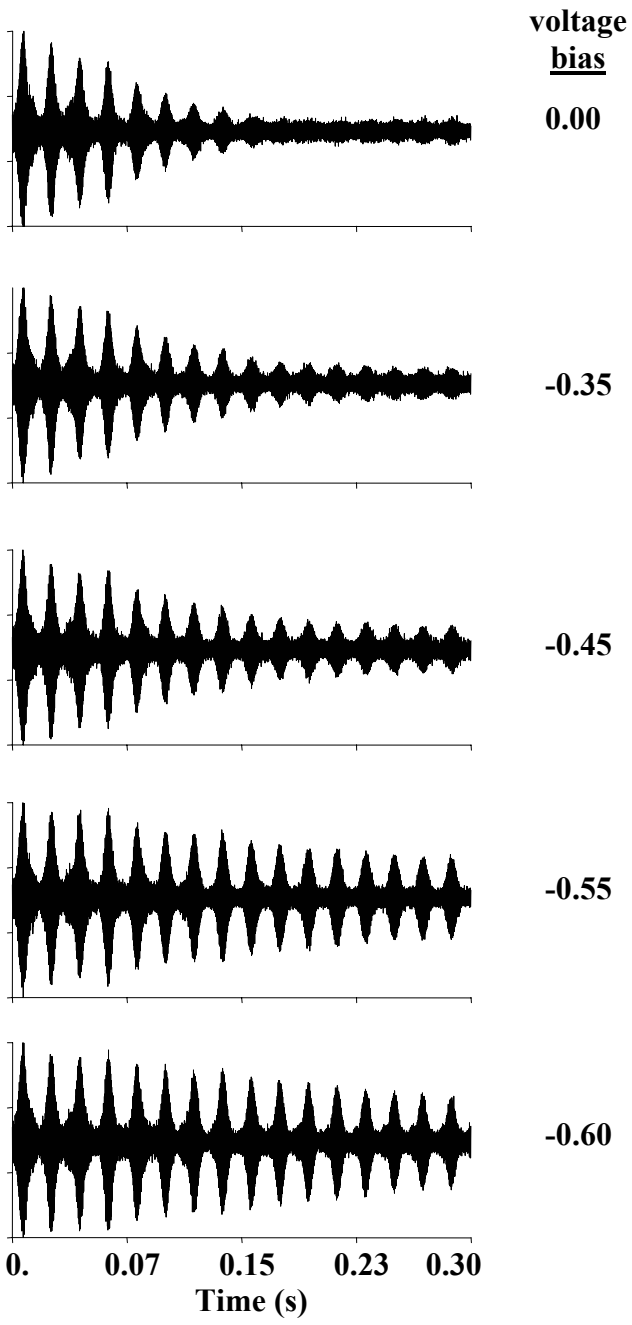

c) The time-domain signal acquired after excitation with voltage of 200 V_{p-p} is shown for different bias voltages applied to the cathode.

Figure 3

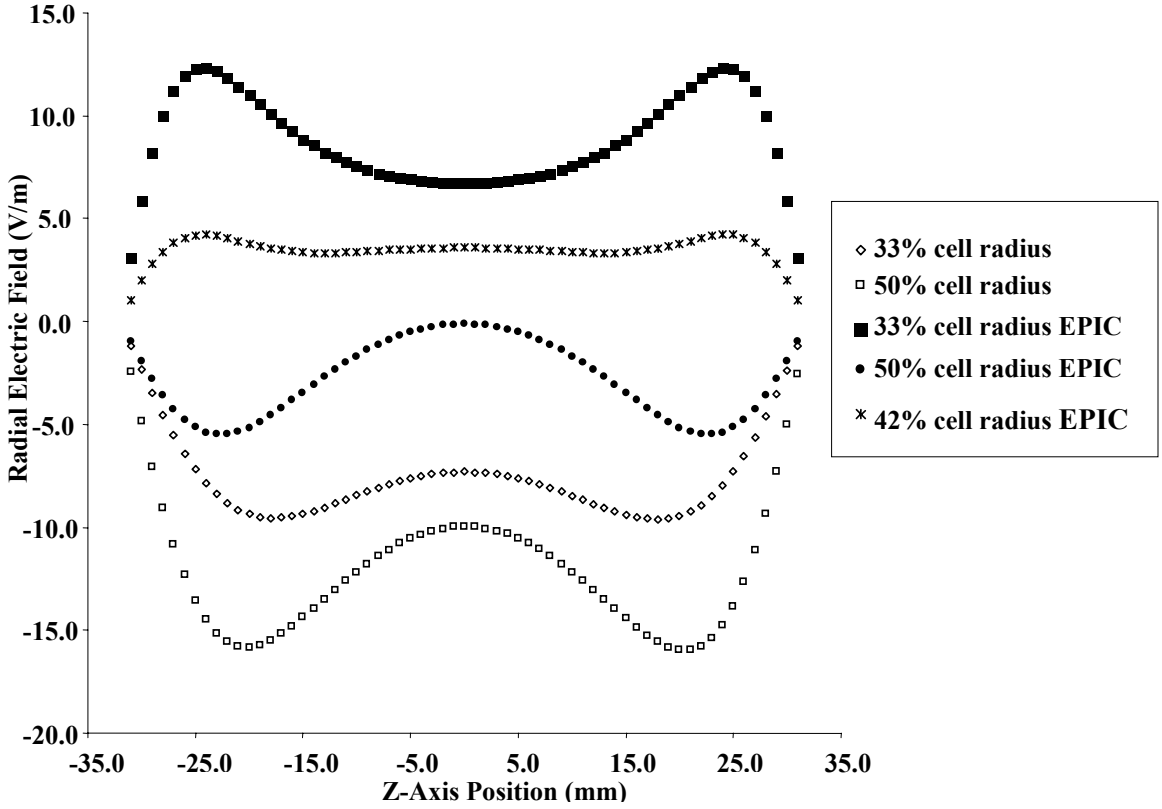

Figure 3) Radial electric fields are shown at set radii across the z-axis of the ICR cell. 1 V applied to the trapping electrodes. The EPIC radial electric fields were constructed with -0.2 V on the central electrode.

Figure 4

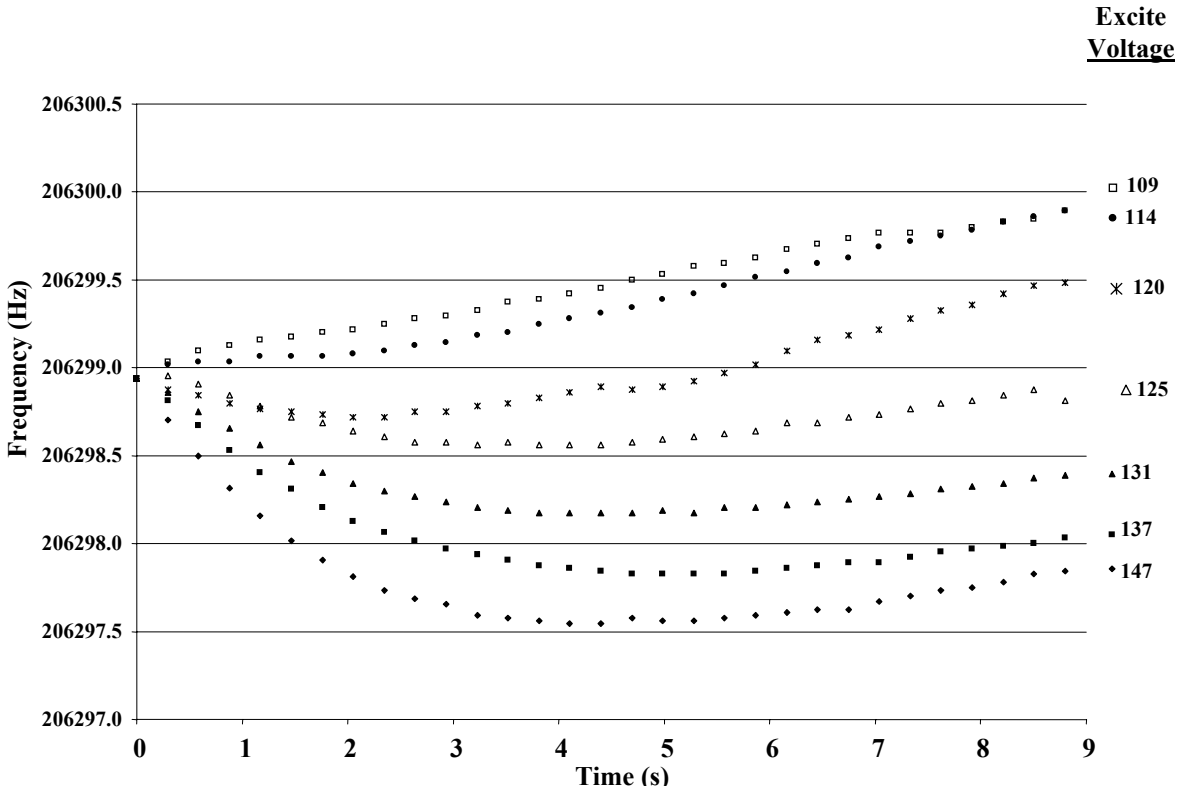

Figure 4) Segments of time-domain signals of bradykinin $(M+2H)^{+2}$ collected in heterodyne mode were sampled to monitor the frequency with time while maintaining the same voltage bias to the cathode. Application of various excitation voltages illustrated that the ions pass through the inflection point at different time points based on the initial excited cyclotron radius. The frequencies were normalized to the detected initial frequency from each acquisition to better illustrate the detected frequency shift with time.

Figure 5

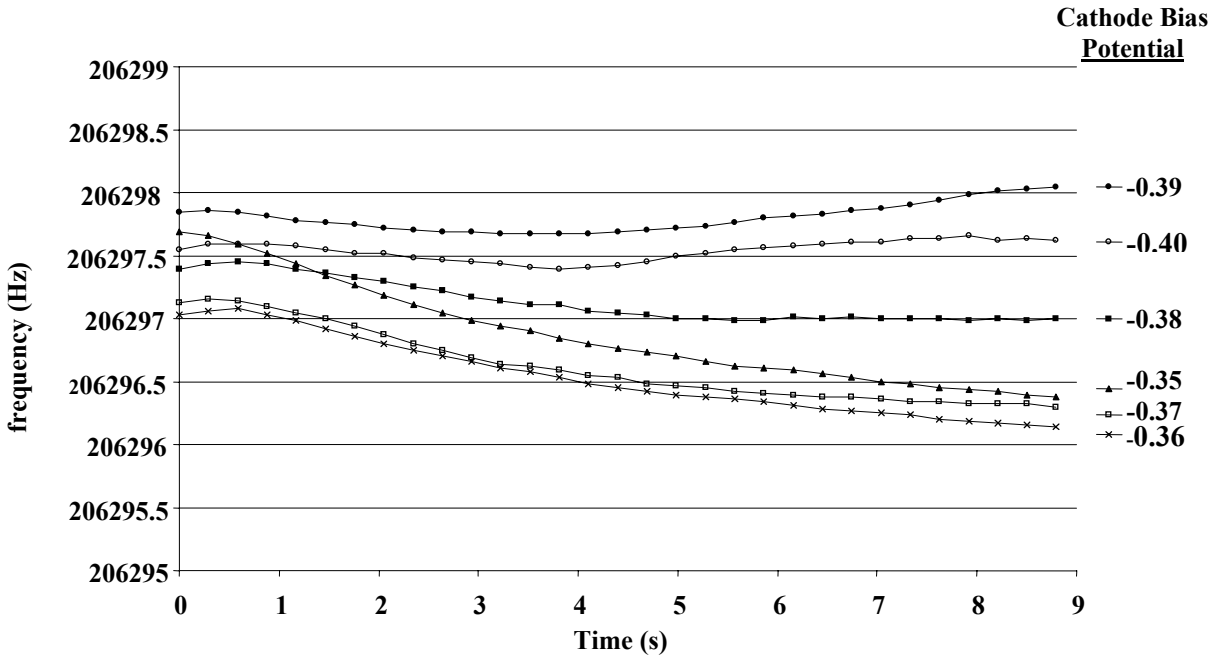

Figure 5) Segmented FFT analysis of time-domain signals of bradykinin $(M+2H)^{+2}$ ions. Various cathode bias potentials were applied to demonstrate how the detected frequency changes with time while maintaining the same excited cyclotron radius. At low applied bias potentials the frequency decreases with time. At higher applied bias potentials the frequency increases with time.

Figure 6

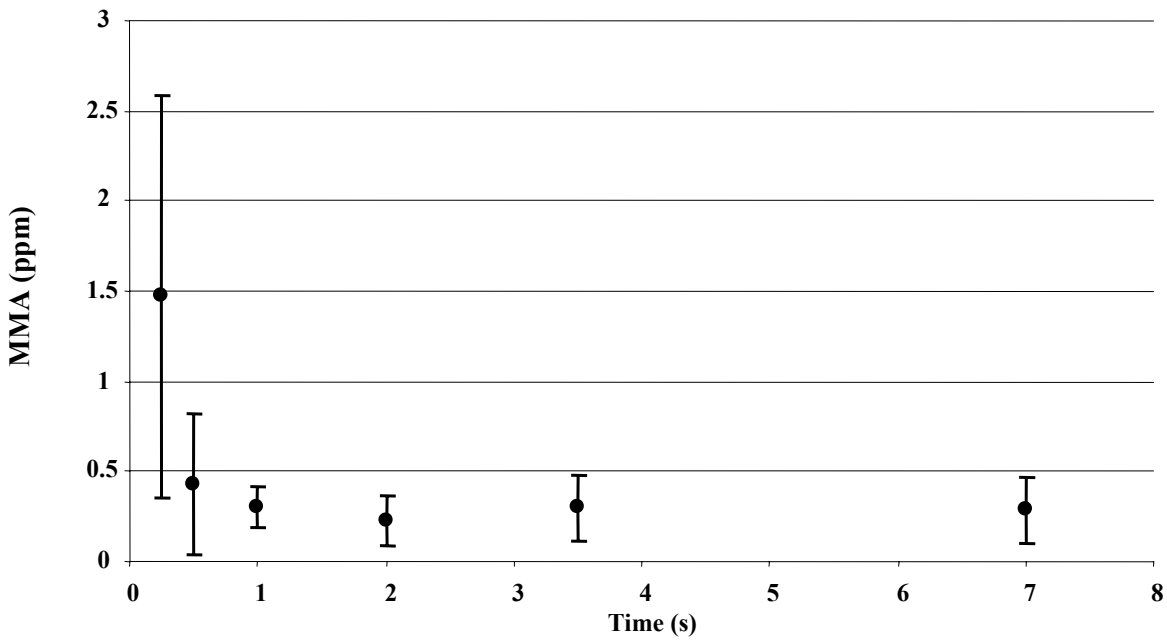

Figure 6) Broadband spectrum of BSA tryptic digest peptides from a recorded 7 second ICR signal acquisition. The resultant time-domain of a single acquisition period was truncated at time intervals of, 0.25, 0.50, 1.0, 2.0, 3.5, 7.0 seconds. The spectrum was calibrated with 5 peptides after each truncation. The average mass measurement error of 8 other peptides in the spectrum is plotted with time. The error bars show +/- one standard deviation.

Figure 7

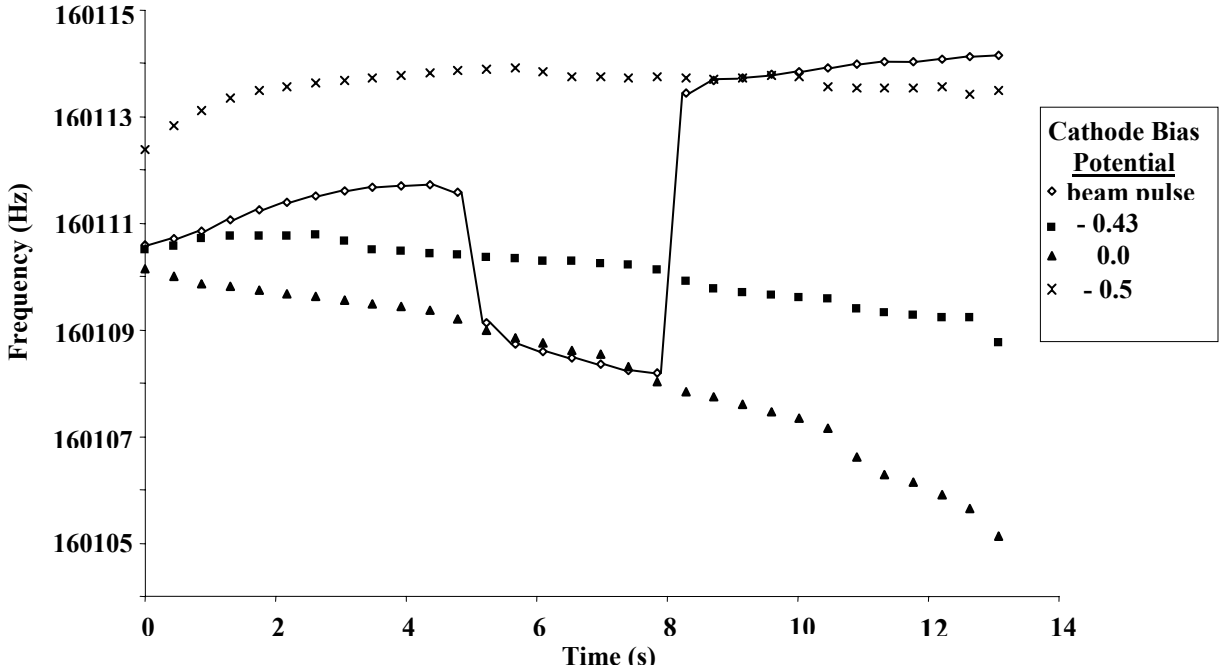

Figure 7) The effect observed by altering the applied cathode potential during ICR signal acquisition. The frequency of Substance p ions was measured throughout the transient signals by segmented FFT analysis. The detected frequency was observed to change abruptly as the electron beam was turned on and off. The detected frequencies obtained at static bias potentials are also shown for comparison.

Figure 8

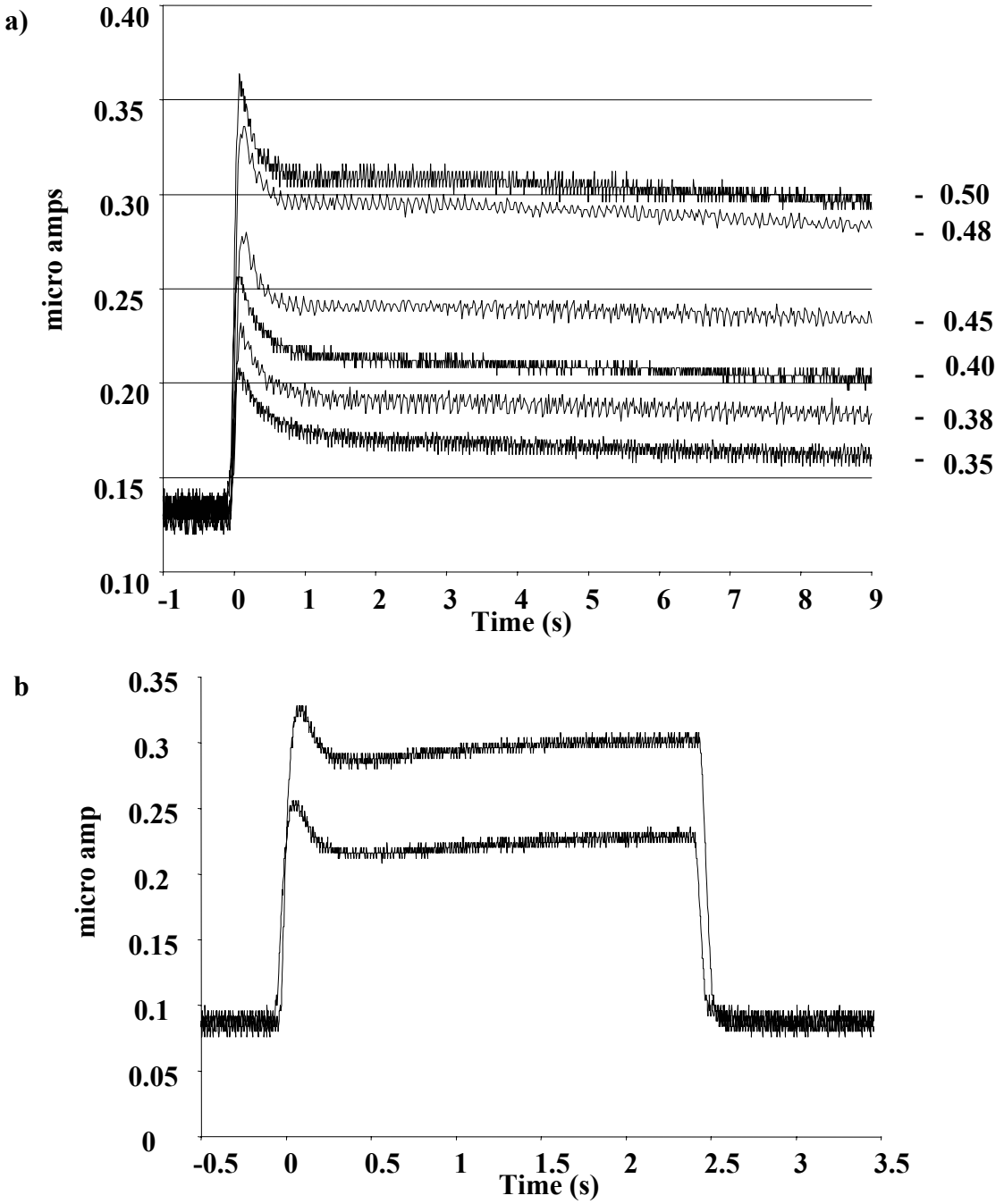

Figure 8) Time-dependence of electron beam current collected on the lens. a) The measured electron current resultant from application of various voltage biases to the cathode. The electron current follows the same general drift in current with time. b) The upper electron current trace was recorded taken after the cathode remained idle for 5 minutes. The lower current trace was detected immediately after 20 previous signal acquisition periods.

CHAPTER 5

Reduction of Axial Kinetic Energy Induced Perturbations on Observed Cyclotron Frequency

Abstract

With Fourier Transform Ion Cyclotron Resonance (FTICR) mass spectrometry one determines the mass-to-charge ratio of an ion by measuring its cyclotron frequency. However, the need to contain ions to the trapping region of the ICR cell with electric fields induces deviations in the unperturbed cyclotron frequency. Additional perturbations to the observed cyclotron frequency are often attributed to changes in space charge conditions. This study presents a detailed investigation of the observed ion cyclotron frequency as a function of ion *z*-axis kinetic energy. In a perfect three-dimensional quadrupolar field, cyclotron frequency is independent of position within the trap. However, in most ICR cell designs, this ideality is approximated only near the trap center and deviations arise from this ideal quadrupolar field as the ion moves both radially and axially from the center of the trap. To allow differentiation between deviations in observed cyclotron frequency caused from changes in space charge conditions or differences in oscillation amplitude, ions with identical molecular weights but different axial kinetic energy, and therefore, amplitude of *z*-axis motion, were simultaneously trapped within the ICR cell. This allows one to attribute deviations in

observed cyclotron frequency to differences in the average force from the radial electric field experienced by ions of different axial amplitude. Experimentally derived magnetron frequency is compared with the magnetron frequency calculated using SIMION 7.0 for ions of different axial amplitude. Electron Promoted Ion Coherence, or EPIC, is used to reduce the differences in radial electric fields at different axial positions. Thus with the application of EPIC, the differences in observed cyclotron frequencies are minimized for ions of different axial oscillation amplitudes.

Introduction

Fourier Transform Ion Cyclotron Resonance (FTICR) mass spectrometry [1, 2] has become the ideal mass analyzer for the analysis of multiply charged ions produced by electrospray ionization with its ability to provide high resolution and accurate mass measurements. It has become common practice to couple electrospray ionization to liquid chromatography for online analysis of complex mixtures with FTICR-MS [3-5]. To effectively sample the chromatographic peaks as they elute from the column, a short duty cycle is needed. However, with ICR mass spectrometers the mass resolving power, sensitivity, and mass measurement accuracy decrease with shorter acquisition time periods. Therefore, the majority of the time ions spend in the ICR cell is used for detection and not on some form of ion manipulation event such as ion accumulation, ion focusing, or ion selection. In order to meet the demand for high-throughput analysis while utilizing the high performance that FTICR mass spectrometers offer, ions are usually accumulated external to the magnetic field and then trapped in the ICR cell with

some variation of gated trapping [3, 6-8]. Hybrid instruments allow for ion selection and fragmentation to take place external to the magnetic field. Minimizing individual spectrum acquisition time increases the number of MS and MS/MS acquisitions that can be obtained during an LC-MS analysis. Therefore, little time is spent on ion manipulation inside the ICR cell.

Ions are trapped in the ICR cell perpendicular (*x*-*y*) to the cell axis by the magnetic field and along the ICR cell axis (*z*) by a static potential applied to the trapping electrodes. The finite dimensions of the ICR cell result in two further motions in addition to cyclotron motion within the ICR cell, a trapping oscillation along the *z*-axis and magnetron motion. The ability to produce a three dimensional axial quadrupolar potential is needed to obtain an ion cyclotron resonance frequency that is independent of the ion location within the ICR cell. This ideal electric field shape can only be achieved with a hyperbolic shaped cell [9]. However, by applying the same dc voltage to each of the trapping electrodes of just about any trap geometry will approximate a quadrupolar electrostatic trapping potential near the center of the ICR cell [10]. This idealized electrostatic field is only present at the center of the ICR cell and as the ions are moved axially and/or radially away from the ICR cell center, the electric field deviates from quadrupolar. Therefore, the observed cyclotron frequency becomes dependent on its position inside the ICR cell. The variation in cyclotron frequency as a function of *z*-axis position has been of concern in to researchers in the ICR field for a long time [11, 12]. The first trapped cell experiments by McIver and coworkers had hyperbolic shaped electrodes to minimize these effects [13]. Many groups have identified that detailed knowledge of frequency shifts due to non-ideal electric fields was required to maximize

instrument performance [14-16]. Mitchell developed a theory of trapped ion motion in the non-quadrupolar electrostatic potential of a cubic ICR cell [17]. At a large radial or axial distance from center of the ICR cell the rapid periodic cyclotron and axial motions of a single ion time averages spatial nonidealities in the electric and magnetic fields [18]. However, these same nonidealities also disrupt the ion motion of a coherent ion packet, increasing the rate of signal decay [19]. There are a number of trap configurations that have been proposed or tested to decrease these nonidealities [20-25].

With the three-dimensional quadrupolar potential achieved at the center of the ICR cell it becomes desirable to reduce the ion oscillation amplitude so that ions are located primarily at the center of the ICR cell during excitation and detection. In addition, quadrupolar axialization improves virtually every aspect of FTICR performance [26]. Higher performance measurements are usually obtained with some form of ion cooling method as well as a reduction of trap plate potentials prior to ion detection [27, 28]. There are a number of different methods that have been used to reduce ion axial motion in the ICR cell such as introducing a collision gas into the ICR cell [29], side-kick [8], evaporative cooling [30, 31], and adiabatic cooling [27]. The method we describe here has great potential in combination with these methods to further minimize differences in magnetron frequency for ions of different *z*-axis oscillation amplitudes.

Gated trapping is attractive because it can decrease the data acquisition time period by accumulating ions external to the ICR cell. However, when gated trapping is performed ions can have different *z*-axis kinetic energies in the ICR cell. However, due to time-of-flight effects and the ion distribution as they exit the accumulation cell, all ions do not reach the center of the ICR cell at the same time [32]. The position of the ions at

the moment the potential applied on the front plate is increased will result in different trapping oscillation amplitudes. Ions located at the center of the trap will be efficiently trapped. However, ions located at the edges of the trapping regions when the potential is increased will result in those ions having larger *z*-axis oscillation amplitudes. This results in a dispersion of ions along the *z*-axis of the ICR cell. This will result in a change in the observed cyclotron frequency based on ion axial position and/or rapid de-phasing of the ion cloud [6, 19, 33, 34]. Therefore, scan-to-scan variation of ion kinetic energy will change the observed cyclotron frequency and also should cause non-linear calibration errors. *Z*-axis motion is an important parameter to consider when performing high performance measurements, since ions of different *z*-axis amplitude may experience different average magnetic field strength and radial electric field strength. It has been reported that during the detection period, the trapping motion effectively averages out differences in electric or magnetic field over *z*-axis amplitudes [18, 35]. This is explained by motional averaging of the radial electric field. That is, the *z*-axis oscillation frequency is usually much higher than the magnetron frequency. Thus, motional averaging of the radial electric field during *z*-axis oscillation yields an average of the radial electric field experienced by an ion [36]. Vartanian and Laude showed that for an open cylindrical cell modulation of the *z*-axis oscillation amplitude induced changes in the magnetron frequency [37].

Motion of ions in the ICR cell is complex and still not fully understood. Though fairly simple for a single ion, the complexity of ion motion increases with increasing number of ions within the ICR cell. Small perturbations in the observed cyclotron frequency from scan-to-scan are often attributed to changes in space charge conditions.

This work focuses on changes in the observed cyclotron frequency as a function of *z*-axis oscillation amplitude. We show that ions with the same mass but different axial kinetic energies exhibit different observed cyclotron frequencies. We also present a further utility of the technique called Electron Promoted Ion Coherence [38-40] or EPIC, in which the application of an electron beam through the center of the ICR cell during detection alters the radial electric fields to produce longer transients. This technique is similar the wire ion guide ICR cell designed by Russell and coworkers, which utilized a charged wire suspended along the axis of the ICR cell for modification of the trapping electric field [41, 42]. In our first paper we showed that with EPIC we could achieve a 3x improvement in resolution and sensitivity by changing the electric fields. In the second paper we demonstrated that high mass measurement accuracy is possible with the technique, and characterized the effects the electron beam has on the observed cyclotron frequency. Here we present the underlying principle for the improvements this technique presents. In this research the use of EPIC produces an observed cyclotron frequency that is independent of *z*-axis oscillation amplitude.

Experimental

Ions were produced using electrospray ionization by applying ~2.5 kV to the entrance to the mass spectrometer. The electrospray solution was 49:49:2 by volume of water:methanol:acetic acid. Ions were analyzed with a Bruker Daltonics 7T ApexQ FTICR mass spectrometer (Billerica, MA). The instrument utilizes the Infinity cell [43] for image current detection. The mass spectral data was acquired with Xmass version

7.0.6 as the data acquisition software. Bradykinin, melittin, and insulin were purchased from Sigma (St. Louis, MO). 10μM solutions of peptides were infused by direct injection with a syringe pump at a rate of 0.4 μL/min. Ions were accumulated in a hexapole following isolation with the mass selective quadrupole. Ion intensity was varied by changing the ion accumulation time in the hexapole. The accumulation time varied between 0.1 ms and 2.0 s. Ions were trapped in the ICR cell with the use of gated trapping. The ions were typically excited to cyclotron radius between 30 – 40% of the ICR cell radius. The data was analyzed with ICR-2LS [44]. To determine frequencies, all transients were Welch apodized followed by one zero-fill before Fourier transformation to the frequency domain. Ion abundances used for space charge frequency corrections were calculated by taking the initial amplitude from the extracted transient of the monoisotopic peak in the frequency domain [45, 46]. This process was done instead of obtaining ion abundances directly from the peak intensity because the peak intensity will change for ions with different signal decay rates.

The pulse sequence to simultaneously trap ions with different axial kinetic energies in the ICR cell called a "Double Trap" experiment is shown in **Figure 1a**. Bradykinin $(M+2H)^{2+}$ was accumulated in the hexapole region and then sent to the ICR cell followed by injection of a cooling gas (argon) with a pulse length of 1.5ms. After an 8 second delay, a second ion packet of Bradykinin $(M+2H)^{2+}$ is accumulated in the hexapole and sent to the ICR cell, followed immediately by excitation and detection. The pulse sequence was set up to individually control the ion accumulation time period for each ion injection event. The trapping potentials were set at 1.5 V for all "Double Trap" experiments.

The magnetron frequency was calculated with SIMION 7.0 software (SIMION 7.0 3D, version 7.0, D.A. Dahl, Idaho National Engineering Laboratory, Idaho Falls, ID). The magnetic field strength was set at 7 Tesla for the magnetron frequency simulations. The ICR cell used for the simulations was a closed cylindrical cell with dimensions of 64mm in length and with a diameter of 60mm. The radial electric fields were also calculated with SIMION 7.0 at 1mm intervals along the *z*-axis, at different cell radii. The segmented trap plates of the infinity cell were treated as if they were a single electrode. This will only cause minor deviations in the calculations very near the surface of the electrodes, and would not alter the calculated fields presented here.

In order to initiate larger *z*-axis amplitude, ions were first cooled axially with a pulse valve event. 1.5 volts were applied to both trap plates. After an 8 second delay the back trap plate was dropped to ground for defined period of time (51us to 2000us), then raised back to 1.5 V for 400usec, before being dropped back to ground. The front trap plate remained at 1.5 V. The number of times that the back trap plate was lowered and raised was varied between 1 and 10.

EPIC was carried out with a hollow cathode originally installed to conduct electron capture dissociation experiments. The cathode was heated with 1.5 to 1.6 amps of current. To send electrons through the center of the ICR cell during detection the potential to the cathode was pulsed negative (0.0 V to -1.0 V). At all other times the potential applied on the cathode was held at a positive 10 V. The cathode is pulsed negative after the excitation event and remained negative throughout the detection event.

Results and Discussion

Simultaneous detection of ions with different kinetic energies:

Though it has been shown that motional averaging of the radial electric field results in a single observed cyclotron frequency for a range of different axial kinetic energies, it is possible to observe separate peaks within the same spectrum for ions with the same mass value but distinctly different axial kinetic energies. **Figure 1b** shows the results from the double trap experiment in which the first ion packet is injected into the ICR cell followed by a pulse gas event. This was done to cool the axial motion and allow the ions to be focused axially to the center of the ICR cell. After an 8 second delay to allow the cooling gas to be pumped away, a second ion packet is injected into the ICR cell. This allows for two packets of ions with the exact same mass value that differ only in kinetic energy to be trapped in the ICR cell. The cooled ions will have small *z*-axis oscillation amplitudes while the ion from the second injection will have much larger *z*-axis oscillation amplitude. The resulting mass spectrum yields two peaks for the same mass value. In Figure 1b, the accumulation time for the first ion injection event was varied while the accumulation time for the second ion injection event remained constant. As expected increasing the accumulation time for the first ion injection event results in an increase in peak intensity for the corresponding peak in the spectra, while the peak intensity resultant from the second ion injection event remained constant. This demonstrates independent control over the number of ions injected into the ICR cell for the separate ion injection events. The results from the double trap experiment were compared with a single ion injection event that mimicked either the first or second ion

injection event of the double trap experiment. The result from only a single ion injection for the first injection event is represented by the dotted line in Figure 1b. The result for the single ion injection for the second ejection event is shown in **Figure 1c**. The pulse sequence remained the same between the single ion injection event and the double trap experiment, with the exception of altering a voltage parameter in the source region to gate the ions. For the same ion accumulation times, the peak intensities are similar between the single ion injection and the corresponding peak in the double trap experiment. The peak for the single injection is shifted to a slightly lower m/z value, indicating higher frequency. This could result from a lower number of total ions trapped in the ICR cell, (one ion injection vs. two ion injections) that results in different space charge conditions. Alternatively, the z-axis oscillation amplitude of the cooled ion packet may have increased slightly during the injection of the second ion packet. The front trap plate was pulsed to ground for the ion flight time (1.5ms) before being raised to 1.5 V for ion detection.

The double trap experiment was designed to minimize differences in space charge conditions that might occur if the experiments were performed separately. If the frequencies had been measured in separate experiments it would be difficult to decipher the contribution between space charge and axial oscillation amplitude on the observed cyclotron frequency. By performing the double trap experiment, we can conclude that the differences in observed frequencies are from the axial oscillation amplitude. In reducing the axial kinetic energy of the ions in the ICR cell with a collision gas, the space charge conditions are also changing. A cooled ion packet likely experiences higher space charge conditions since the spread in axial positions of the ions is decreased. One

might therefore expect cooled ions to exhibit lower cyclotron frequencies due to increased space charge conditions [47, 48]. However, as shown in Figure 1b the cooled ion packet is observed at a lower *m*/*z* value indicating that it has a *higher* observed cyclotron frequency. The difference in frequency results from the difference in average radial electric field experienced by the ions. **Figure 2** shows the calculated magnitude of the outward directed radial electric field along the *z*-axis at 45% of the ICR cell radius with 1 V applied to the trap electrodes. The magnitude of the radial electric field changes with ion position along the *z*-axis. Increasing the trap plate voltage will increase the difference in magnitude of the radial electric field across the *z*-axis of the ICR cell. Therefore, as an ion oscillates between the trap plates it will experience differences in the magnitude of the radial electric field. The resultant magnetron frequency is correlated to the average radial electric field experienced by the ions. Therefore, changes in the average radial electric field produced from differences in axial motion will be reflected in the magnetron frequency. The magnetron frequency is also shown in Figure 2 for ions with different axial oscillation amplitudes. Ions with different axial kinetic energy in the ICR cell will have different axial oscillation amplitudes, and thus will experience a different average radial electric force. Dunbar and coworkers were able map out electric field imperfections in a cubic ICR cell by monitoring the magnetron frequency of the ions [49]. A cooled ion packet will have small axial oscillation amplitude and be located at the center of the ICR cell, and experience little change in the radial electric field along the *z*-axis. In Figure 2, the magnetron frequency is smallest at the center of the ICR cell. As the kinetic energy or amplitude of *z*-axis motion increases, the magnetron frequency increases. An ion with small amplitude of *z*-axis motion will have a greater observed

cyclotron frequency because it has a smaller magnetron frequency. This relationship is shown in Equation (1) where ω_+ is the observed cyclotron frequency, ω_c is the unperturbed cyclotron frequency, and ω_- is the magnetron frequency [1].

$$\omega_+ = \omega_c - \omega_- \qquad (1)$$

Effect of ion cooling on observed cyclotron frequency:

Ion kinetic energies were varied to observe the effect of different axial oscillation amplitude on observed cyclotron frequency. Ions are cooled either through a pulsed gas event or by the addition of a significant delay between ion injection into the ICR cell and excitation. The results for the experiments are shown in **Figure 3**. The highest observed cyclotron frequency occurs after the ions have been cooled to the middle of the ICR cell. Three sets of data are illustrated in this figure. The duration between the pulse valve event following ion injection and cyclotron excitation (**o**) was varied. Increasing the duration between the pulse event showed no noticeable trend in measured cyclotron frequencies. This indicates that ions are cooled axially to the middle of the ICR cell. No time points were taken with a delay of 2 seconds or less due to the deleterious effects the high pressure has on ICR signal detection. Thus, the delay period between ion cooling and ion excitation had no observable effect on the axial position of the ions. The next set of experiments examined the frequency difference for ions that were subjected to variable delay times between ion injection into the ICR cell and cyclotron excitation with no pulsed valve (■). With a delay of approximately 10μs between ion injection and excitation the ions have the lowest observed frequency, which indicates that these ions have the largest axial motion immediately after ion injection. As the delay period

increases the observed frequency increases, which results from ions being cooled to the middle of the ICR cell through either ion-neutral or ion-ion interactions. The signal amplitude remained constant for each delay period, indicating that ions are not lost from the ICR cell during the delay period. Therefore, the change in frequency can be attributed to a change in axial position, rather than alterations in space charge conditions. After approximately a 7 second delay the observed frequency leveled off at the same frequency one would expect if the ions were cooled to the center of the ICR cell with the addition of a cooling gas. This indicates two things: first, after some set time period the axial oscillation amplitude was not being reduced further, and second the ion axial amplitude with the delay between ion injection and excitation approaches the ion axial amplitude following the pulse gas event. This experiment was also carried out with melittin and insulin to test for mass-dependence of this axial relaxation. All three tested species exhibited the same effect of increased frequency with delay time before leveling off at observed frequencies that agreed with those recorded with corresponding pulse gas experiments. Figure 3 also shows result of the experiments in which a pulse gas event was followed by a variable delay time before ion injection into the ICR cell (♦). When the pulse gas event is immediately followed by ion injection, there are enough neutral molecules in the ICR cell to cool the ions the same as if the ions were trapped and cooled with a pulse gas event. This is evident from the data in Figure 3 since the measured frequencies with this delay period of 0.5 seconds or less agreed closely with those measured for cooled ions (**o**). It should be noted that, if the delay period between the pulse gas event and ion injection was less than two seconds an additional delay was added so that the total time between the pulse gas and cyclotron excitation was greater

than 2 seconds to allow time for the residual neutral molecules to be pumped away. As the delay period between the pulse gas and ion injection increases, the observed frequency decreases. This results from the neutral gas molecules being pumped away and therefore, when ions reach the ICR cell there are insufficient ion-neutral collisions to promote complete cooling of axial ion motion. Furthermore, a delay of 1 second or more results in observed frequencies that are in close agreement with those acquired with no pulsed valve (■). Importantly, these data illustrate the degree to which the ions are cooled changes their axial oscillation amplitude and thus, their observed frequencies.

Determination of magnetron frequency:

Magnetron frequency was determined experimentally for both the pulsed gas and the non-pulsed gas experiments. This was achieved by varying the trap plate potentials from 3.0 V to 0.5 V. The application of trap plate potentials induces the radial electric field which drives magnetron motion. Increasing the applied trap plate potentials increases the force from the outward directed radial fields and results in higher magnetron frequencies. The results from investigation of trap potential effects on observed frequencies with and without pulsed gas both produced a linear increase with a decrease in trap plate potential. The observed frequencies for the cooled ions were larger at every trap plate potential. The difference between the two data sets becomes greater with increased trap plate potential. The observed cyclotron frequency for the non-pulsed gas experiments decreases (as trap potentials are increased) at a greater rate. These results are illustrated in **Figure 4a**. This indicates that the radial electric fields are changing more at greater *z*-axis position with increased trap plate potentials. By

extrapolating the trend line of the measured cyclotron frequency to 0 V on the trapping plates one will obtain the unperturbed cyclotron frequency. With 0 V applied to the trapping plates, the ions will not experience any radial fields and there should be an absence of magnetron motion. The difference between the y-intercept and the observed cyclotron frequency is the result of the magnetron frequency in the absence of space charge conditions. Differences in ion intensity at the different trap plate potentials were corrected for with the method developed by Easterling *et al*. [50]. Separate ion intensity calibration curves were constructed for the pulsed gas and non-pulsed gas experiments. Each frequency was corrected by adding the correct shift (based on ion intensity) to obtain a frequency with minimal space charge conditions. The two experiments have different calculated magnetron frequencies that result from differences in the *z*-axis oscillation amplitudes. As the trap plate potentials increase, the difference in magnetron frequency increases. This result is compared with the magnetron frequency calculated with SIMION 7.0, and is shown in **Figure 4b**. The magnetron frequency is calculated with *z*-axis amplitude of 2mm and a radius of 10mm to compare with the pulsed gas event, and also with *z*-axis amplitude of 38mm and a radius of 10mm to compare to the non-pulse gas experiment. The radius of 10mm is chosen to match the calculated excited cyclotron radius; ions will experience the radial electric force at the position they are located in the ICR cell. The experimental and calculated magnetron frequencies match closely indicating that ions of different *z*-axis oscillation amplitudes have different magnetron frequencies.

At 1 V trap potential, the frequency difference between the two experiments is ~2.5 Hz. A 1-2 Hz shift in frequency will result in a 9-18 ppm error for *m*/*z* value of

1,000 for an FTICR instrument equipped with a 7 Tesla magnet. Ions which do not have the same ion kinetic energy from scan-to-scan will have a slight variation in the observed cyclotron frequency. Thus, degradation in the observed mass measurement accuracy is expected under these conditions. Also, one might expect ions of the same cyclotron frequency but different magnetron frequency to de-phase more rapidly. A 1-2 Hz difference indicates that ions with extreme differences in *z*-axis motion (2 mm – 38 mm) will be 180^{o} out of phase within 0.5-0.25 seconds. This is in general agreement with experimental observations. The magnetron frequency decreases proportionally with increased magnetic field strength; thus the difference in magnetron frequency resultant from different oscillation amplitudes also decreases. Doubling the magnetic field strength should double the time it takes for ions to become 180^{o} out of phase. Therefore, working with higher field magnets will help, but ultimately not circumvent these problems. Improved performance must involve further ICR cell technology development.

Increased z-axis amplitude through excitation of trapping motion:

The *z*-axis motion of a cooled ion packet was excited to further probe the effect of *z*-axis distribution on observed ion cyclotron frequency. The *z*-axis motion was excited by first cooling the ion packet to the middle of the ICR cell with cooling gas followed by dropping the back trap plate to ground successive times for a total of 10 cycles. The time period that the back trap plate was held at ground was varied. This was done to excite the *z*-axis motion and move the ions from the middle of the trap. **Figure 5** illustrates the results observed by varying the duration of the "pulse length" to ground on the back trap

plate. When the back trap plate potential was dropped for a time period that approximated one period of trapping motion, the ions changed their axial distribution. The calculated trapping oscillation period for bradykinin $(M+2H)^{2+}$ with 1.5 V trapping potential was 0.323ms. If the "pulse length" was too long or too short the observed cyclotron frequency shifted back to the original frequency. The frequency of the trap plate oscillation was estimated to be one half the trapping frequency when the pulse length matched the trapping oscillation period. Therefore, at this pulse length it is possible to directly excite the axial motion and thus, increase the amplitude of ion axial oscillation . The total ion intensity shown in Figure 5 remained relatively constant indicating that ions are not being ejected from the ICR cell when the trap plate was dropped to ground. However, if the time period that the back trap plate was dropped was too long (~2ms or greater) the ion intensity decreased. This result agrees with our previous results that showed that ions with larger axial kinetic energies have lower observed cyclotron frequencies. The frequency shift observed in the experiment when the ions are given larger *z*-axis amplitude is ~4.5 Hz lower frequency. The magnetron frequency difference calculated with SIMION 7.0 for an ion with *z*-axis amplitudes of 2mm - 38mm at a 10 mm radius with 1.5 V applied trapping potential was ~4.1 Hz. The experimental results compare well with the calculated value. The decrease in the observed cyclotron frequency by increasing the *z*-axis amplitude results from a change in the magnetron frequency.

EPIC results:

EPIC was carried out to determine the effect it has on the observed cyclotron frequency as a function of *z*-axis oscillation amplitude. For the SIMION model a solid electrode is used to approximate the electron beam. Though it is not an exact solution, the model does provide a first order approximation of the electric fields inside the ICR cell with EPIC and agrees well with our previous results [40]. It is possible that the large numbers of electrons in the beam behave more like negatively charged plasma, and occupies the space between the cathode and the source trap electrode of the ICR cell. The application of EPIC flattens the radial electric field across the *z*-axis of the ICR cell at some non-zero cell radius. The radius which EPIC results in minimal change in radial field across the *z*-axis is a function of the applied trap plate potential and the number of electrons traversing the ICR cell. The ability to produce invariable radial electric fields along the *z*-axis with EPIC is shown in **Figure 6** [40]. The trapping potential was set to 1 volt on both trapping electrodes. The electrostatic potential was calculated at 1mm intervals at 42% of the cell radius with EPIC Figure 6a and under normal operation Figure 6b. Radial electric fields are also calculated and overlaid on top of the electrostatic trapping potentials. The ion oscillation length is also shown for two different ion kinetic energies. In the non-EPIC case, Figure 6b, there is a larger difference in the radial electric force experienced by ions with different kinetic energies. With EPIC the ions of different kinetic energies will experience similar radial electric fields. When the ion cyclotron radius is excited to this particular cell radius, the ions will experience the same radial force regardless of their axial distribution. Therefore, magnetron frequency and thus the observed cyclotron frequency will become independent of *z*-axis amplitude.

EPIC was carried out with a variety of applied cathode bias potentials which changes the numbers of electrons that transverse the ICR cell for both the pulse gas and non-pulsed gas experiments individually. The changes in detected cyclotron frequency observed with changing EPIC conditions for pulsed gas and non-pulsed gas experiments are shown in **Figure 7a**. With 0 volts applied to the heated cathode, the difference in observed frequency between the two experiments is approximately 6 Hz. This difference in frequency has been consistent throughout all of our experiments, with the pulse gas having a higher frequency than the non-pulse gas experiment. This also indicates that there were not enough electrons being sent through the center of the ICR cell to significantly alter the radial electric fields. As the cathode potential is biased more negatively, the observed cyclotron frequency increases for both experiments. The rates at which the frequencies increase for the two sets of experiments are different. This indicates that the radial electric field is changing greater at further distance from the center of the ICR cell. At ~ -0.38 V bias to the cathode, there is no difference in the observed cyclotron frequencies between the two different experiments. This signifies that with the application of EPIC, the radial electric fields are constant across the ICR cell at the excited cyclotron radius of the ions. If the cathode potential is further increased (negatively), the two frequencies diverge. The observed frequency with the non-pulse gas becomes greater than the pulse gas experiment. The increase in frequency is resultant from the change in magnitude and direction of the radial electric field experienced by the ions. This indicates that with careful adjustment of the number of electrons sent through the ICR cell, the observed cyclotron frequency becomes independent of the ion's *z*-axis oscillation amplitude.

To further test the effect EPIC has on the observed cyclotron frequency with *z*-axis oscillation amplitude the "double trap" experiment was conducted with EPIC. The results are shown in **Figure 7b-e.** In the non-EPIC conditions there are two separate peaks that are visible in the spectrum for the "double trap" experiment, as would be expected based on the results from Figures 1b and 7a. Results from the cooled and un-cooled single ion injection experiments are overlaid for reference of peak position. With -0.4 V applied to the cathode there is only one peak that is visible for the "double trap" experiment. This corresponds to the data from Figure 7a, where the ions from the separate ion injection events exhibited the same observed frequencies. The frequency from the single ion injection experiments with EPIC match with the double ion injection experiments with EPIC. The ion intensity for the EPIC result in the "double trap" experiment is higher than the single ion injection, since the "double trap" experiment had more ions resulting from two different ion injection events. This shows that with EPIC there is no change in observed cyclotron frequency between cooled and un-cooled ions. This is especially important for gated trapping when trapped ions may have differences in trapping oscillation amplitudes.

In our previous publication, we showed that the application of EPIC can improve the resolution and sensitivity by approximately 3-fold. Even after the ions were cooled with a collision gas and the trap plates set at low voltage potentials we were still able to see these same improvements. In the double trap experiments ions were forced to have different kinetic energies to study the change in frequency based on *z*-axis oscillation. Typically an instrument is tuned to minimize large differences in axial kinetic energy. If the instrument is not properly tuned this energy distribution may lead to peak splitting

and rapid de-phasing of the ion packet. However, in almost all cases a distribution of *z*-axis kinetic energy still persists. This is important because these ions will have slightly different reduced cyclotron frequencies which will not result in corresponding peaks in the mass spectra but rather a decrease in ion intensity as the ion packets de-phase as well as peak broadening.

Conclusions

The observed cyclotron frequency for ions that have been cooled to the middle of the ICR cell is higher than for ions with larger *z*-axis oscillation amplitudes. Space charge effects did not appear to have a significant impact on the measured ion cyclotron frequency. However, the dominant divergence in observed cyclotron frequency between ion packets of distinctly different kinetic energy can be attributed to the difference in axial oscillation amplitude of the ions along the center of the ICR cell. Bradykinin $(M+2H)^{2+}$ ions of different axial kinetic energies were detected in the same spectrum to minimize differences that are associated with changing space charge conditions. At the excited ion cyclotron radii, the ion will experience differences in the radial electric field as it transverses the ICR cell. These differences become larger as difference in the ion kinetic energy increases. Since the force from the radial electric field produces magnetron motion, the magnetron frequency will change at different axial positions. Ions of different axial amplitude exhibit different magnetron frequencies which were determined experimentally and correlated well with the theoretical magnetron frequencies calculated in SIMION 7.0. Changes in magnetron frequency produce

differences in observed cyclotron frequency. With the application of EPIC, changes in the radial electric field across the *z*-axis of the ICR cell at a selected cyclotron radius can be minimized. Therefore, as the ions of different kinetic energy oscillate along the *z*-axis of the ICR cell, they will experience little change in the radial electric field. Thus, the observed cyclotron frequency becomes independent of *z*-axis position. This can have significance in terms of ion de-phasing.

Acknowledgements

The authors acknowledge helpful discussions with Drs. Jean Futrell and Göhkan Baykut. This material is based upon work supported by the National Science Foundation under Grant No. 0352451; Murdock Charitable Trust; Office of Science (BER), U. S. Department of Energy, Grant No. DE-FG02-04ER63924, and the National Institutes of Health Biotechnology Training Grant.

References

1. Marshall, A. G., Hendrickson, C. L., Jackson, G. S., Fourier transform ion cyclotron resonance mass spectrometry: a primer, *Mass Spectrometry Reviews*. **1998,** *17*, 1-35.

2. Comisarow, M. B., Marshall, A. G., Fourier transform ion cyclotron resonance spectroscopy, *Chemical Physics Letters*. **1974,** *25*, 282-283.

3. Senko, M. W., Hendrickson, c. L., Emmett, M. R., Shi, S. D. H., Marshall, A. G., External accumulation of ions for enhanced electrospray ionization Fourier transform ion cyclotron resonance mass spectrometry, *Journal of the American Society for Mass Spectrometry*. **1997,** *8*, 970-976.

4. Sharma, S., Simpson, D. C., Tolic, N., Jaitly, N., Mayampurath, A. M., Smith, R. D., Pasa-Tolic, L., Proteomic Profiling of Intact Proteins Using WAX-RPLC 2-D Separations and FTICR Mass Spectrometry, *Journal of Proteome Research*. **2007,** *6*, 602-610.

5. Belov, M. E., Anderson, G. A., Wingerd, M. A., Udseth, H. R., Tang, K., Prior, D. C., Swanson, K. R., Buschbach, M. A., Strittmatter, E. F., Moore, R. J., Smith, R. D., An automated high performance capillary liquid chromatography-Fourier transform ion cyclotron resonance mass spectrometer for high-throughput proteomics, *Journal of the American Society for Mass Spectrometry*. **2004,** *15*, 212-232.

6. Gorshkov, M. V., Masselon, C. D., Anderson, G. A., Udseth, H. R., Harkewicz, R., Smith, R. D., A dynamic ion cooling technique for FTICR mass spectrometry, *Journal of the American Society for Mass Spectrometry*. **2001,** *12*, 1169-1173.

7. Alford, J. M., Williams, P. E., Trevor, D. J., Smalley, R. E., Metal cluster ion cyclotron resonance. Combining supersonic metal cluster beam technology with FT-ICR, *International Journal of Mass Spectrometry and Ion Processes*. **1986,** *72*, 33-51.

8. Caravatti, P., Method and Apparatus for The Accumulation of Ions in a Trap of an Ion Cyclotron Resonance Spectrometer, by Transferring the Kinetic Energy of the Motion Parallel to the Magnetic Field into Directions Perpendicular to the Magnetic Field., *US Patent. 4,924,089.* **1990.**

9. Marto, J. A., Marshall, A. G., Schweikhard, L., A two-electrode ion trap for Fourier transform ion cyclotron resonance mass spectrometry, *International Journal of Mass Spectrometry and Ion Processes*. **1994,** *137*, 9-30.

10. Guan, S., Marshall, A. G., Ion traps for Fourier transform ion cyclotron resonance mass spectrometry: principles and design of geometric and electric configurations, *International Journal of Mass Spectrometry and Ion Processes*. **1995,** *146/147*, 261-296.

11. McIver, R. T., Jr., Baranyi, A. D., High resolution ion cyclotron resonance spectroscopy, *International Journal of Mass Spectrometry and Ion Physics*. **1974,** *14*, 449-458.

12. Marshall, A. G., Theory for ion cyclotron resonance absorption line shapes, *J Chem Phys*. **1971,** *55*, 1343-1354.

13. McIver, R. T., Jr., Ledford, E. B., Jr., Miller, J. S., Proposed method for mass spectrometric analysis for ultra-low vapor pressure compounds, *Analytical Chemistry*. **1975,** *47*, 692-697.

14. Brown, L. S., Gabrielse, G., Geonium theory: physics of a single electron or ion in a Penning trap, *Reviews of Modern Physics*. **1986,** *58*, 233-311.

15. Holliman, C. L., Rempel, D. L., Gross, M. L., A mechanism for poor high mass performance in Fourier transform mass spectrometry, *Journal of the American Society for Mass Spectrometry*. **1992,** *3*, 460-463.

16. Hartmann, H., Chung, K. M., Baykut, G., Wanczek, K. P., Dependence of ion cyclotron frequency on electric field inhomogeneity, *J Chem Phys*. **1983,** *78*, 424-431.

17. Mitchell, D. W., Theory of trapped ion motion in the non-quadrupolar electrostatic potential of a cubic ion cyclotron resonance cell, *International Journal of Mass Spectrometry and Ion Processes*. **1995,** *142*, 1-22.

18. Comisarow, M., Fourier transform ion cyclotron resonance spectroscopy, *Advances in Mass Spectrometry*. **1978,** *7B*, 1042-1046.

19. Mitchell, D. W., Smith, R. D., Prediction of a space charge induced upper molecular mass limit towards achieving unit mass resolution in Fourier transform ion cyclotron resonance mass spectrometry, *Journal of Mass Spectrometry*. **1996,** *31*, 771-790.

20. Bruce, J. E., Anderson, G. A., Lin, C.-Y., Gorshkov, M., Rockwood, A. L., Smith, R. D., A novel high-performance Fourier transform ion cyclotron resonance cell for improved biopolymer characterization, *Journal of Mass Spectrometry*. **2000,** *35*, 85-94.

21. Vartanian, V. H., Hadjarab, F., Laude, D. A., Open cell analog of the screened trapped-ion cell using compensation electrodes for Fourier transform ion cyclotron resonance mass spectrometry, *International Journal of Mass Spectrometry and Ion Processes*. **1995,** *151*, 175-187.

22. Barlow, S. E., Tinkle, M. D., "Linearizing" an ion cyclotron resonance cell, *Review of Scientific Instruments*. **2002,** *73*, 4185-4200.

23. Wang, M., Marshall, A. G., A "screened" electrostatic ion trap for enhanced mass resolution, mass accuracy, reproducibility, and upper mass limit in Fourier-transform ion cyclotron resonance mass spectrometry, *Analytical Chemistry*. **1989,** *61*, 1288-1293.

24. Jackson, G. S., White, F. M., Guan, S., Marshall, A. G., Matrix-shimmed ion cyclotron resonance ion trap simultaneously optimized for excitation, detection, quadrupolar axialization, and trapping, *Journal of the American Society for Mass Spectrometry*. **1999,** *10*, 759-769.

25. Rempel, D. L., Ledford, E. B., Jr., Huang, S. K., Gross, M. L., Parametric mode operation of a hyperbolic Penning trap for Fourier transform mass spectrometry, *Analytical Chemistry*. **1987,** *59*, 2527-2532.

26. Guan, S., Wahl, M. C., Wood, T. D., Marshall, A. G., Enhanced mass resolving power, sensitivity, and selectivity in laser desorption Fourier transform ion cyclotron resonance mass spectrometry by ion axialization and cooling, *Anal Chem*. **1993,** *65*, 1753-1757.

27. Shi, S. D. H., Hendrickson, C. L., Marshall, A. G., Counting individual sulfur atoms in a protein by ultrahigh-resolution Fourier transform ion cyclotron resonance mass spectrometry: experimental resolution of isotopic fine structure in proteins, *Proceedings of the National Academy of Sciences of the United States of America*. **1998,** *95*, 11532-11537.

28. Winger, B. E., Hofstadler, S. A., Bruce, J. E., Udseth, H. R., Smith, R. D., High-resolution accurate mass measurements of biomolecules using a new electrospray ionization ion cyclotron resonance mass spectrometer, *Journal of the American Society for Mass Spectrometry*. **1993,** *4*, 566-577.

29. Sack, T. M., Gross, M. L., Pulsed valve interface for gas chromatography/Fourier transform mass spectrometry, *Analytical Chemistry*. **1983,** *55*, 2419-2421.

30. Hogan, J. D., Laude, D. A., Jr., Suspended trapping procedure for alleviation of space charge effects in gas chromatography/Fourier-transform mass spectrometry, *Analytical Chemistry*. **1990,** *62*, 530-535.

31. Dunbar, R. C., Weddle, G. H., Ion cyclotron resonance time-of-flight spectroscopy. Kinetic energy of p-iodotoluene photodissociation fragment ions, *J Phys Chem*. **1988,** *92*, 5706-5709.

32. Wilcox, B. E., Hendrickson, C. L., Marshall, A. G., Improved ion extraction from a linear octopole ion trap: SIMION analysis and experimental demonstration, *J Am Soc Mass Spectrom*. **2002,** *13*, 1304-1312.

33. Mitchell, D. W., Realistic simulation of the ion cyclotron resonance mass spectrometer using a distributed three-dimensional particle-in-cell code, *Journal of the American Society for Mass Spectrometry*. **1999,** *10*, 136-152.

34. Tinkle, M. D., Barlow, S. E., Image charge forces inside conducting boundaries, *J Appl Phys*. **2001,** *90*, 1612-1624.

35. Marshall, A. G., Milestones in Fourier transform ion cyclotron resonance mass spectrometry technique development, *International Journal of Mass Spectrometry*. **2000,** *200*, 331-356.

36. Bloom, M., Riggin, M., Theory of ion cyclotron resonance, *Can J Phys*. **1974,** *52*, 436-455.

37. Vartanian, V. H., Laude, D. A., Motional averaging of ions for control of magnetron motion in Fourier transform ion cyclotron resonance open-geometry trapped-ion cells, *International Journal of Mass Spectrometry*. **1998,** *178*, 173-186.

38. Kaiser, N. K., Bruce, J. E., Observation of Increased Ion Cyclotron Resonance Signal Duration through Electric Field Perturbations, *Analytical Chemistry*. **2005,** *77*, 5973-5981.

39. Kim, S., Choi, M. C., Kim, S., Hur, M., Kim, H. S., Yoo, J. S., Blakney, G. T., Hendrickson, C. L., Marshall, A. G., Modification of Trapping Potential by Inverted Sidekick Electrode Voltage during Detection To Extend Time-Domain Signal Duration for Significantly Enhanced Fourier Transform Ion Cyclotron Resonance Mass Resolution, *Analytical Chemistry*. **2007,** *79*, 3575-3580.

40. Kaiser, N. K., Bruce, J. E., Reduction of ion magentron motion and space charge using radial electric field modulation, *International Journal of Mass Spectrometry*. **2007,** 265, 271-280.

41. Gillig, K. J., Bluhm, B. K., Russell, D. H., Ion motion in a Fourier transform ion cyclotron resonance wire ion guide cell, *International Journal of Mass Spectrometry and Ion Processes*. **1996,** *157/158*, 129-147.

42. Solouki, T., Gillig, K. J., Russell, D. H., Detection of High-Mass Biomolecules in Fourier Transform Ion Cyclotron Resonance Mass Spectrometry: Theoretical and Experimental Investigations, *Analytical Chemistry*. **1994,** *66*, 1583-1587.

43. Caravatti, P., Allemann, M., The infinity cell: a new trapped-ion cell with radiofrequency covered trapping electrodes for Fourier transform ion cyclotron resonance mass spectrometry, *Organic Mass Spectrometry*. **1991,** *26*, 514-518.

44. Anderson, G. A., Bruce J.E., Smith R.D., ICR-2LS, Richland, WA, **1996**.

45. Bresson, J. A., Anderson, G. A., Bruce, J. E., Smith, R. D., Improved isotopic abundance measurements for high resolution Fourier transform ion cyclotron resonance mass spectra via time-domain data extraction, *Journal of the American Society for Mass Spectrometry*. **1998,** *9*, 799-804.

46. Du, Y., Parks, B. A., Sohn, S., Kwast, K. E., Kelleher, N. L., Top-Down Approaches for Measuring Expression Ratios of Intact Yeast Proteins Using Fourier Transform Mass Spectrometry, *Analytical Chemistry*. **2006,** *78*, 686-694.

47. Francl, T. J., Sherman, M. G., Hunter, R. L., Locke, M. J., Bowers, W. D., McIver, R. T., Jr., Experimental determination of the effects of space charge on ion cyclotron resonance frequencies, *International Journal of Mass Spectrometry and Ion Processes*. **1983,** *54*, 189-199.

48. Ledford, E. B., Jr., Rempel, D. L., Gross, M. L., Space charge effects in Fourier transform mass spectrometry. Mass calibration, *Anal Chem*. **1984,** *56*, 2744-2748.

49. Dunbar, R. C., Chen, J. H., Hays, J. D., Magnetron motion of ions in the cubical ICR cell, *International Journal of Mass Spectrometry and Ion Processes*. **1984,** *57*, 39-56.

50. Easterling, M. L., Mize, T. H., Amster, I. J., Routine part-per-million mass accuracy for high-mass ions: space-charge effects in MALDI FT-ICR, *Analytical Chemistry*. **1999,** *71*, 624-632.

Figure 1

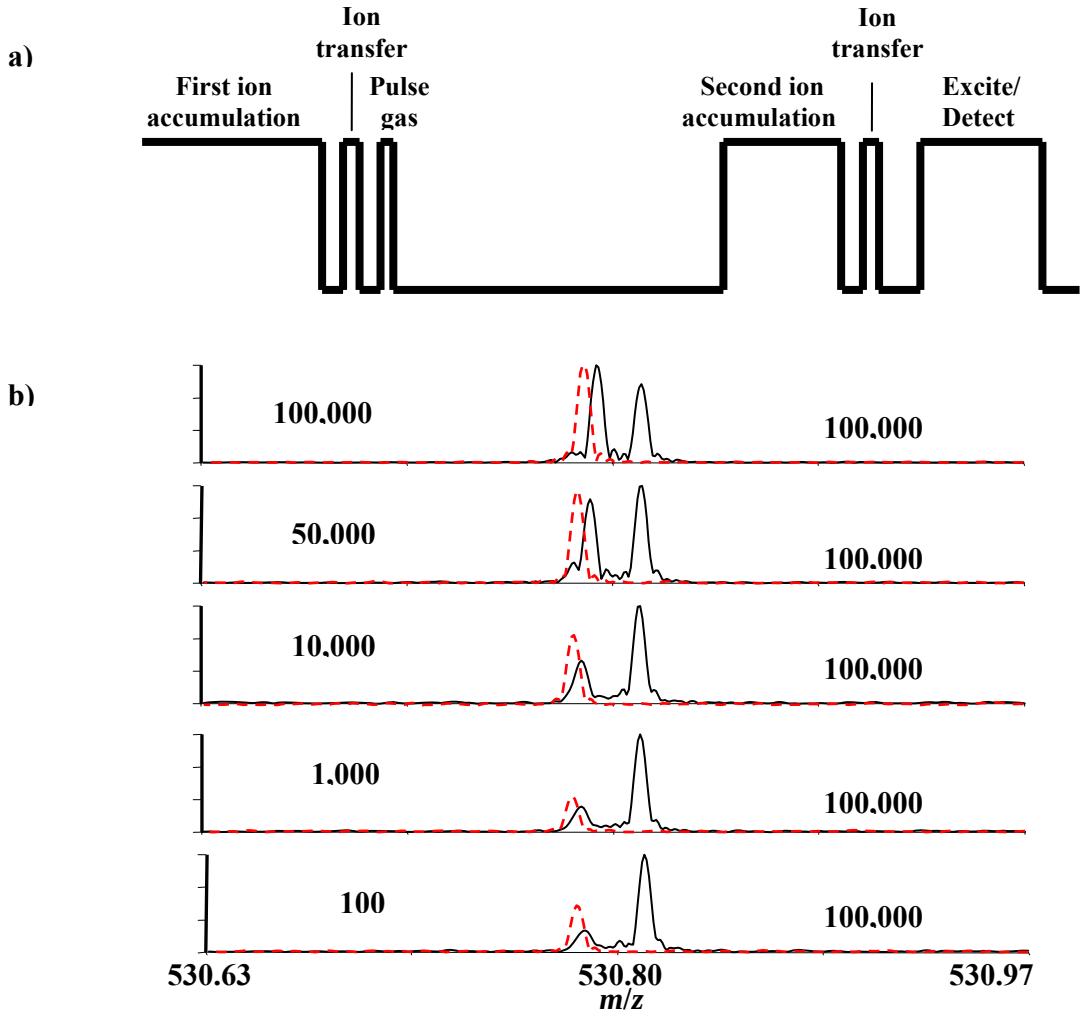

Figure 1. "Double trap" experiment. a) Pulse sequence for the "double trap" experiment that includes two separate ion injection events. b) The monoisotopic peak of Bradykinin $(M+2H)^{2+}$ with different ion accumulation time periods given in μs. Solid line represents the "double trap" experiment. The first ion accumulation time period (located left of the peak) was varied while the second ion accumulation time period (located to the right of the peak) remained constant. The dotted line represents a single ion injection which corresponds to the first ion injection event (cooled ion packet) of the "double trap" experiment. The accumulation for the single ion injection experiment was also varied.

Figure 1 c)

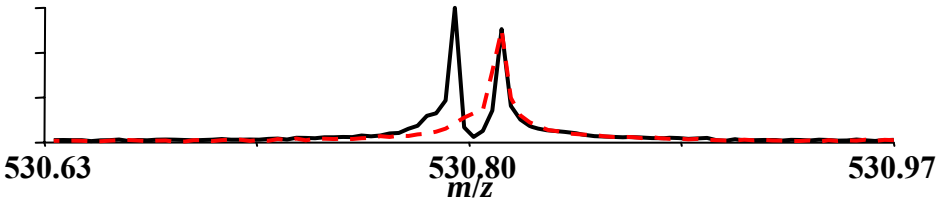

. c) The solid line is the "double trap" experiment and the dotted line is a single ion injection which corresponds to the second ion injection event of the double trap experiment.

Figure 2

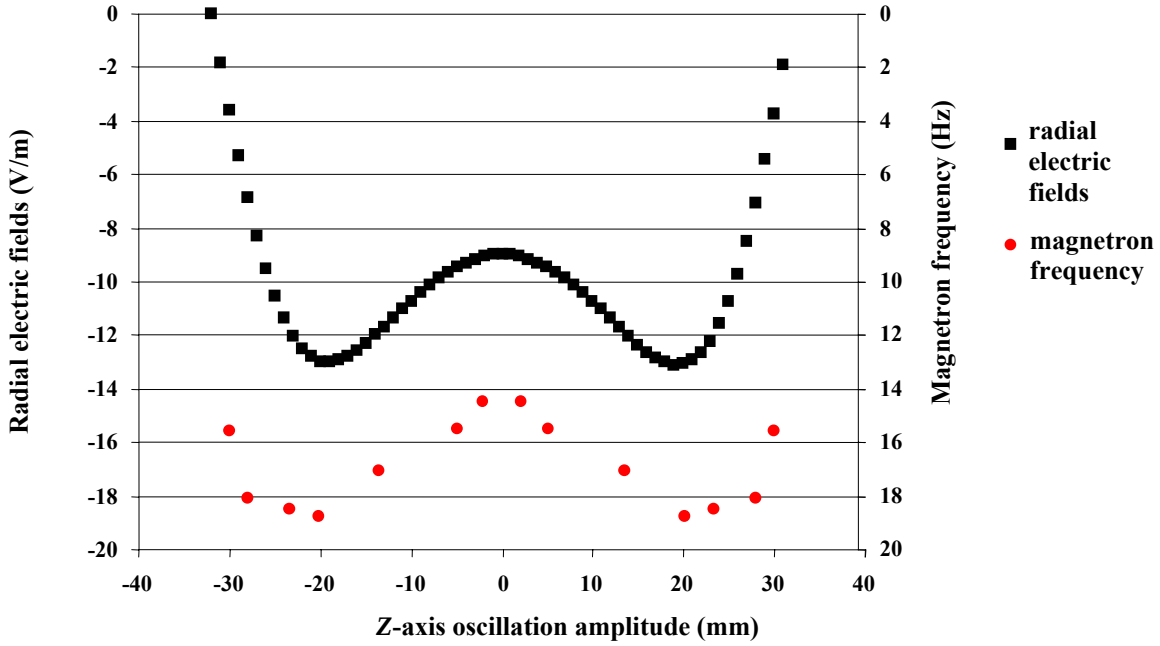

Figure 2. SIMION calculated radial electric fields and magnetron frequency at 45% of the ICR cell radius with 1V applied to the trap electrodes. The center of the ICR cell is set at 0 mm.

Figure 3

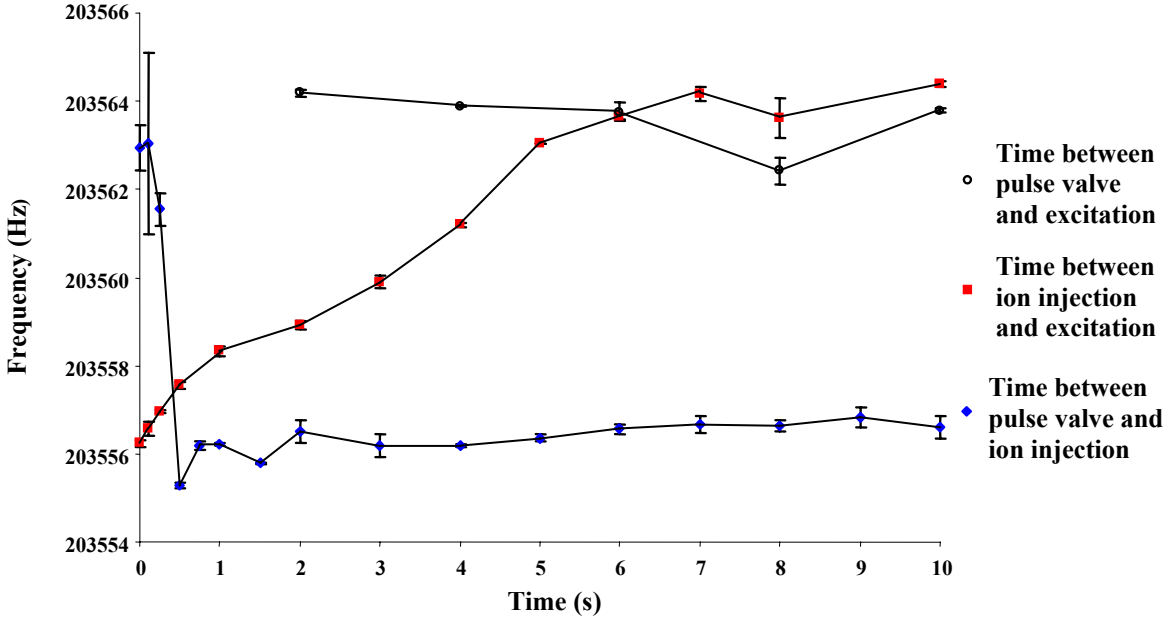

Figure 3. Observed cyclotron frequency of the monoisotopic peak from bradykinin $(M+2H)^{2+}$ with different time delays between events. The error bars represent the maximum and minimum values obtained for each data set.

Figure 4

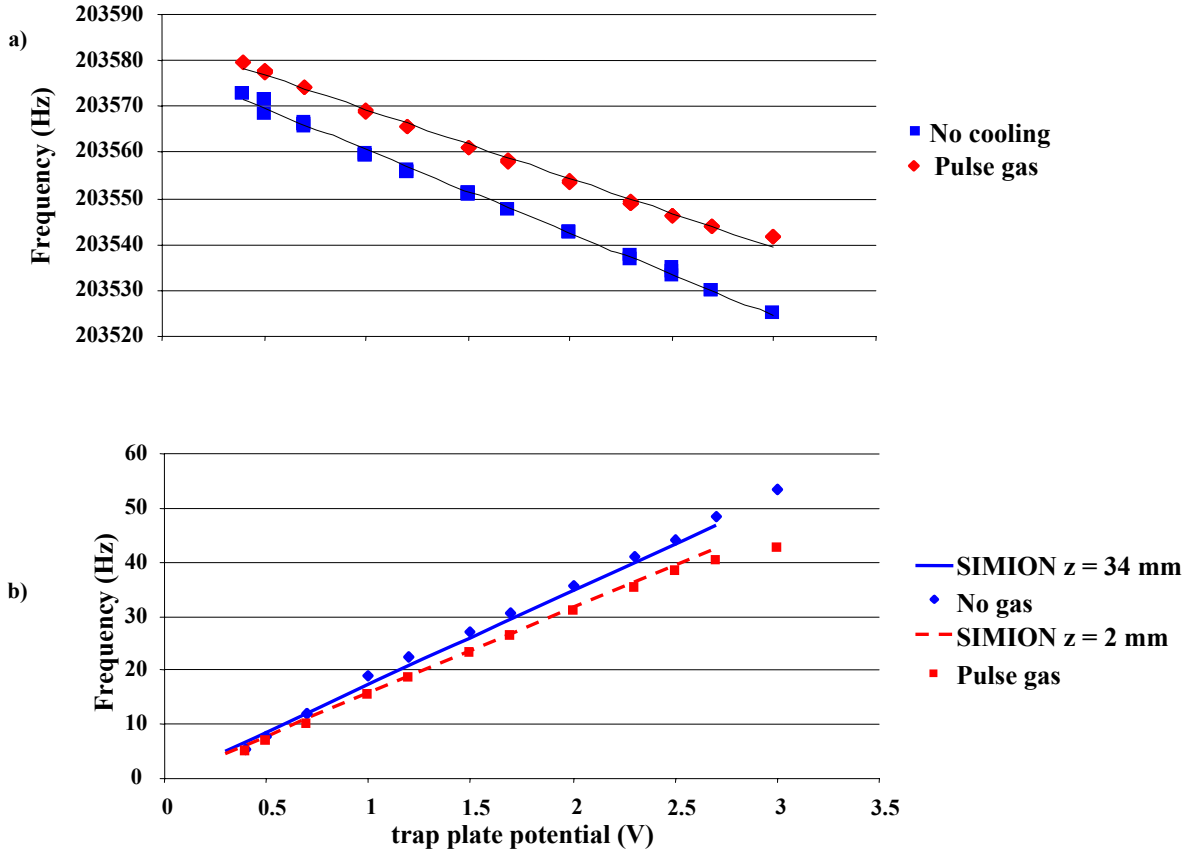

Figure 4. a) Observed cyclotron frequency of bradykinin $(M+2H)^{2+}$ at different trap plate potentials with the pulsed gas and non-pulsed gas experiments. b) The experimentally derived magnetron frequencies at different trap plate potentials for the pulsed gas and non-pulsed gas experiment are compared to the magnetron frequencies calculated with SIMION.

Figure 5

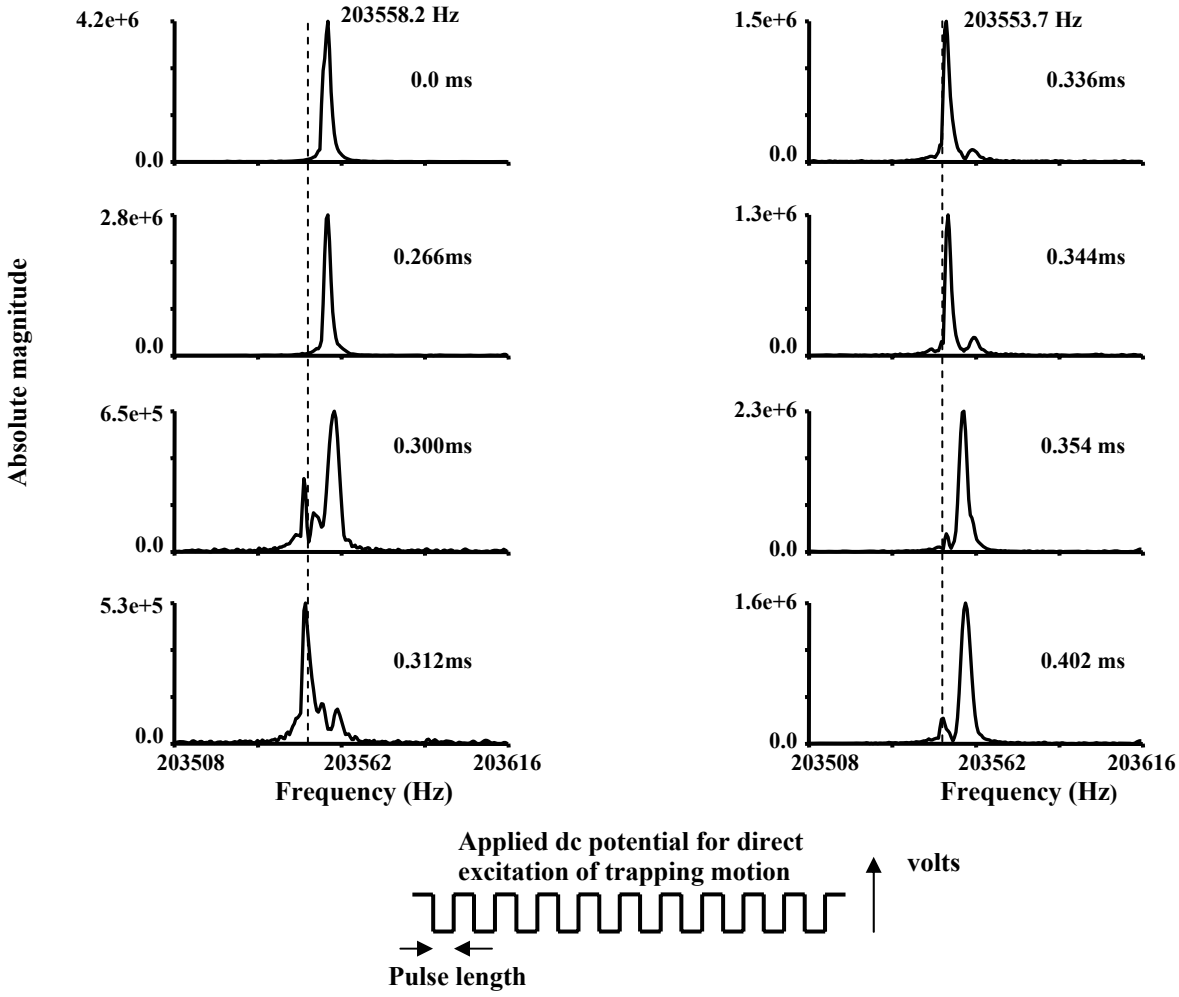

Figure 5. Observed cyclotron frequency of bradykinin $(M+2H)^{2+}$ after *z*-axis excitation. Ions are first cooled with a pulse gas event, and then displaced axially by dropping the back trap plate 10 times. The time given represents the "pulse length" or time period the back trap plate was dropped to ground. The dashed line represents the same frequency in both columns and is added to provide a reference point for the frequency shift.

Figure 6

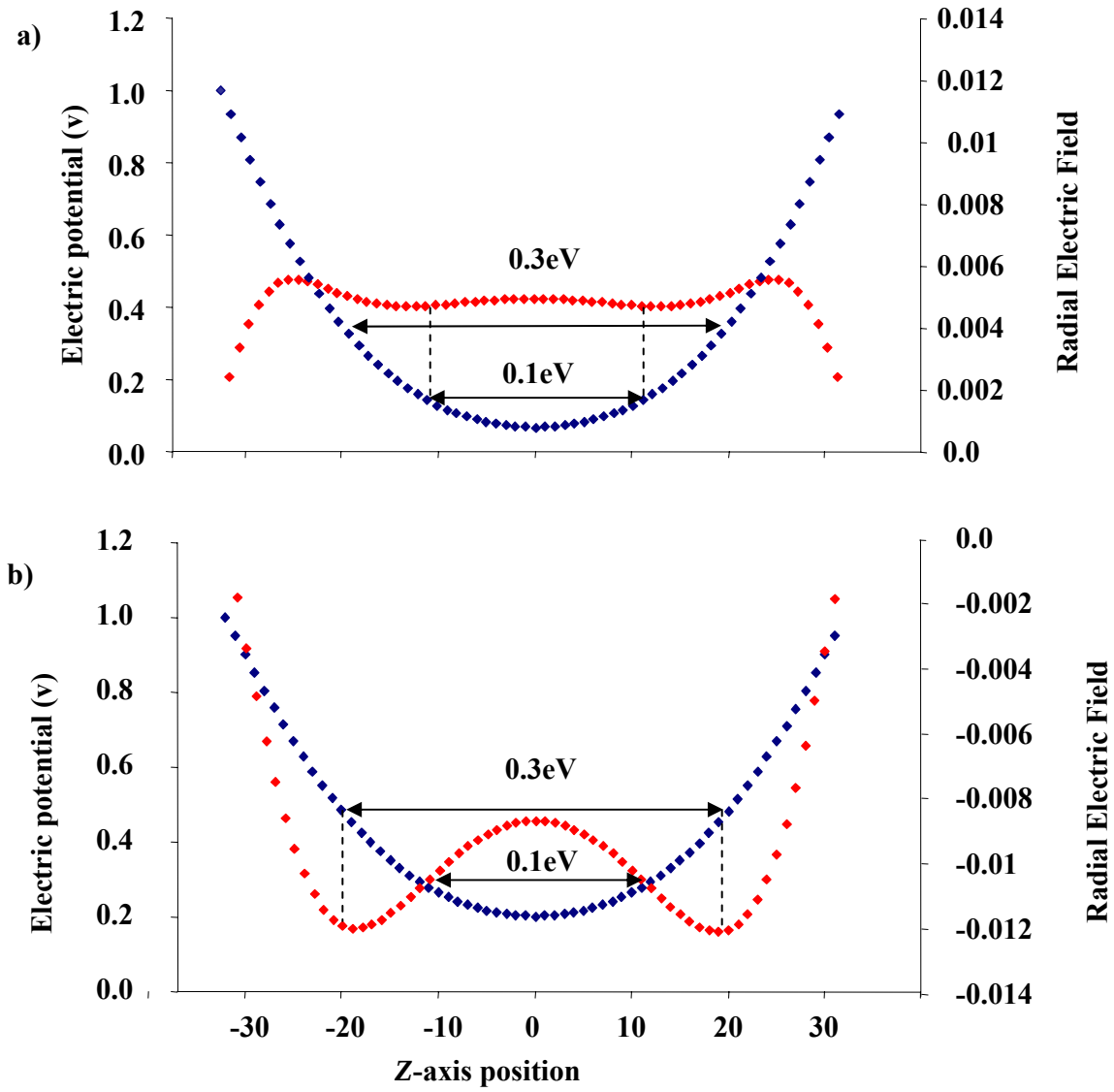

Figure 6. SIMION calculations of the radial electric field and electric potential at 42% of the ICR cell radius. a) EPIC with -0.2 V applied to the central electrode and 1 volt applied to the trap electrodes. b) Closed cylindrical cell with 1 volt applied to the trap electrodes.

Figure 7

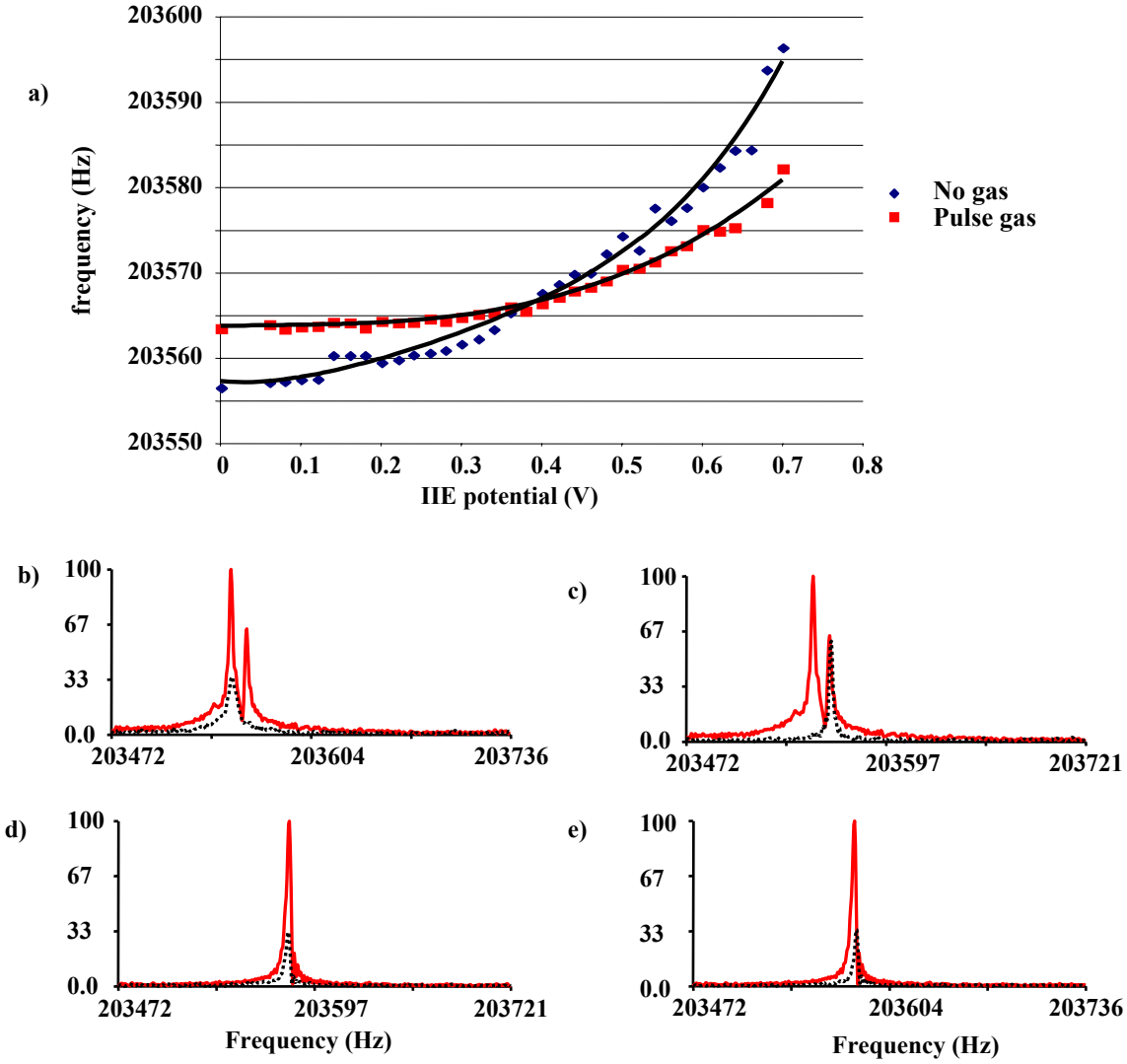

Figure 7. EPIC experiments a) Comparison of the observed cyclotron frequency for the monoisotopic peak of bradykinin $(M+2H)^{2+}$ for the pulsed gas and non-pulsed gas experiment with EPIC at different bias potentials applied to the heated cathode.
b) non-EPIC conditions, the dotted line represents the second ion injection event only. c) non-EPIC conditions, the dotted line represents the first ion injection only. d) Cathode potential set at -0.4 V, the dotted line represents the second ion injection event only. e) Cathode potential set at -0.4 V, the dotted line represents the first ion injection event only. The "double trap" experiment is indicated by the solid line, the single ion injection experiment is indicated by the dotted line.

CHAPTER 6

Restrained Ion Population Transfer: A Novel Ion Transfer Method for Mass Spectrometry

Abstract

With modern Fourier transform ion cyclotron resonance (FTICR) mass spectrometers the ion accumulation event takes place in a region of higher pressure which allows ions to be thermally cooled before being accelerated toward the ICR cell where they are decelerated and re-trapped. This transfer process induces mass discrimination due to time-of-flight effects. Also, trapping ions with substantial axial kinetic energy can decrease the performance of the ICR instrument when compared to the analysis of thermally-cooled ions located at the trap center. Therefore, it is desirable to limit the energy imparted to the ions within the ICR cell as well as minimize time-of-flight effects. The approach presented here for ion transfer called restrained ion population transfer or RIPT is designed to provide complete axial containment of an ion population throughout the entire transfer process from the accumulation region to the ICR cell eliminating mass discrimination associated with time-of-flight separation. This is accomplished by utilization of a number of quadrupole segments arranged in series with independent control of the dc bias voltage applied to each segment of the quadrupole ion guide. The dc bias voltage is applied in such a way to minimize the energy imparted to the ions allowing transfer of ions with low kinetic energy from the ion accumulation region to the ICR cell. Initial ICR data is presented which illustrates the feasibility of RIPT. The

technique was also modeled with SIMION 7.0 and simulation results that support our feasibility studies of the ions transfer process are presented.

Introduction:

Fourier transform ion cyclotron resonance mass spectrometry[1] (FTICRMS) is well-suited for the analysis of biological molecules and complex mixtures[2-7]. In most modern FTICR mass spectrometers, ions are created external to the mass analyzer. External ion production allows for large populations of ions to be accumulated before transfer to the ICR cell for mass analysis. External ion accumulation has been shown to improve the signal-to-noise ratio and mass resolving power, and increase the duty cycle to nearly 100% [8, 9]. Ions are typically accumulated inside an ion trap a significant distance from the ICR cell to allow for multiple stages of differential vacuum pumping and reduce interference resultant from fringe magnetic fields produced from the high field magnet needed for ICR analysis. Though gated trapping has proven to be an extremely useful technique it is not without limitations. The ions which are originally trapped in the accumulation region are accelerated toward the ICR cell with no axial constraints and are to be decelerated and re-trapped once they reach the ICR cell. A number of different ion transfer devices have been developed to transfer ions to the ICR cell, such as, a number of RF multipole devices[10, 11], stacked-ring electrostatic guide[12], charged wire ion guide[13], and electrostatic focusing elements[14].

In ICR instruments which have external ion sources, there is typically a meter or more separation in distance between the accumulation region and the ICR cell. This separation in space leads to time-of-flight dispersion of the injected ions which can result in significant mass discrimination when ions are pulsed to and trapped in an ICR cell

using gated trapping[15, 16]. Therefore, all *m*/*z* species trapped in the accumulation region are not equally represented in ICR cell. Pulsed extraction of ions to the ICR cell limits the *m*/*z* range that can be detected in a single scan. Therefore, gated trapping may require multiple ion injection events with varied trapping delays to sample the entire mass range of interest[17]. Ions with different *m*/*z* ratios will have different optimal ion transfer times. Another aspect to consider when performing gated trapping of ions in the ICR cell is that not all ions are pulsed from the accumulation region through the ion guide at the same time. The length of a multipole ion trap is usually chosen to be much larger than its width to store a large number of ions without excessive space-charge repulsion. This results in low penetration of the trapping dc potential field in a multipole storage device in the central region of the trap. Therefore, ions of the same *m*/*z* but with different axial position or velocity trapped in the accumulation region will be ejected at slightly different times, which will reduce the efficiency of gated trapping in the ICR cell. Since the ion transfer process can result in a loss of ions, longer accumulation times are required. Also, the rate of ion injection depends on the space-charge repulsion resultant from the total number of ions present in the multipole ion trap[9, 18].

It has been shown that by producing an axial potential gradient inside a multipole ion trap, the ion exit time distribution can be reduced by an order of magnitude relative to the application of potentials only to the trapping lenses[19]. Thomson *et. al*. investigated various methods to produce axial potential gradients in the quadrupole collision cell of a triple quadrupole instrument to decrease ion transient time while maintaining the same ion transmission efficiency[20]. Axial potential gradients have been produced within the accumulation region through a variety of methods, such as an angled wire arrangement

between parallel rods of a multipole[19, 21, 22], the introduction of conical multipole rods[23], encasing the multipole with segmented rings[24], and by segmenting the multipole rods[9, 20]. Though these methods can reduce the ion exit time distribution and increase the number of ions reaching the ICR cell at the same time, there are still time-of-flight effects present when trapping a wide *m*/*z* range. In the accumulation region of an FTICR instrument, low energy collisions with background gas can cool ions both internally and translationally. However, raising the potential of the accumulation cell to push the ions toward the ICR cell gives ions axial kinetic energy; this can result in the requirement of larger trapping potentials in the ICR cell. High trap plate potentials increase the ion capacity in the ICR cell, resulting in the detection of a larger number of ions.[16, 25, 26] However, increased trap plate potentials typically increase radial ion ejection[26], space charge frequency shifts[27-29], and peak coalescence[30, 31] which result in lower quality spectral data and make the mass calibration less accurate. Longer transients and higher resolution spectra are more readily attained at lower trap plate potentials[32-34]. It can be desirable to perform quadrupolar excitation in the presence of a collision gas once ions reach the ICR cell, so that ions collect axially near the trap center where there is a near-perfect quadrupolar electrostatic trapping potential[35, 36]. However, this results in an undesirable pumping delay to reestablish an optimal pressure in the ICR cell region before ion excitation and detection. Thus, it is not suitable when high duty cycle is required. Ultimately, it would be attractive to trap ions with low initial axial kinetic energy in the ICR cell which leads to increased instrument performance[37].

In this paper we present a novel ion transfer technique, called Restrained Ion Population Transfer, or RIPT, which provides complete axial containment of the ions

from the accumulation region to the ICR cell by controlling their position in the ion guide. This technique utilizes a number of quadrupole sets arranged in series with each other. The ion guide has individually controllable dc potentials applied to each quadrupole set to allow control of the axial position of the ions. A similar approach to control ion axial position has been used to increase the efficiency of ion transfer through intermediate pressure regions using individually controllable dc potentials with a stacked ring ion guide[38-40]. That technique utilizes a traveling dc wave coupled to a RF stacked ring collision cell or ion accumulation region to reduce the exit time of a packet of ions from the cell. With this method the kinetic energy of the ions can be reduced by slowing down the waveform and allowing more time for ions to collide with neutral gas molecules. The rate at which the traveling dc potential wave moves through cell does not allow time for the ions to oscillate between waveforms (~300m/s); therefore, the ions are typically located at the leading edge of the waveform as they are pushed through the device. Each voltage step will cause an increase in ion kinetic energy which is then offset by collisions with neutral molecules. Unfortunately, FTICR measurements are done at pressures orders of magnitude lower than the technique mentioned above. Thus for every voltage step there are few ion neutral collisions to minimize the kinetic energy imparted to the ions as in the previous method.

To overcome this problem, our dc ramp sequence is designed to limit the amount of energy distributed to the ion, without needing a collision gas to continually cool the ions. The rate at which the ions move through the ion guide is also much slower (<10m/s) which allows the ions to oscillate within each quadrupole segment which is crucial in minimizing the kinetic energy imparted to the ions. Our technique is designed

to offer an alternative ion transfer technique under ultra-high vacuum conditions needed for FTICRMS. However, this ion guide could be used in any type of mass spectrometer to transfer ion packets with low kinetic energies. Instead of pulsing the ion packet out of the accumulation region, which introduces time-of-flight *m*/*z* discrimination and requires re-trapping of the ions at the ICR cell, we maintain complete containment of the ion packet throughout the entire ion transfer process. This technique eliminates time-of-flight effects associated the ion transfer process by injecting all ions in the ICR cell at the same time, as well as minimizes axial kinetic energy imparted to the ions.

Experimental:

SIMION SIMULATIONS:

Ion trajectory modeling was performed with SIMION 7.0 software (SIMION 7.0 3D, version 7.0, D.A. Dahl. Idaho National Engineering Laboratory, Idaho Falls, ID) running on a 2.80 GHz Pentium 4 PC with 768 MB RAM. For the simulation, nine quadrupoles were arranged in series. Each of the quadrupole segments was 200 mm in length, with a 6 mm space between each segment. Simulations were run at two different settings; RF voltage amplitude = 500 $V_{p\text{-}p}$, and frequency, $\Omega/2\pi$ = 1.6 MHz, and RF voltage = 220 $V_{p\text{-}p}$ and frequency 860 kHz. The initial ion kinetic energy (mass-to-charge ratio, *m*/*z* = 2,000, 1,000, and 400) was set at 0.1 eV for all simulations. The final kinetic energy, ion time-of-flight, and final ion *z*-axis position were recorded when the ion reached the end of the last quadrupole segment. Ions were created with 0.1 eV of

kinetic energy at the entrance of the ion guide on the central axis with various initial angles (within 4^{o} of center in both the *x* and *y* direction). After an initial delay period which allowed time for the ions to reach the second segment (1-2 ms), the dc bias applied to the first segment was ramped up to trap the ions. The ions are trapped in a region of the ion guide created by a low dc bias voltage applied to quadrupole segment (x) and a higher dc voltage bias applied to the quadrupole segments on either side. Throughout all simulations, the low dc bias voltage was set at 0 V, and the high dc bias voltage was set at 10 V unless otherwise noted. Ion transfer is accomplished by the application of a dc bias voltage ramp on quadrupole segments (x+1) and (x-1) while maintaining segment x at 0 V, the same RF voltage applied to all segments. At the start of each ramp cycle, the initial bias voltage applied to segment (x) and (x-1) was at 0 V, all other segments were held at a bias voltage of 10 V. Ions are transferred through the ion guide by holding segment (x) at 0 V and then simultaneously raising the voltage bias on segment (x-1) until it reaches 10 V and lowering the voltage bias on segment (x+1) until it reaches the same voltage bias as segment (x). The rates at which the voltages on the quadrupole segments are raised and lowered were varied to investigate the effects that the ramp times have on the ion kinetic energy as they exit the ion guide. Each ion trajectory was simulated individually; ion-ion Coulombic repulsion was not included in these simulations. The overall goal of the simulations was to determine the effects that the dc ramping rates have on the resultant ion kinetic energy, which to a first approximation, are independent of ion-ion repulsion. Experimentally, long accumulation times may result in excessive ion-ion repulsion causing discrimination against higher charge states and lower *m*/*z* species[41].

INSTRUMENTATION:

All peptides were purchased from Sigma (St. Louis, MO). They were dissolved in a solution of 49:49:2 by volume of methanol, water, and acetic acid and diluted to 10 μM. Electrospray was used as the ionization source. A syringe pump was used to infuse the sample at a rate of 0.4 μL/min. Approximately 2.6 kV was applied to the spray solution through a metal union. Ions entered the vacuum system through a flared inlet metal capillary[42, 43]. The FTICR mass spectrometer developed in our laboratory will be described in full detail in CHAPTER 7. Ions were accumulated in the first quadrupole region of the instrument at a pressure of 7.9×10^{-3} Torr. The RIPT quadrupole shown in **Figure 1** was divided into 19 segments 3" long. The gaps between the segments were 0.20". The total length of the ion guide was approximately 61". The spacers in the high vacuum region (6×10^{-6} Torr) were constructed out of Ultem, and the spacers in the ultra high vacuum region $<1 \times 10^{-6}$ Torr were constructed out of Macor. The quadrupole was constructed with a solid 0.25" aluminum rod that runs the entire length of the ion guide. 4-40 vented bolts which thread into the aluminum rods are used to secure the rods against the spacers. The RF voltage is applied directly to these aluminum rods. Aluminum tube 0.27" I.D. and 0.38" O.D are placed over these solid rods. Small mylar sheets were rolled up and placed between the solid aluminum rods and aluminum tubes. The mylar sheet acted as an insulator between the surface of the rod and the tube to allow separate dc voltages to be applied to each tube and capacitive coupling of RF to each segment. The RF voltage was coupled from the rods to the tubes at approximately 75 – 80%

efficiency. Kapton wire was used to carry the electric potential from the feedthrough to each segment. The potential split through 2 resistors (1 MΩ) in parallel, one for each phase of RF. The dc potential was applied to each of the tubes through a terminal held in place with a 2-56 screw that was threaded into the aluminum tube; there were screws at each end of the tubes to secure the tubes tight to the aluminum rods. These bolts are also used to secure the tubes in place. The RF voltage applied directly to the rods was 400 V_{p-p} at a frequency of 600 kHz. The ions then pass through a 2mm conductance limit into the RIPT quadrupole ion guide. There are 5 dc sections before the next conductance limit of 4mm and then another 3 sections before the last conductance limit of 5mm. There is an aluminum plate at the end of the quadrupole rods with a 6mm hole. To transfer ions, the first dc voltage profile was coupled to the first three segments. The following dc voltage profiles were coupled to two segments each. There were a total of eight voltage biases. The last two segments were held at ground.

The ion signal was initially detected using an electron multiplier located at the end of the quadrupole rods in which the pressure was $1x10^{-7}$ Torr. The detector response from the electron multiplier was recorded using a Tektronix THS 730A oscilloscope (Beaverton, OR). After the initial testing phase was complete a closed cylindrical ICR cell was secured at the end of the quadrupole rods for mass detection of the transferred ions. MIDAS[44] was used as the data acquisition software the FTICR parameters. The timing and voltage generation for the RIPT program were located on a separate computer (National Instruments board PCI-6723) and initiated with a TTL pulse from the MIDAS data station. ICR-2LS[45] was used for all data analysis. The pressure at the detector during ICR experiments was ~$3x10^{-9}$ Torr.

Results and Discussion:

SIMION SIMULATIONS:

The objective behind development of a segmented quadrupole for ion transfer from the accumulation region to the ICR cell is to eliminate any time-of-flight effects associated with the ion transfer process while minimizing the axial kinetic energy that is distributed to the ions. SIMION modeling was performed to investigate how the kinetic energy of the ions would be altered in the absence of ion-neutral collisions during the transfer process. The actual ion transfer processes would have limited ion-neutral collisions; this factor may cause slight deviations in experimental RIPT results and the presented simulations. The simulations illustrate that an ion oscillates a number of periods within the trapping region of the ion guide throughout the transfer process. **Figure 2a** provides a visual representation of how an ion will oscillate while being transferred through the ion guide by plotting the *z*-axis position as a function of time. Once an ion becomes trapped in a segment it oscillates back and forth while its total energy remains constant. However, when an ion is being transferred from one segment to the next it is possible for the ion to gain or lose energy. This can be seen in Figure 2a by looking at the number of oscillations that occur within a given segment and in **Figure 2b** which shows the kinetic energy. As the ion kinetic energy increases, the number of oscillations increases. An ion can be located in one of three possible segments, one that has its dc voltage bias staying constant (x), ramping up (x-1), or ramping down (x+1). Ions located in segment x (held at a constant potential) will experience no change in

energy. However, when an ion is located within segment (x-1) in which the dc bias voltage is increasing, the ion will gain potential energy. Conversely, when an ion is located in segment (x+1) on which the dc bias voltage is decreasing, the ion will lose potential energy. **Figure 3** illustrates how the voltage ramps affect the potential energy of an ion as it moves through the ion guide. For an ion to proceed from segment (x) to (x+1) or (x-1) during the ramp sequence, it may have to overcome a potential energy barrier. After an ion enters one of these ramping segments its kinetic energy is conserved while traversing that segment; however, its potential energy will change resulting in a net change in total energy. The kinetic energy in Figure 2 can be matched against the height of the observed potential energy well formed by the ion in Figure 3. The higher the kinetic energy, the higher the ion moves up the potential energy well. The correlation of the two ramps is important in limiting the amount of energy imparted to the ions. For example, if only the bias voltage on the x-1 segment was ramped up and the voltage bias on the x+1 segment was dropped instantaneously, then there would be a larger probability in a net gain of energy. That is, there would be a much greater chance for an ion to be located in the x-1 segment being ramped up than located at the x+1 side of the trapping well when the voltage bias on segment x+1 is dropped instantaneously. Therefore, it is important to understand how the change in the voltage bias can affect the ion kinetic energy as it travels through the ion guide.

The ramp times and high dc bias voltage were changed to investigate how the kinetic energy is affected. The results are shown in **Table 1.** The results indicate that as the ramp time increases and the dc bias voltages are lowered, the amount of kinetic energy imparted to the ions is decreased as they exit the RIPT ion guide. In both cases,

either changing the ramp time while holding the high dc potential constant or by holding the ramp time constant and changing the high dc potential, the rate (V/ms) of the dc bias is being changed. This would indicate that going to higher dc potentials would result in longer ramp times to achieve comparable ion kinetic energy. In Table 1, a ramp time of 10 ms at 5 V in the first column is comparable to a ramp time of 20 ms at 10 V in the second column; both had a voltage ramp rate of 0.5 V/ms. Since the time it takes for an ion to traverse a segment is small relative to the time during which the bias voltage is ramped, the energy imparted to the ions can be minimized. By increasing to longer ramp times or decreasing the high dc bias potential, the rate of the voltage ramp is decreased, which decreases the change in voltage experienced per ion oscillation. When the voltage on either segment (x+1 and x-1) is larger than the ion kinetic energy, the ions do not penetrate into either segment and oscillate without change in total energy, (as seen in Figure 3 part D). The most critical time of the transfer event is when the kinetic energy of the ion is similar to the value of the voltage being applied to the ramped segments and the ion is able to overcome the potential energy barrier. If the ramping rate is too fast, a wider distribution of ion kinetic energy results and there is a greater possibility for ions to be lost from the trapping region. Increasing the ramp rate by making the ramp times longer or lowering the high voltage minimizes the total energy distributed to the ions. The modeling results suggest optimal conditions can be achieved by orchestrating the two ramps so energy imparted to the ions is effectively offset by energy removed from the ions through ramping of the voltage bias. Additionally, simulation of ions of different *m*/*z* values (400, 1000, and 2,000) had the same kinetic energy distribution under the same ramp conditions. Simulations were performed at two different settings; (RF

voltage 220 V_{p-p}, 860 kHz) and (RF voltage 500 V_{p-p}, 1.6 MHz). There was no difference in the final kinetic energy distribution between the two simulation settings. The two settings were carried out to see if the RF voltage or frequency had any effect on the ion kinetic energy. The total time it took for ions of different *m*/*z* values to traverse the ion guide was entirely dependent upon the ramp times used (31.3ms for a 5ms ramp: 61.9ms for a 10ms ramp: 133.4 ms for a 20ms ramp). These simulations indicate that the use of ramp times of approximately 20 ms or greater with <10 V potential well results in minimized kinetic energy imparted to the ions.

ION GUIDE EXPERIMENTAL RESULTS:

A dc voltage program was written in Visual Basic to support this study and is flexible in the type of voltage ramp profile that can be produced. **Figure 4** is an example of a typical voltage ramp profile that can be generated. The first voltage profile is the voltage applied to the first segment with respect to time, and the second voltage profile is the voltage applied to the second segment with respect to time. The first waveform starts at a low potential to allow ions accumulated in the front quadrupole to enter the RIPT ion guide. There is a time period when both the first and second segments are held at the same low voltage potential. During this time period, the ions are able to move freely through both the first and second segments. The dc potential on the first segment is slowly increased (on the order of ms time scale) to allow the trapped ions to move exclusively into the second segment. A voltage applied to the conductance limit at the entrance to the RIPT ion guide stops ions from continually entering the device. Ions are

then trapped between the first and third segment. In this way the ions can be transported one segment at a time to the mass analyzer.

The initial cooling of ions through collisions with neutral gas molecules before entering the multipole device will focus the ions axially toward the center of the quadrupole segments. This cooling also reduces the kinetic energy in the axial direction and leads to significant increase in ion travel time through the instrument. Also, keeping the ions contained by transferring them one segment at a time increases the time period for ion transfer compared to having the entire ion packet pulsed to the mass analyzer. ~2-5 ms for gated trapping compared to ~300 ms with RIPT. However, it is possible to have multiple potential wells present simultaneously. Thus, while one ion packet is being accumulated multiple ion packets could be moving toward the mass analyzer while another ion packet could be analyzed in the ICR cell. The accumulation process can start again once the ion packet has been moved into the first segment and the potential to the conductance limit which serves as the entrance to the ion guide is increased. We have been able to simultaneously move three ion packets through the ion guide with our current setup of 8 voltage profiles. For experiments that involve rapid chromatographic separations, or the implementation of strategies like selective accumulation[46] or gas phase fractionation[47], this capability to simultaneously transfer several populations of ions to the mass spectrometer will be extremely useful.

The feasibility of ion transfer via a contained packet was first tested with an electron multiplier outside the magnetic field. The ability to transfer ions with RIPT is shown in **Figure 5a**. This indicates that we are able to effectively trap and transport ions as a restrained ion population through the RIPT ion guide. There is no time-of-flight with

this technique, since there is a constant axial constraint on the ions. The ions remain trapped in a voltage well through the entire transfer process. Results shown in **Figure 5b** indicate the ion kinetic energy as they exit the ion guide. The voltage well in this experiment had a high of 20 volt and a low of -10 volt, and the voltage applied to the last two segments was varied. The ramp time was set at 30ms. The ions exited the ion guide when the voltage bias to the last well was approximately 1 volt higher than the bias applied to the last two segments. This indicates that the trapped ions are not gaining kinetic energy during the transfer process.

There is one point worth further consideration. In order to transfer ions from near zero magnetic field strength to the high magnetic field region required for ICR analysis, they must pass through the fringe magnetic fields. Ions not directly on the central axis of the solenoid are subjected to an impeding force (magnetic mirror effect) as they pass into the high field region of the magnet[48]. A rf quadrupole device has been successfully used to transport ions through the fringe fields for many years[49]. As indicated by McIver, this successful transmission is due to the quadrupole focusing of ions into a beam with less than a millimeter radius. When this beam is correctly aligned along the axis of the magnet, the decelerating force which causes the magnetic mirror effect is equal to zero. Also, calculations by McIver *et al.* showed that the electrical force from the quadrupole is several orders of magnitude greater than the impeding magnetic force, thus the trajectory of an ion is determined primarily by the operating conditions of the quadrupole[50].

The RIPT ion guide is able to successfully transport a contained ion packet from the accumulation region through the magnetic field to the ICR cell. The ramp function used to transport ions is shown in **Figure 6a**. Ions were accumulated in the front

quadrupole for 0.1 seconds before transfer to the RIPT ion guide. The voltage ramp-down and ramp-up were both 15 ms. The resulting mass spectrum of the ions transferred with RIPT is shown in **Figure 6b**. To ensure that ions were not continually entering the RIPT ion guide the voltage applied to the first conductance limit was raised to10 V once the voltage bias to the first RIPT segment reached its high value. The kinetic energy of the ions entering the ICR cell was approximated by changing the voltage to the back trap plate of the ICR cell. If the voltage applied to the back trap plate was too low then ions with larger kinetic energy entering the ICR cell would not be trapped. Gated trapping can be preformed with the RIPT ion guide by holding all the dc segments at 0 V, and biasing the accumulation quadrupole to ~7 V. For the same relative ion intensity the back trap plate was typically 3-4 volts lower with RIPT. Thus, the kinetic energy of the ions entering the ICR cell is smaller than one might encounter with gated trapping alone. It should be noted that the absolute ion intensity was slightly greater using gated trapping when compared to RIPT. The ion transfer process with RIPT allowed us to keep the potentials applied to the trap plates low during ion detection, which is advantageous for collecting quality spectra.

The distribution of m/z species with RIPT and with gated trapping is shown in **Figure 7**. For the gated trapping ions are accumulated in the front quadrupole for 0.1 s by applying 10 v to the first conductance limit. To eject the ions the front quadrupole was biased to 7 v, and the first conductance limit is dropped to ground. The bias voltages to each of the RIPT segments were set to 0 volts. Data in **Figure 7a** was acquired with a 3 ms time period between ion ejection from the accumulation quadrupole and raising the front trap plate of the ICR cell while **Figure 7b** has a time period of 2 ms. The difference

in time-of-flight between high or low *m*/*z* species results in a dispersion of ions. These results indicate that by defining a set flight time for an experimental setup, discrimination against high or low *m*/*z* species will occur. These spectra are compared to a spectrum in which RIPT was used to transfer ions from the accumulation region to the ICR cell. This result is shown in **Figure 7c**. The transfer parameters were the same as those shown in Figure 4, with an initial ion accumulation time period of 0.1 s. With the RIPT transfer method the observed intensity appear to be an average of those observed with short (2ms) and long (3ms) ion transfer conditions shown in Figure 7a & b. Importantly, these data show the ability to simultaneously detect low *m*/*z* and high *m*/*z* species.

Conclusions

We present a novel approach for ion transfer, RIPT, which has been created as part of a novel FTICR mass spectrometer under development in our lab. This ion transfer process allows for the transfer of low axial kinetic energy ion packets from the accumulation region to the ICR cell while imparting little axial kinetic energy to the ions. The transfer process was modeled with SIMION 7.0 to demonstrate the ability to minimize axial kinetic energy imparted to the ions with optimal ramping functions. Initial testing of the ion guide was carried out to demonstrate the feasibility of transferring ions in a restrained ion population. This approach should eliminate any mass discrimination due to time-of-flight effects, since all ions initially trapped in the accumulation region remain confined axially and are deposited directly into the ICR cell for mass analysis. Though the ion guide transfers ions at a slower rate, the ability to create multiple trapping regions in the ion guide should allow the duty cycle of the instrument to remain relatively unchanged. Also, the analysis of ions with lower axial kinetic energy leads to lower applied trap plate potentials.

Acknowledgments

We greatly apprciate the National High Magnetic Field Labortory to lone us a MIDAS data station to carry out ICR experiments. This material is based upon work supported by the National Science Foundation under Grant No. 0352451; Murdock Charitable Trust;

Office of Science (BER), U. S. Department of Energy, Grant No. DE-FG02-04ER63924, and the National Institutes of Health Biotechnology Training Grant.

References

1. Comisarow MB, Marshall AG. *Chemical Physics Letters* 1974; **25**: 282

2. Masselon C, Anderson GA, Harkewicz R, Bruce JE, Pasa-Tolic L, Smith RD. *Analytical Chemistry* 2000; **72**: 1918

3. Kelleher NL, Zubarev RA, Bush K, Furie B, Furie BC, McLafferty FW, Walsh CT. *Analytical Chemistry* 1999; **71**: 4250

4. He F, Emmett MR, Hakansson K, Hendrickson CL, Marshall AG. *Journal of Proteome Research* 2004; **3**: 61

5. Little DP, Speir JP, Senko MW, O'Connor PB, McLafferty FW. *Analytical Chemistry* 1994; **66**: 2809

6. Sze SK, Ge Y, Oh H, McLafferty FW. *Proceedings of the National Academy of Sciences of the United States of America* 2002; **99**: 1774

7. Jebanathirajah JA, Pittman JL, Thomson BA, Budnik BA, Kaur P, Rape M, Kirschner M, Costello CE, O'Connor PB. *Journal of the American Society for Mass Spectrometry* 2005; **16**: 1985

8. Senko MW, Hendrickson cL, Emmett MR, Shi SDH, Marshall AG. *Journal of the American Society for Mass Spectrometry* 1997; **8**: 970

9. Belov ME, Nikolaev EN, Anderson GA, Udseth HR, Conrads TP, Veenstra TD, Masselon CD, Gorshkov MV, Smith RD. *Analytical Chemistry* 2001; **73**: 253

10. Huang Y, Guan S, Kim HS, Marshall AG. *International Journal of Mass Spectrometry and Ion Processes* 1996; **152**: 121

11. Lebrilla CB, Amster IJ, McIver RT, Jr. *International Journal of Mass Spectrometry and Ion Processes* 1989; **87**: R7

12. Guan S, Marshall AG. *Journal of the American Society for Mass Spectrometry* 1996; **7**: 101

13. Limbach PA, Marshall AG, Wang M. *International Journal of Mass Spectrometry and Ion Processes* 1993; **125**: 135

14. Van Vaeck L, Van Espen P, Gijbels R, Baykut G, Laukien FH. *European Journal of Mass Spectrometry* 2000; **6**: 277

15. Beu SC, Hendrickson CL, Marshall AG. *53rd ASMS Conference on Mass Spectrometry and Allied Topics*, San Antonio, TX, 2005.

16. Patrie SM, Charlebois JP, Whipple D, Kelleher NL, Hendrickson CL, Quinn JP, Marshall AG, Mukhopadhyay B. *Journal of the American Society for Mass Spectrometry* 2004; **15**: 1099

17. Wong RL, Amster IJ. *Journal of the American Society for Mass Spectrometry* 2006; **17**: 205

18. Belov ME, Nikolaev EN, Harkewicz R, Masselon CD, Alving K, Smith RD. *International Journal of Mass Spectrometry* 2001; **208**: 205

19. Wilcox BE, Hendrickson CL, Marshall AG. *Journal of the American Society for Mass Spectrometry* 2002; **13**: 1304

20. Javahery G, Thomson B. *Journal of the American Society for Mass Spectrometry* 1997; **8**: 697

21. Loboda A, Krutchinsky A, Loboda O, McNabb J, Spicer V, Ens W, Standing K. *European Journal of Mass Spectrometry* 2000; **6**: 531

22. Taban IM, McDonnell LA, Roempp A, Cerjak I, Heeren RMA. *International Journal of Mass Spectrometry* 2005; **244**: 135

23. Mansoori BA, Dyer EW, Lock CM, Bateman K, Boyd RK. *Journal of the American Society for Mass Spectrometry* 1998; **9**: 775

24. Thomson BA, Jolliffe CL. *PCT Int. Appl.*, 9707530, 1997.

25. May MA, Grosshans PB, Marshall AG. *International Journal of Mass Spectrometry and Ion Processes* 1992; **120**: 193

26. Arkin CR, Laude DA. *Journal of the American Society for Mass Spectrometry* 2005; **16**: 422

27. Easterling ML, Mize TH, Amster IJ. *Analytical Chemistry* 1999; **71**: 624

28. Francl TJ, Sherman MG, Hunter RL, Locke MJ, Bowers WD, McIver RT, Jr. *International Journal of Mass Spectrometry and Ion Processes* 1983; **54**: 189

29. Ledford EB, Jr., Rempel DL, Gross ML. *Analytical Chemistry* 1984; **56**: 2744

30. Mitchell DW, Smith RD. *Physical Review. E. Statistical Physics, Plasmas, Fluids, and Related Interdisciplinary Topics* 1995; **52**: 4366

31. Naito Y, Inoue M. *Journal of the Mass Spectrometry Society of Japan* 1994; **42**: 1

32. Easterling ML, Pitsenberger CC, Kulkarni SS, Taylor PK, Amster IJ. *International Journal of Mass Spectrometry and Ion Processes* 1996; **157/158**: 97

33. Stults JT. *Analytical Chemistry* 1997; **69**: 1815

34. Shi SDH, Hendrickson CL, Marshall AG. *Proceedings of the National Academy of Sciences of the United States of America* 1998; **95**: 11532

35. Guan S, Kim HS, Marshall AG, Wahl MC, Wood TD, Xiang X. *Chemical Reviews* 1994; **94**: 2161

36. Guan S, Wahl MC, Wood TD, Marshall AG. *Analytical Chemistry* 1993; **65**: 1753

37. Gorshkov MV, Masselon CD, Anderson GA, Udseth HR, Harkewicz R, Smith RD. *Journal of the American Society for Mass Spectrometry* 2001; **12**: 1169

38. Giles K, Pringle SD, Worthington KR, Little D, Wildgoose JL, Bateman RH. *Rapid Communications in Mass Spectrometry* 2004; **18**: 2401

39. Colburn AW, Giannakopulos AE, Derrick PJ. *European Journal of Mass Spectrometry* 2004; **10**: 149

40. Bateman RH, Pringle S, Giles K. *Eur. Pat. Appl.*, 1378930, 2004.

41. Belov ME, Gorshkov MV, Alving K, Smith RD. *Rapid Communications in Mass Spectrometry* 2001; **15**: 1988

42. Wu S, Zhang K, Kaiser NK, Bruce JE, Prior DC, Anderson GA. *Journal of the American Society for Mass Spectrometry* 2006; **17**: 772

43. Prior DC, Price J, Bruce JE. *U.S. Patent 6,455,8646*, 2002.

44. Senko MW, Canterbury JD, Guan S, Marshall AG. *Rapid Communications in Mass Spectrometry* 1996; **10**: 1839

45. Anderson GA, Bruce J.E., Smith R.D. *ICR-2LS,* Richland, WA, 1996.

46. Bruce JE, Anderson GA, Smith RD. *Analytical Chemistry* 1996; **68**: 534

47. Yi EC, Marelli M, Lee H, Purvine SO, Aebersold R, Aitchison JD, Goodlett DR. *Electrophoresis* 2002; **23**: 3205

48. Chen FF. *Introduction to Plasma Physics and Controlled Fusion,*. Plenum Press: New York, 1984;

49. McIver RT, Jr., Hunter RL, Bowers WD. *International Journal of Mass Spectrometry and Ion Processes* 1985; **64**: 67

50. McIver RT, Jr. *International Journal of Mass Spectrometry and Ion Processes* 1990; **98**: 35

Figure 1

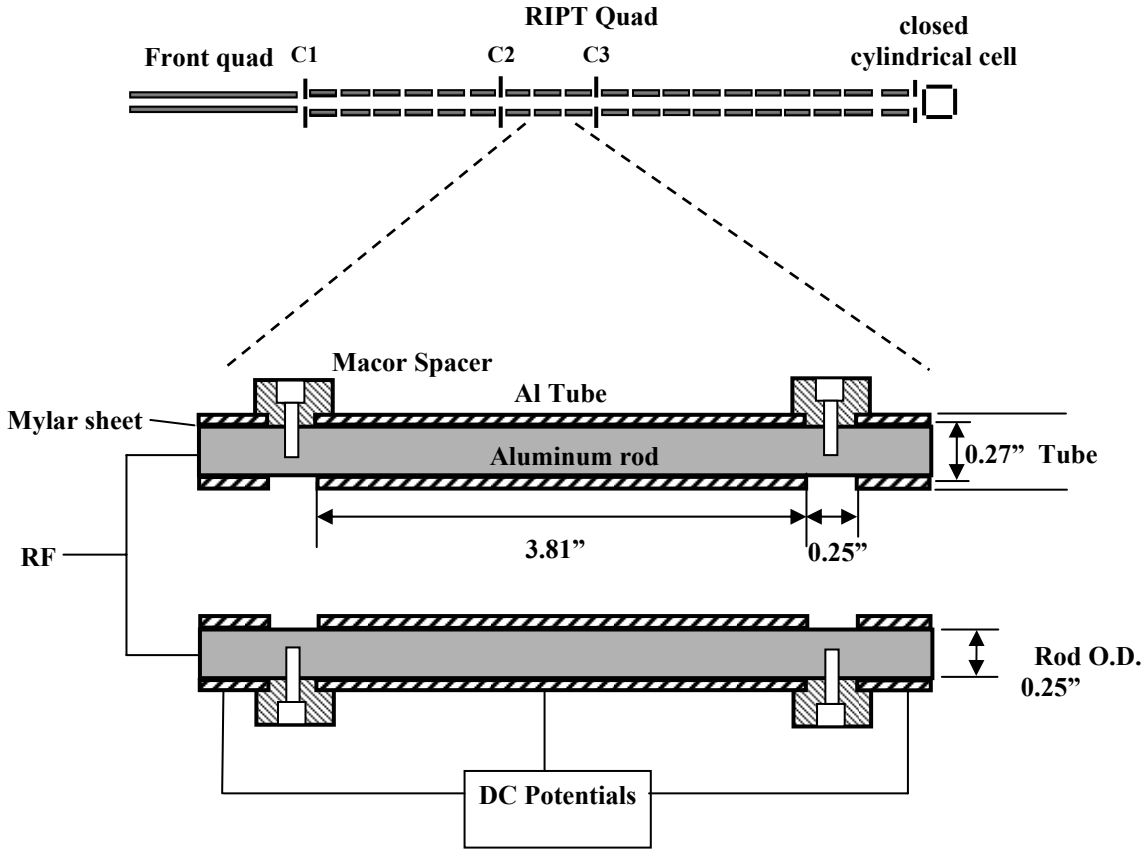

Figure 1. A visual representation of the experimental set-up that was used to measure ion current. C1, C2, C3 are the conductance limits in the RIPT ion guide. The inset illustrates one segment from the ion guide assembly to show how the outer aluminum tubes and inner aluminum rods are coupled.

Figure 2

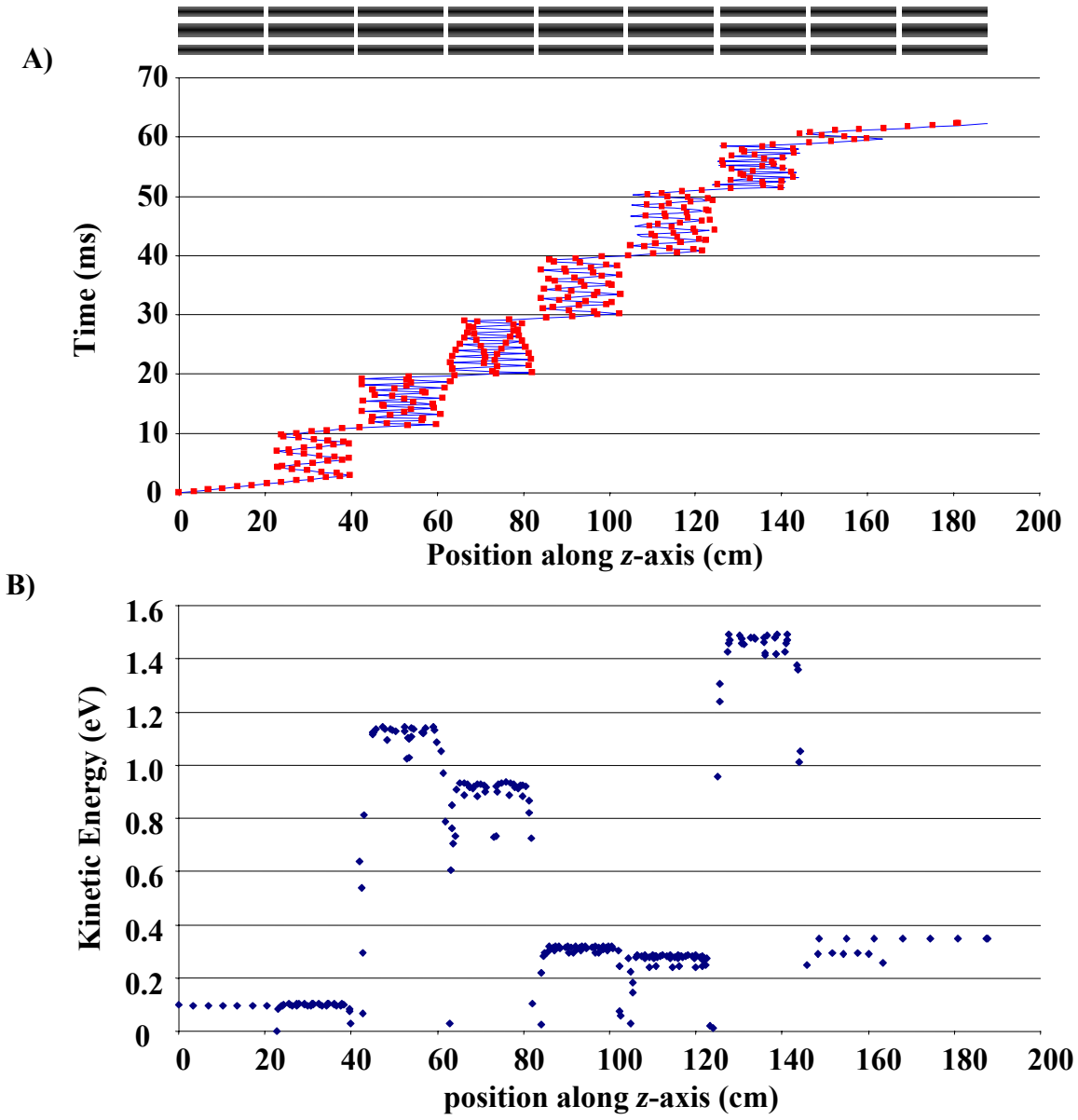

Figure 2. SIMION trajectory results for a single ion (*m/z* 1,000, with an initial KE of 0.10 eV, 10 V for the high dc bias potential, and a 10 ms rise time) is shown throughout the transfer process in the ion guide. A) Plots the position of the ion at every 250 µs time point. The ion guide segments are shown and numbered at the top of the figure. The ion enters the ion guide through segment 1. The ion is transferred into a new segment every 10 ms, as indicated by its position. B) Plots the KE for the same time points taken above. Once an ion becomes trapped in a segment its kinetic energy remains constant. The few points scattered around at lower KE potentials at the edge of the segments is because the ion is located on the edge of the potential well, and its kinetic energy is converted into potential energy.

Figure 3

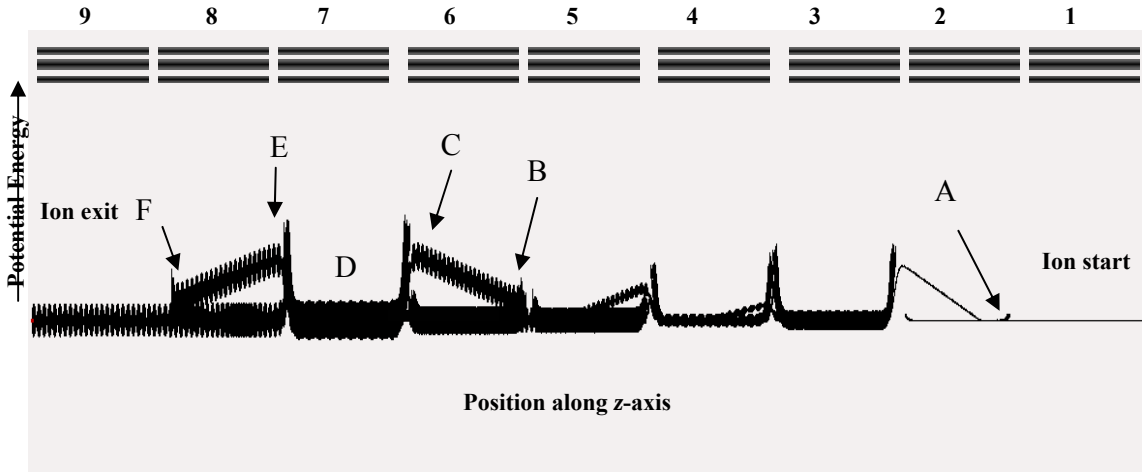

Figure 3. The ion's potential energy trace is plotted for the same ion trajectory in Figure 2. The ion guide segments are numbered; the ions enter the ion guide through segment 1. A number of time points are chosen to describe the ion at that position. A. Ion oscillates in the first trapping region at 0.1eV. B. The voltage bias on the sixth segment increases while the ion is located in the sixth segment. C. The ion's KE is the same as it was at point B, however the potential energy increased resulting in a net gain of energy. D. The ion oscillates at a new energy value in the seventh segment. E. Much of the ion's energy has been converted into potential energy as it has just enough energy to overcome the potential energy barrier to reach the eighth segment. F. The ion's KE is the same as it was at point E, however, the decrease in bias voltage of the seventh segment resulted in a loss of potential energy.

Figure 4

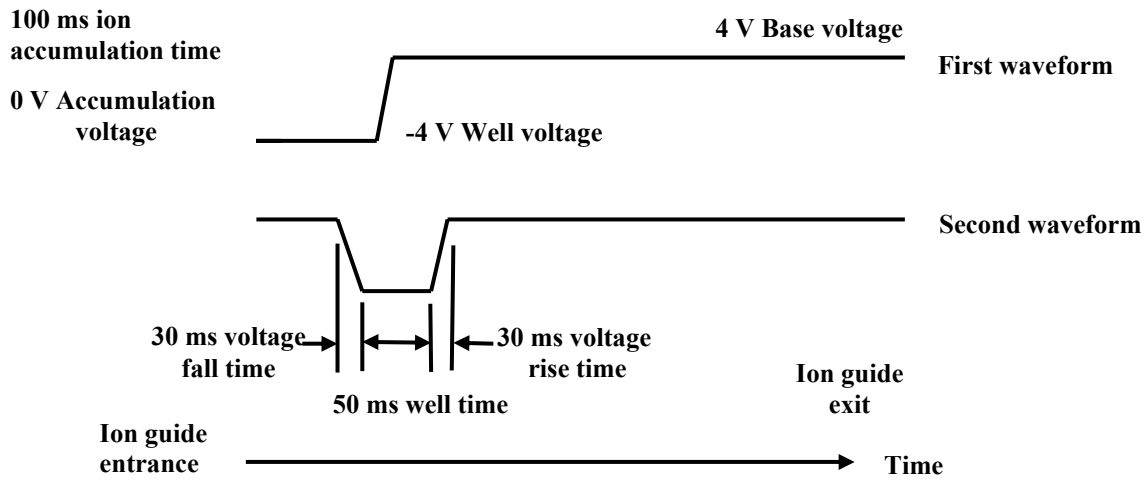

Figure 4. Typical voltage profile for ion transmission with the application of RIPT. The top profile shows the voltage ramp sequence that is applied to the first segment. After the ion accumulation period, the dc voltages applied to each segment are individually adjusted to move the ion trapping region to the exit end of the ion guide. The bottom profile is the voltage ramp sequence that is applied to the second segment.

Figure 5

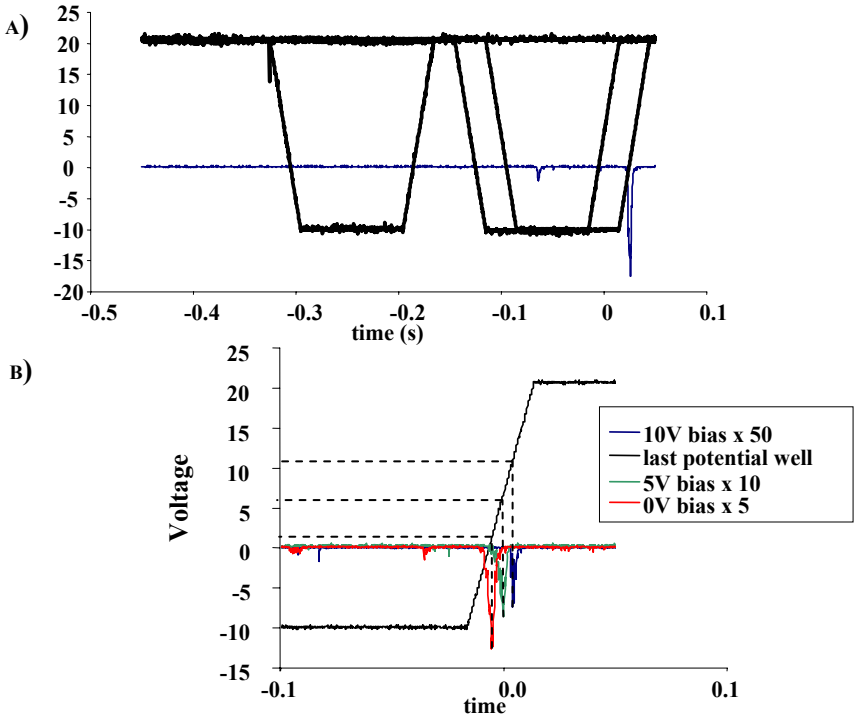

Figure5. The ions exit the ion guide as the voltage applied to the second to last segment nears the bias voltage applied to the last segment of the ion guide. The bias voltage to the last segment was varied. Ion current was measured with the electron multiplier, the current was scaled so that it could be on the same scale as the voltage ramp.

Figure 6

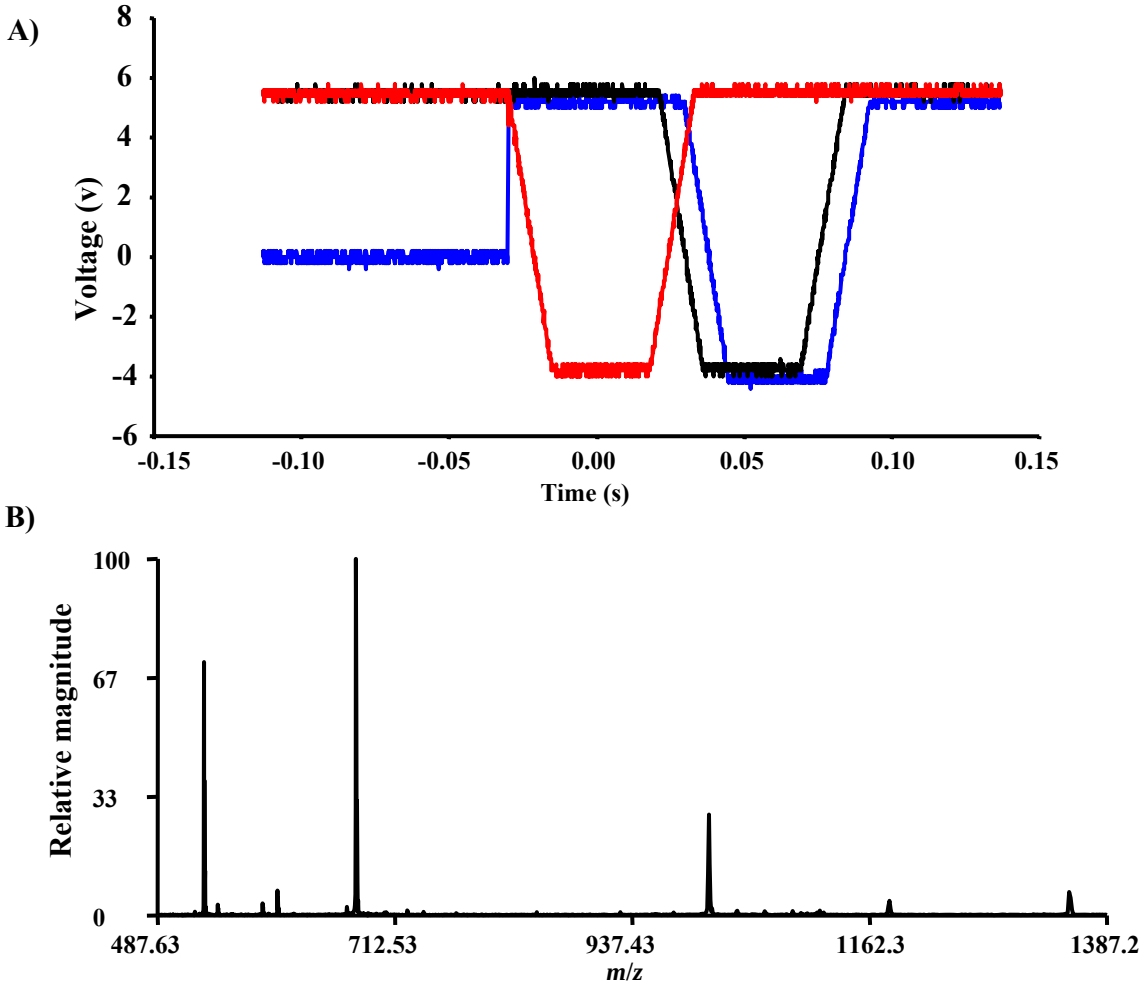

Figure 6. RIPT results A) The applied voltage profile to the first, seventh, and eighth voltage wells. B) The resulting mass spectrum of a peptide mixture consisting of bradykinin, substance p, and oxytocin.

Figure 7

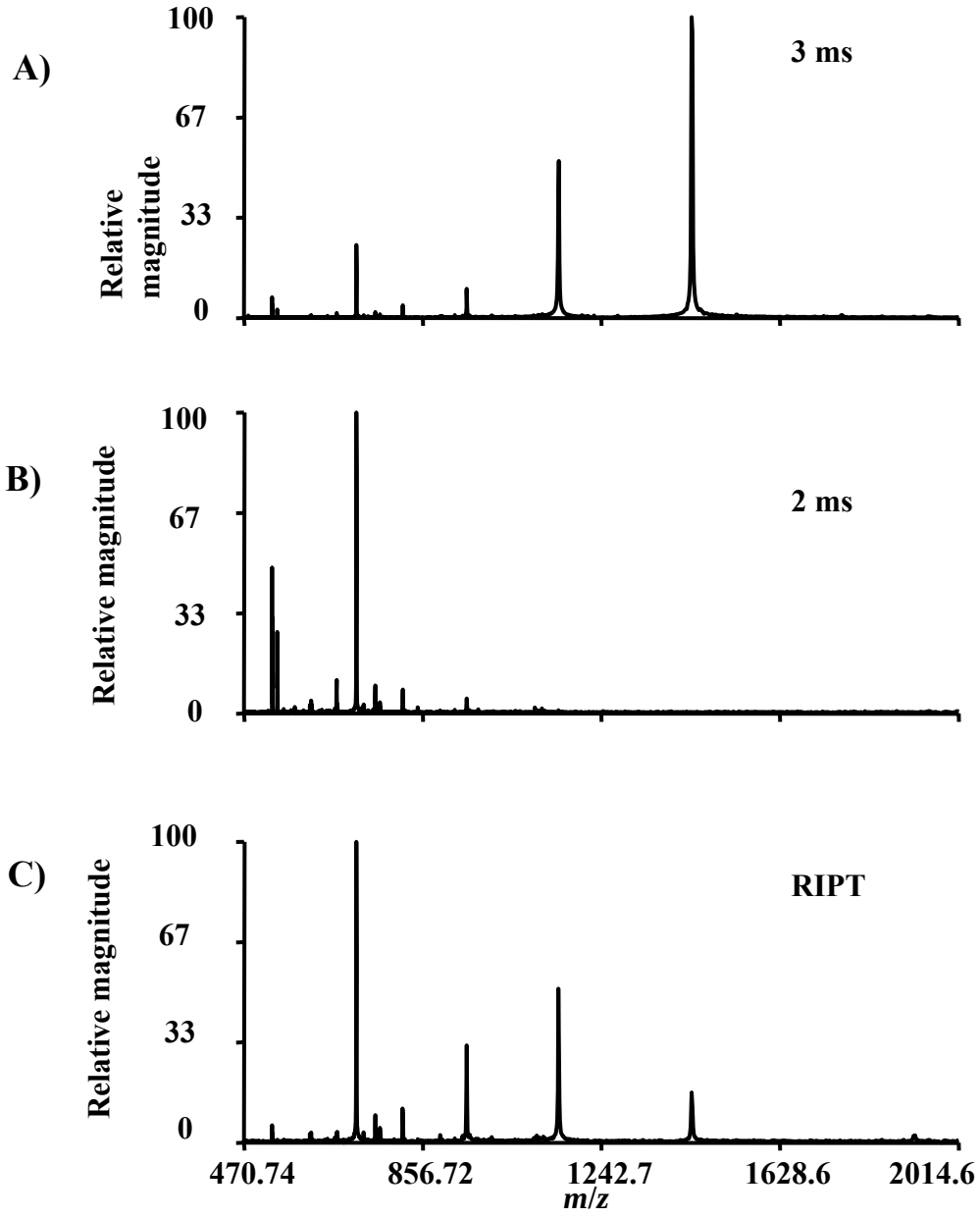

Figure7. Mass spectra of a mixture of bradykinin, melittin, and insulin. A) Ions were accumulated in the ICR cell with gated trapping with a flight time of 3 ms. B) Gated trapping with a 2 ms flight time. C) Ions were accumulated with the RIPT method.

Table 1

Comparison of K.E. for Different Ramp Conditions

Voltage High	Column 1 Average K.E. (ev)	Median K.E. (eV)	Ramp Time	Column 2 Average K.E. (eV)	Median K.E. (eV)
2 V	0.61	0.36	5 ms	3.17	2.62
5V	1.05	0.59	10 ms	1.67	0.94
10 V	1.67	0.94	15 ms	1.11	0.78
18 V	2.25	1.75	20 ms	0.96	0.75
25 V	2.75	2.02			

Table 1. Simulation results from varying the rate (V/ms) of the ramp. Results were obtained with *m/z* = 1000, 500Vp-p, 1.6MHz, and 0.1 initial ion KE. Column 1) The voltage bias change was carried out at ramp time of 10 ms. Column 2) Ramp time increase was carried out with 10 V high bias.

CHAPTER 7

A Novel Fourier Transform Ion Cyclotron Resonance Mass Spectrometer for Biomolecule Analysis

Abstract

A novel Fourier transform ion cyclotron resonance FTICR mass spectrometer has been developed for improved biomolecule analysis. The instrument incorporates a flared metal capillary and an electrodynamic ion funnel for improved ion transmission in the source region of the instrument. A novel ion guide called Restrained Ion Population Transfer, or RIPT, is used to transfer ions from the ion accumulation region to the ICR cell. The RIPT ion guide reduces the mass discrimination that may occur due to time-of-flight during gated trapping, and is able to transfer ions with lower kinetic energy to the ICR cell. A novel ICR cell called, Trapping Ring Electrode Cell, or TREC is employed for ion current detection. With TREC the trapping electric fields can be tailored to reduce de-phasing of the coherent cyclotron motion of an excited ion packet. With TREC we are able to observe a 4X improvement in resolution. The increase in signal duration with TREC results in an enhancement in the signal-to-noise ratio.

Introduction

Mass spectrometers have become an indispensable tool in the area of proteomics. With the desire to understand biology and analyze lower abundant proteins in the proteome, more accurate and sensitive instruments are required [1, 2]. A Fourier transform ion cyclotron resonance FTICR [3, 4] instrument is the highest performance mass spectrometer in terms of resolution and mass measurement accuracy [5-7]. It has the ability to measure thousands of components in a complex mixture in a single spectrum [8, 9]. To attain the high performance capabilities of FTICR-MS there is a trade off in time, because every aspect of FTICR-MS increases with longer acquisition periods [10]. However, this depends on the ability to detect an observable signal for the entire data acquisition period. There are a number of factors which cause the observed signal to rapidly decay [11]. Many of these factors which cause ion could de-phasing are associated with the requirement to confine the ions to a finite space for analysis.

There are a number of advantages to increasing the magnetic field strength such as the data acquisition period decreases linearly for a defined resolution (increased cyclotron frequency), and upper mass limit and the maximum number of ions increase quadradically [12-14]. Also, the number of ions needed for have peak coalescence to occur decreases inverse-quadradically with magnetic field strength [15]. These parameters are especially critical for top-down proteomic experiments [16-18]. To observe ion signal for a period of time ions need to be confined parallel to the magnetic field by electric fields [19]. There are a number of idealized electric fields which the ICR

cell struggles to produce, rf potential parallel to the magnetic field, and a three dimensional quadrupolar potential along the axis of the ICR cell [20]. There is typically a trade-off in the type of electric field produced. A large number of ICR cell designs have been developed to target one or more of these electric fields [21, 22]. The most common ICR cell geometries in use today are designed to produce infinity long excite potentials [23, 24].

Electrospray was successfully coupled to a FTICR mass spectrometer by McLafferty and coworkers for analysis of large molecules [25, 26]. With external ionization sources, ions are usually accumulated outside the magnetic field to allow for differential pumping to produce an ultra high vacuum (UHV) required for FTICR analysis. Accumulation of ions external to the ICR cell has been shown to increase sensitivity [27]. With external ion accumulation some form of gated trapping is typically used to trap ions within the ICR cell [28, 29]. This transfer process from the accumulation region to the ICR cell give ions kinetic energy, to trap the ions in the ICR cell the voltage applied to the trap plates need to be greater than the kinetic energy of the ions entering the ICR cell. Since regions of electric field inhomogeneity increase inside the ICR cell with larger trapping potential it advantageous to perform FTICR measurements at low trapping potentials [30-32]. However with gated trapping, ions trapped in the ICR cell will have a distribution of kinetic energies along the *z*-axis which leads to differences in trapping oscillation amplitude [28, 33]. Lowering the trap plate potentials below the threshold of *z*-axis kinetic energy of the trapped ions will result in a loss of ions from the ICR cell and a decrease in sensitivity [34]. Therefore, to reach low trapping potentials ions are usually cooled with a pulse valve event or a slow reduction of

trapping potential [35]. The addition of a collision gas causes expansion of the magnetron radius. Thus, it is desirable to perform quadrupole axialization which converts magnetron motion to cyclotron motion which is rapidly damped in the presence of a collision gas [36, 37]. However, these ion cooling and axiallization techniques require sufficient time for and are not applicable to be performed on a LC time-scale which requires a high duty cycle. In addition, there is a loss of sensitivity when performing gated trapping in the sense that all the ions trapped in the accumulation region do not exit the accumulation region at the same time and ions reach the ICR cell at different times due to different flight times. The ions can be forced out of the accumulation region over a shorter period of time by putting angled wires between the multipoles of the accumulation cell to induce a voltage gradient within the accumulation region [38]. However, there is still mass discrimination due to time-of-flight effects to overcome [39].

All current commercial vendors of FTICR mass spectrometers have developed hybrid FTICR instruments which have a mass selective device exterior to the magnetic field. This allows for ion isolation of ions before accumulation, and also allows for fragmentation exterior to the ICR cell [40, 41]. This has greatly increased the speed and flexibility of the type of experiments that can be performed. Though the instrument described here is not a hybrid instrument, we seek to modify the instrument configurations to improve the overall FTICR mass spectrometer performance. In this paper we present a novel FTICR mass spectrometer which is designed to overcome some of the weakness in current instrument designs. First we incorporated a heated flared metal inlet capillary [42, 43] followed by an electrodynamic ion funnel [44, 45] for

improved ion transmission from atmospheric pressure through the first vacuum stage. A novel quadrupole ion guide following the ion accumulation region is designed to minimize time-of-flight effects that occur when transmitting ions from the accumulation region to the ICR cell, as well as transfer ions with low kinetic energy to the ICR cell. For ion detection we have developed a novel ICR cell to reducing de-phasing of ion clouds, without the need to lower trap potentials.

Experimental

The home built FTICR instrument implemented into a 3 Tesla magnet (Magnex Scientific, Abingdon, UK). The vacuum system shown in **Figure 1 A** was designed to allow for atmospheric ionization sources such as electrospray ionization to be used. Ions enter the mass spectrometer through a 30.5 cm long flared metal capillary tube (I.D. 0.51mm) (Small Parts Inc, Miami Lakes, FL). The capillary is held in place by a heating block that is heated to 130 ^{o}C with two cartridge heaters (Omega, Stamford, CN). The first stage of pumping is carried out with a rough pump (1.2 Torr). An ion funnel is used to transfer ions through the first pumping stage. A leak valve was added to the first pumping stage to allow control over the pressure for optimized ion transmission through the ion funnel. The ion funnel has 22 electrodes with an outer diameter of 35.5 mm and 1.6 mm thick with 1.0 mm thick nylon washers used as spacers between the electrodes. The inner diameter of the first electrode was 20.3 mm, the inner diameter of the electrodes decreased with the last electrode having an inner diameter of 2.2 mm. The conductance limit at the bottom of the ion funnel is 3.0 mm. The rf voltage that was

applied to the ion funnel was ~200 V_{p-p}. The dc voltage gradient was set up by applying 150 V to the first electrode and 35 V to the last electrode. Following the conductance limit at the end of the ion funnel is a skimmer. The second stage is pumped by the auxiliary port on the drag pump used to pump the third stage. The ions are transmitted through the third pumping stage by a 35.6 cm long quadrupole operated with an RF voltage of 280 V_{p-p} at 1.03 MHz ($7.9x10^{-3}$ Torr). A UHV gate valve (HVA Reno, NV) was added between the third and fourth stage of pumping. The source region of the instrument has a *z*-axis translational UHV bellows (McAllister Technical Services, Coeurd' Alene, ID). This allows the source region to be accessed for modification or cleaning while still maintaining the UHV needed for ICR analysis. A conductance limit of 2 mm separates the ion accumulation region from the novel ion optics used to transfer ions to the ICR cell. The pressure on the high vacuum side of the gate valve ($1x10^{-5}$ Torr) is monitored with a Micro-Ion gauge (Grandville-Phillips, Longmont, CO). The ion guide called restrained ion population transfer, or RIPT is described in detail elsewhere. The pressure in the region UHV region of the instrument was $3x10^{-9}$ Torr monitored with a Stable-Ion gauge (Grandville-phillips, Longmont, CO). The pressure reading on the ion gauge reads approximately half the value when the instrument is rolled into the magnet. After ions were trapped in the ICR cell by transfer with either RIPT or gated trapping, ions were analyzed directly or the axial energy of the ions trapped in ICR cell was cooled with a pulse gas event of 1 ms. Argon was used as the collision gas. A delay of 8-10 seconds was used to allow the collision gas to be pumped away.

Ions were created through electrospray by applying 2.75 kV to a metal union located before the spray tip. The spray solution for all analytical standards purchased

from Sigma (St. Loius, MO) was 49:49:2, by volume water:methanol:acetic acid. Infusion of the electrospray solution was performed with a syringe pump (Cole-Parmer, Vernon Hills, IL) at a flow rate of 1μL/min. There were two types of ICR cells tested in the instrument the first was a capacitively coupled open cylindrical cell and a novel ICR cell called trapping ring electrode cell or TREC which has been described in detail elsewhere. Both ICR cells had an inner diameter of 47.6 mm and a length of 50.8 mm. The open cylindrical cell had three equal segments of 50.8 mm. A MIDAS data station was used to acquire the data [46]. Ions were excited with broadband excitation with a sweep width of 200 kHz. The sweep rate and excitation amplitude were varied to change the excited cyclotron radius. The excitation waveform created by the arbitrary waveform generator was amplified by a novel rf excitation amplifier developed in-house and described in detail elsewhere. The RIPT quadrupole ion guide was only used with the TREC cell when all the rings which make of the front trap plate and all the rings which make up the back trap plate all had the same potentials. Ions were transported in the RIPT with 5 V as the high potential and -4 V as the low potential to form the voltage well. The ramp time down and up were both set at 30ms. A total of eight different voltages were used. ICR -2LS software package was used for data analysis [47].

Results and Discussion

Many problems associated with signal acquisition for FTICR mass spectrometers such as ion cloud de-phasing or Coulombic interaction of ion packets are amplified at low magnetic field strength; though these problems are still present at higher magnetic field

strength they are not as detrimental. FTICR mass spectrometers which have low field magnets, such as the 3 Tesla instrument described here, are not in routinely use because of the disadvantages already mentioned. However, identifying these limitations and trying to correct for them is needed as an alternative to improve performance without investing in a higher field magnet. The performance increases shown on a 3 Telsa instrument will also translate into increased performance with instruments which incorporated higher field magnets.

The trapping ring electrode cell, or TREC, illustrated in **Figure 2** was designed to minimize radial electric fields within the ICR cell. It has been shown that altering the radial fields during ion detection can produce longer transients [48, 49]. Therefore, we have decided to construct a novel ICR cell which gives us unique control over shape of the trapping electric fields. This approach differs from the ICR cells in commercial instruments today, which have been designed to eliminate *z*-axis ejection during excitation [50, 51]. The cell has the geometry of a closed cylindrical cell, but the solid trap plates were replaced with 5 concentric rings with the ability to apply separate voltages to each ring on either trap plate. This allows the electric fields to be modified to decrease the electric field inhomogeneity inside the ICR cell. All the rings were kept at the same voltages during ion accumulation and then switched to individual potentials between excitation and detection. The voltages on the TREC were tuned by iteratively changing the ring potentials. **Figure 3** shows a comparison of the two ICR cells that were employed in the instrument. In both cases a collision gas was introduced into the ICR cell to cool the ions. The ion signal in the time-domain lasts approximately 3X as long when obtained with the TREC compared to the open cylindrical cell. These results

show that the ability to modify the trapping electric fields with TREC decreases electric field inhomogeneity inside the ICR cell is important for improving FTICR signal. With TREC the excited ion clouds are able to remain as a coherent packet for a longer time period. This results in higher resolving power, signal-to-noise ratio as can be seen from Figure 3.

With a closed cylindrical cell the ions will experience *z*-axis excitation and possibly ejection from the ICR cell during excitation of cyclotron motion. The larger the *z*-axis oscillation amplitude of the ions the more likely *z*-axis excitation will be a problem. Therefore, with the current design of TREC we have made the trade off in electric field profile in favor of trapping electric field over the excitation electric field. However, *z*-axis excitation can be reduced by coupling the excitation on to the trap rings, similarly to the Infinity cell. Ion cooling with a collision gas is desirable to reduce the *z*-axis oscillation amplitude of the ions so they are located at the center of the ICR cell. **Figure 4** compares spectra between TREC and non-TREC conditions with the ion cooling for mellitin. Figure 4A is the non-TREC spectrum in which the excitation conditions were optimized, the calculated cyclotron radius was approximately 0.6 cm. 1.2 volts were placed on all the ring electrodes. The resolution obtained was ~100,000 with a signal duration of ~6 seconds. Figure 4B is the spectrum obtained with TREC, in which ions were excited to a cyclotron radius approximately half the ICR cell radius. The signal duration lasts longer than the data acquisition period of 13 seconds, with a resolution of over 400,000. There is also little observed frequency drift with observation time with TREC [52, 53]. After the 13 second data acquisition the resolution of the peak is still at the theoretical limit, which can be approximated by *frequency* * *time* =

resolution. The reason that ions can be excited to a larger cyclotron radius with TREC is because the electric field inhomogeneities increase the further the ions are from the central axis of the ICR cell, thus leading to faster de-phasing rates under non-TREC conditions. With TREC the electric fields can be tailored to decrease these electric field inhomogeneities at larger ICR cell radius. This is important because the signal intensity increases with cyclotron radius because the ion cloud is closer to the detection electrodes. In addition, space charge frequency shifts from varying number of ions from one data acquisition period to the next are more prominent at smaller cyclotron radii. Because, for the same number of ions the charge density is larger at smaller radii, this results in increased Coulombic interactions. It should be noted that even though the resolution is good enough to define fine structure, none is observed due to the peak coalescence which is more prominent at lower magnetic field strength. In comparing the spectra in Figure 4 the frequencies of the peaks are shifted since the radial electric fields are different. Since the radial electric forces drive magnetron motion, the ion clouds in the two trapping cell (TREC vs. non-TREC) will exhibit different magnetron frequencies. In this figure the peaks in the TREC spectrum are shifted to a lower frequency. The voltages applied to the ring electrodes from inner to outer ring is 0.2, 1.2, 2.0, 2.4, 2.8 V. In this case the magnitude of the radial force is greater (lower observed cyclotron frequency) but the electric fields have been altered to make this force more constant along the *z*-axis of the ICR cell.

The other novel feature of the instrument is the RIPT ion guide. This segmented quadrupole can work in two modes: 1) Static, in which all segments maintain the same dc voltage at all times. 2) RIPT, in which voltages applied to the quadrupole segments are

varied individually to form a potential well to transport ions. In the static mode ions are transferred to the ICR cell by biasing the front quadrupole to ~8 volts while holding the dc voltage for all segments of the RIPT quadrupole at ground, and employing gated trapping to trap ions in the ICR cell. The segmented ion guide resembles a solid set of quadrupole rods in this mode of operation. The segmented regions do not appear to have any negative effect on the ion transmission efficiency. It is desirable to transfer ions with low kinetic energy because it takes lower trapping voltages to trap the ions. The higher the applied voltages the greater the inhomogeneity of the electric fields within the ICR cell which translates to faster de-phasing rates. The kinetic energy of ions entering the ICR cell with RIPT and gated trapping is shown in **Figure 5**. The normalized signal intensity is an average of three standards: bradykinin $(M+2H)^{2+}$, mellitin $(M+4H)^{4+}$, and insulin $(M+5H)^{5+}$. The voltage applied to the back trap plate is varied. If the voltage is lower than the kinetic energy of the ions entering the ICR cell the ions will pass through the ICR cell. If the ions have less kinetic energy than the applied voltage potential, the ions will slow down and be forced to change direction. This increases the duration in which the ions are located in the trapping region, and thus the likelihood that the ions will be trapped with gated trapping. Figure 5 illustrates that with RIPT we are able to transfer ions to the ICR cell with lower kinetic energy. The RIPT ion guide and TREC use the same hardware device; therefore, we are currently unable to perform both tasks simultaneously. We are planning to couple them together in the very near future.

Conclusions

A novel FTICR mass spectrometer has been designed and initial performance described. The TREC design allows ions to be excited to larger cyclotron radii by reducing electric field inhomogeneity. TREC offers a 4X improvement in resolution compared to the same voltage applied to all ring electrodes. Exciting ions to larger cyclotron radii will increase sensitivity and the signal-to-noise ratio. The RIPT ion guide can reduce time-of-flight effects as well as reduce the kinetic energy of the ions entering in the ICR cell. This allows the voltage applied to the trapping electrodes to be lower. Lower voltages results in decreased electric field inhomogeneity and thus decreased de-phasing rates.

Acknowledgements

This material is based upon work supported by the National Science Foundation under Grant No. 0352451; Murdock Charitable Trust; Office of Science (BER), U. S. Department of Energy, Grant No. DE-FG02-04ER63924, and the National Institutes of Health Biotechnology Training Grant.

Reference

1. He, F., Emmett, M. R., Hakansson, K., Hendrickson, C. L., Marshall, A. G., Theoretical and experimental prospects for protein identification based solely on accurate mass measurement, *J Proteome Res*. **2004,** *3*, 61-67.

2. Clauser, K. R., Baker, P., Burlingame, A. L., Role of Accurate Mass Measurement (+-10 ppm) in Protein Identification Strategies Employing MS or MS/MS and Database Searching, *Analytical Chemistry*. **1999,** *71*, 2871-2882.

3. Comisarow, M. B., Marshall, A. G., Fourier transform ion cyclotron resonance spectroscopy, *Chemical Physics Letters*. **1974,** *25*, 282-283.

4. Comisarow, M. B., Marshall, A. G., Frequency-sweep Fourier transform ion cyclotron resonance spectroscopy, *Chemical Physics Letters*. **1974,** *26*, 489-490.

5. He, F., Hendrickson, C. L., Marshall, A. G., Baseline mass resolution of peptide isobars: A record for molecular mass resolution, *Analytical Chemistry*. **2001,** *73*, 647-650.

6. Williams, D. K., Jr., Muddiman, D. C., Parts-Per-Billion Mass Measurement Accuracy Achieved through the Combination of Multiple Linear Regression and Automatic Gain Control in a Fourier Transform Ion Cyclotron Resonance Mass Spectrometer, *Analytical Chemistry*. **2007,** *79*, 5058-5063.

7. Shi, S. D. H., Hendrickson, C. L., Marshall, A. G., Counting individual sulfur atoms in a protein by ultrahigh-resolution Fourier transform ion cyclotron resonance mass spectrometry: experimental resolution of isotopic fine structure in proteins, *Proceedings of the National Academy of Sciences of the United States of America*. **1998,** *95*, 11532-11537.

8. McLafferty, F. W., Fridriksson, E. K., Horn, D. M., Lewis, M. A., Zubarev, R. A., Techview: biochemistry. Biomolecule mass spectrometry, *Science*. **1999,** *284*, 1289-1290.

9. Hughey, C. A., Rodgers, R. P., Marshall, A. G., Resolution of 11,000 Compositionally Distinct Components in a Single Electrospray Ionization Fourier Transform Ion Cyclotron Resonance Mass Spectrum of Crude Oil, *Analytical Chemistry*. **2002,** *74*, 4145-4149.

10. Marshall, A. G., Hendrickson, C. L., Fourier transform ion cyclotron resonance detection: principles and experimental configurations, *International Journal of Mass Spectrometry*. **2002,** *215*, 59-75.

11. Peurrung, A. J., Kouzes, R. T., Long-term coherence of the cyclotron mode in a trapped ion cloud, *Physical Review. E. Statistical Physics, Plasmas, Fluids, and Related Interdisciplinary Topics*. **1994,** *49*, 4362-4368.

12. Mitchell, D. W., Realistic simulation of the ion cyclotron resonance mass spectrometer using a distributed three-dimensional particle-in-cell code, *Journal of the American Society for Mass Spectrometry*. **1999,** *10*, 136-152.

13. Mitchell, D. W., Smith, R. D., Prediction of a space charge induced upper molecular mass limit towards achieving unit mass resolution in Fourier transform ion cyclotron resonance mass spectrometry, *Journal of Mass Spectrometry*. **1996,** *31*, 771-790.

14. Marshall, A. G., Guan, S., Advantages of high magnetic field for Fourier transform ion cyclotron resonance mass spectrometry, *Rapid Communications in Mass Spectrometry*. **1996,** *10*, 1819-1823.

15. Mitchell, D. W., Smith, R. D., Cyclotron motion of two Coulombically interacting ion clouds with implications to Fourier-transform ion cyclotron resonance mass spectrometry, *Physical Review. E. Statistical Physics, Plasmas, Fluids, and Related Interdisciplinary Topics*. **1995,** *52*, 4366-4386.

16. Bogdanov, B., Smith, R. D., Proteomics by FTICR mass spectrometry: Top down and bottom up, *Mass Spectrometry Reviews*. **2005,** *24*, 168-200.

17. Kelleher, N. L., Lin, H. Y., Valaskovic, G. A., Aaserud, D. J., Fridriksson, E. K., McLafferty, F. W., Top Down versus Bottom Up Protein Characterization by Tandem High-Resolution Mass Spectrometry, *Journal of the American Chemical Society*. **1999,** *121*, 806-812.

18. Sze, S. K., Ge, Y., Oh, H., McLafferty, F. W., Top-down mass spectrometry of a 29-kDa protein for characterization of any posttranslational modification to within one residue, *Proc Natl Acad Sci U S A*. **2002,** *99*, 1774-1779.

19. McIver, R. T., Jr., Ledford, E. B., Jr., Miller, J. S., Proposed method for mass spectrometric analysis for ultra-low vapor pressure compounds, *Analytical Chemistry*. **1975,** *47*, 692-697.

20. Guan, S., Marshall, A. G., Ion traps for Fourier transform ion cyclotron resonance mass spectrometry: principles and design of geometric and electric configurations, *International Journal of Mass Spectrometry and Ion Processes*. **1995,** *146/147*, 261-296.

21. Anderson, J. S., Vartanian, H., Laude, D. A., Evolution of trapped ion cells in Fourier transform ion cyclotron resonance mass spectrometry, *Trends Anal Chem*. **1994,** *13*, 234-239.

22. Vartanian, V. H., Anderson, J. S., Laude, D. A., Advances in trapped ion cells for Fourier transform ion cyclotron resonance mass spectrometry, *Mass Spectrometry Reviews*. **1995,** *14*, 1-19.

23. Caravatti, P., Allemann, M., The infinity cell: a new trapped-ion cell with radiofrequency covered trapping electrodes for Fourier transform ion cyclotron resonance mass spectrometry, *Organic Mass Spectrometry*. **1991,** *26*, 514-518.

24. Beu, S. C., Laude, D. A., Jr., Elimination of axial ejection during excitation with a capacitively coupled open trapped-ion cell for Fourier transform ion cyclotron resonance mass spectrometry, *Analytical Chemistry*. **1992,** *64*, 177-180.

25. Henry, K. D., Williams, E. R., Wang, B. H., McLafferty, F. W., Shabanowitz, J., Hunt, D. F., Fourier-transform mass spectrometry of large molecules by electrospray ionization, *Proceedings of the National Academy of Sciences*. **1989,** *86*, 9075-9078.

26. Loo, J. A., Quinn, J. P., Ryu, S. I., Henry, K. D., Senko, M. W., McLafferty, F. W., High-resolution tandem mass spectrometry of large biomolecules, *Proc Natl Acad Sci*. *89*, 286-289.

27. Senko, M. W., Hendrickson, c. L., Emmett, M. R., Shi, S. D. H., Marshall, A. G., External accumulation of ions for enhanced electrospray ionization Fourier transform ion cyclotron resonance mass spectrometry, *Journal of the American Society for Mass Spectrometry*. **1997,** *8*, 970-976.

28. Gorshkov, M. V., Masselon, C. D., Anderson, G. A., Udseth, H. R., Harkewicz, R., Smith, R. D., A dynamic ion cooling technique for FTICR mass spectrometry, *Journal of the American Society for Mass Spectrometry*. **2001,** *12*, 1169-1173.

29. Caravatti, P., US Patent. 4,924,089.; **1990.**

30. Easterling, M. L., Pitsenberger, C. C., Kulkarni, S. S., Taylor, P. K., Amster, I. J., A 4.7 Tesla internal MALDI-FTICR instrument for high mass studies: performance and methods, *International Journal of Mass Spectrometry and Ion Processes*. **1996,** *157/158*, 97-113.

31. Stults, J. T., Minimizing peak coalescence: high-resolution separation of isotope peaks in partially deamidated peptides by matrix-assisted laser desorption/ionization Fourier transform ion cyclotron resonance mass spectrometry, *Analytical Chemistry*. **1997,** *69*, 1815-1819.

32. Solouki, T., Emmett, M. R., Guan, S., Marshall, A. G., Detection, number, and sequence location of sulfur-containing amino acids and disulfide bridges in peptides by ultrahigh-resolution MALDI FTICR mass spectrometry, *Anal Chem*. **1997,** *69*, 1163-1168.

33. Nikolaev, E. N., Miluchihin, N., Inoue, M., Evolution of an ion cloud in a Fourier transform ion cyclotron resonance mass spectrometer during signal detection: its influence on spectral line shape and position, *International Journal of Mass Spectrometry and Ion Processes*. **1995,** *148*, 145-157.

34. Wong Richard, L., Amster, I. J., Sub part-per-million mass accuracy by using stepwise-external calibration in fourier transform ion cyclotron resonance mass spectrometry, *J Am Soc Mass Spectrom*. **2006,** *17*, 1681-1691.

35. Winger, B. E., Hofstadler, S. A., Bruce, J. E., Udseth, H. R., Smith, R. D., High-resolution accurate mass measurements of biomolecules using a new electrospray ionization ion cyclotron resonance mass spectrometer, *Journal of the American Society for Mass Spectrometry*. **1993,** *4*, 566-577.

36. Guan, S., Kim, H. S., Marshall, A. G., Wahl, M. C., Wood, T. D., Xiang, X., Shrink-wrapping an ion cloud for high-performance Fourier transform ion cyclotron resonance mass spectrometry, *Chemical Reviews*. **1994,** *94*, 2161-2182.

37. Guan, S., Gorshkov, M. V., Marshall, A. G., Circularly polarized quadrature excitation for Fourier-transform ion cyclotron resonance mass spectrometry, *Chemical Physics Letters*. **1992,** *198*, 143-148.

38. Wigger, M., Eyler, J. R., Benner, S. A., Li, W., Marshall, A. G., Fourier transform-ion cyclotron resonance mass spectrometric resolution, identification, and screening of non-covalent complexes of Hck Src homology 2 domain receptor and ligands from a 324-member peptide combinatorial library, *J Am Soc Mass Spectrom*. **2002,** *13*, 1162-1169.

39. Wong, R. L., Amster, I. J., Combining Low and High Mass Ion Accumulation for Enhancing Shotgun Proteome Analysis by Accurate Mass Measurement, *Journal of the American Society for Mass Spectrometry*. **2006,** *17*, 205-212.

40. Belov, M. E., Rakov, V. S., Nikolaev, E. N., Goshe, M. B., Anderson, G. A., Smith, R. D., Initial implementation of external accumulation liquid chromatography/electrospray ionization Fourier transform ion cyclotron resonance with automated gain control, *Rapid Communications in Mass Spectrometry*. **2003,** *17*, 627-636.

41. Belov, M. E., Nikolaev, E. N., Anderson, G. A., Udseth, H. R., Conrads, T. P., Veenstra, T. D., Masselon, C. D., Gorshkov, M. V., Smith, R. D., Design and performance of an ESI interface for selective external ion accumulation coupled to a fourier transform ion cyclotron mass spectrometer, *Analytical Chemistry*. **2001,** *73*, 253-261.

42. Prior, D. C., Price, J., Bruce, J. E., U.S. Patent 6,455,8646; **2002**.

43. Wu, S., Zhang, K., Kaiser, N. K., Bruce, J. E., Prior, D. C., Anderson, G. A., Incorporation of a Flared Inlet Capillary Tube on a Fourier Transform Ion Cyclotron Resonance Mass Spectrometer, *Journal of the American Society for Mass Spectrometry*. **2006,** *17*, 772-779.

44. Shaffer, S. A., Prior, D. C., Anderson, G. A., Udseth, H. R., Smith, R. D., An ion funnel interface for improved ion focusing and sensitivity using electrospray ionization mass spectrometry, *Anal Chem*. **1998,** *70*, 4111-4119.

45. Shaffer, S. A., Tolmachev, A., Prior, D. C., Anderson, G. A., Udseth, H. R., Smith, R. D., Characterization of an Improved Electrodynamic Ion Funnel Interface for Electrospray Ionization Mass Spectrometry, *Analytical Chemistry*. **1999,** *71*, 2957-2964.

46. Senko, M. W., Canterbury, J. D., Guan, S., Marshall, A. G., A high-performance modular data system for Fourier transform ion cyclotron resonance mass spectrometry, *Rapid Communications in Mass Spectrometry*. **1996,** *10*, 1839-1844.

47. Anderson, G. A., Bruce J.E., Smith R.D., ICR-2LS, Richland, WA, **1996**.

48. Kaiser, N. K., Bruce, J. E., Observation of Increased Ion Cyclotron Resonance Signal Duration through Electric Field Perturbations, *Analytical Chemistry*. **2005,** *77*, 5973-5981.

49. Kim, S., Choi, M. C., Kim, S., Hur, M., Kim, H. S., Yoo, J. S., Blakney, G. T., Hendrickson, C. L., Marshall, A. G., Modification of Trapping Potential by Inverted Sidekick Electrode Voltage during Detection To Extend Time-Domain Signal Duration for Significantly Enhanced Fourier Transform Ion Cyclotron Resonance Mass Resolution, *Analytical Chemistry*. **2007,** *79*, 3575-3580.

50. Van de Guchte, W. J., Van der Hart, W. J., Excitation of the z motion of ions in cubic and elongated ion cyclotron resonance cells, *International Journal of Mass Spectrometry and Ion Processes*. **1990,** *95*, 317-326.

51. Van der Hart, W. J., Van de Guchte, W. J., Excitation of the z-motion of ions in a cubic ICR cell, *International Journal of Mass Spectrometry and Ion Processes*. **1988,** *82*, 17-31.

52. Bruce, J. E., Anderson, G. A., Hofstadler, S. A., Winger, B. E., Smith, R. D., Time-base modulation for the correction of cyclotron frequency shifts observed in long-lived transients from Fourier-transform ion-cyclotron-resonance mass spectrometry of electrosprayed biopolymers, *Rapid Communications in Mass Spectrometry*. **1993,** *7*, 700-703.

53. Guan, S., Wahl, M. C., Marshall, A. G., Elimination of frequency drift from Fourier transform ion cyclotron resonance mass spectra by digital quadrature heterodyning: ultrahigh mass resolving power for laser-desorbed molecules, *Anal Chem*. **1993,** *65*, 3647-3653.

Figure 1

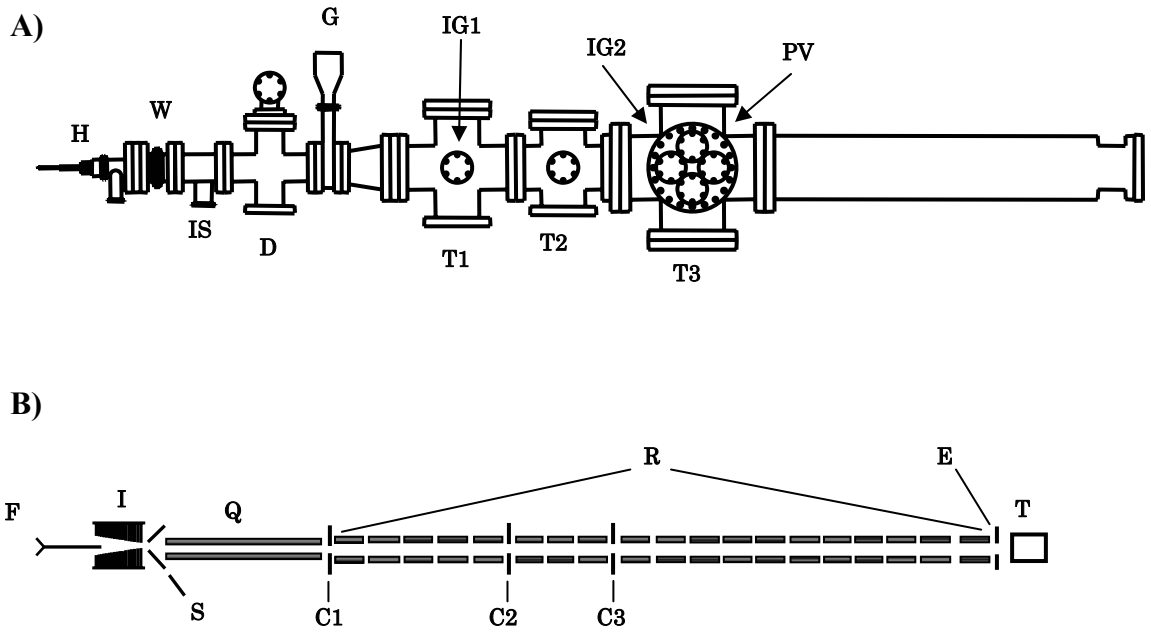

Figure 1. Novel FTICR-MS instrument developed in-house. A. Vacuum system of 3T instrument. F = Flared capillary inlet, H = heating block, W = bellows, IS = interstage pumping from the drag pump (10 l/s) , D = turbomolecular drag pump (220 l/s), G = gate valve, IG1 = ion gauge, IG2 = ion gauge 2, T1 = turbo pump 1 (350 l/s), T2 = turbopump 2 (200 l/s), T3 turbopump 3 (400 l/s). B. Ion optics within the vacuum system. I = ion funnel, Q = front quadrupole, C1, C2, C3 = are conductance limits, R = RIPT ion guide, TC = TREC ICR cell

Figure 2

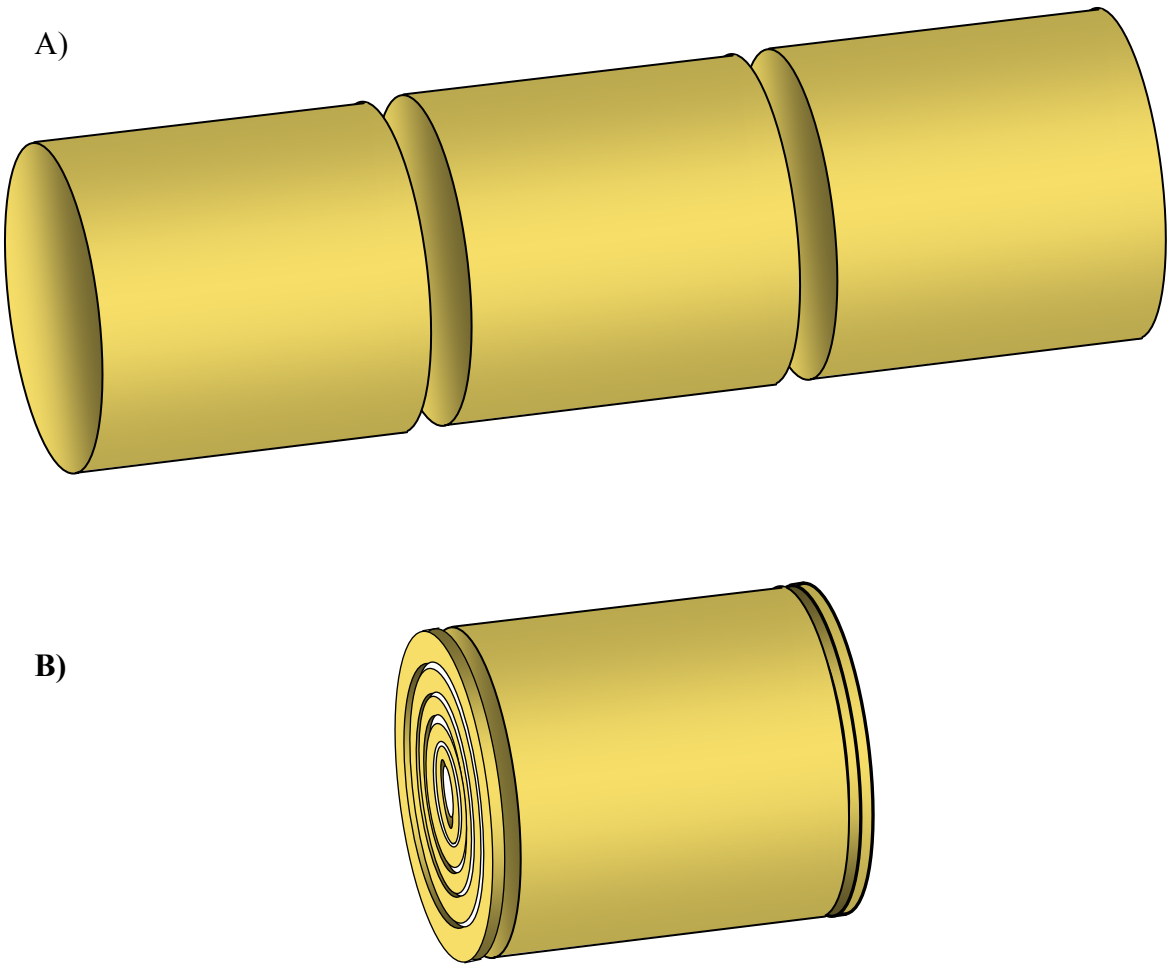

Figure 2. ICR cell designs employed in the instrument A) capacitively coupled open cylindrical cell B) TREC cell

Figure 3

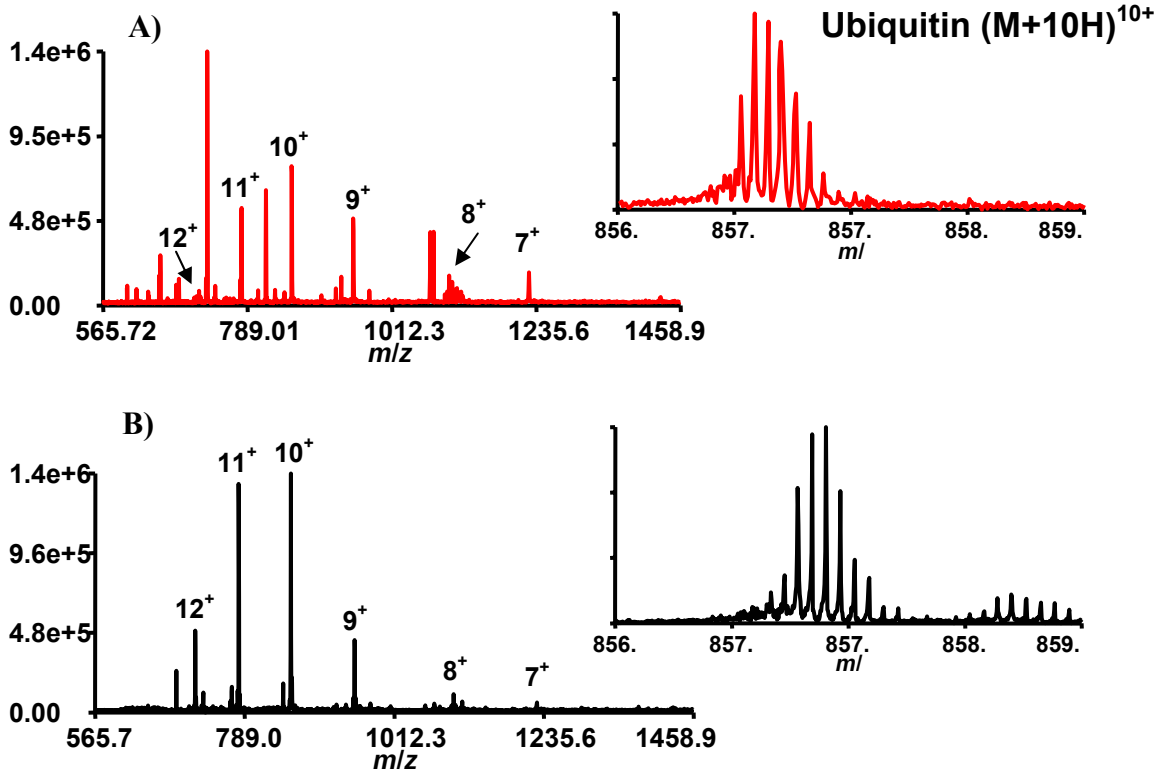

Figure 3. Ubiquitin spectra acquired with the different ICR cell designs, both are single scans. A) spectrum acquired with the capacitively coupled open cylindrical cell B) spectrum acquired with TREC. There was some fragmentation that occurred in the open cell experiment to account for the other peaks in the spectrum. The inset shows the zoomed in region of the $(M+10)^{10+}$ charge state.

Figure 4

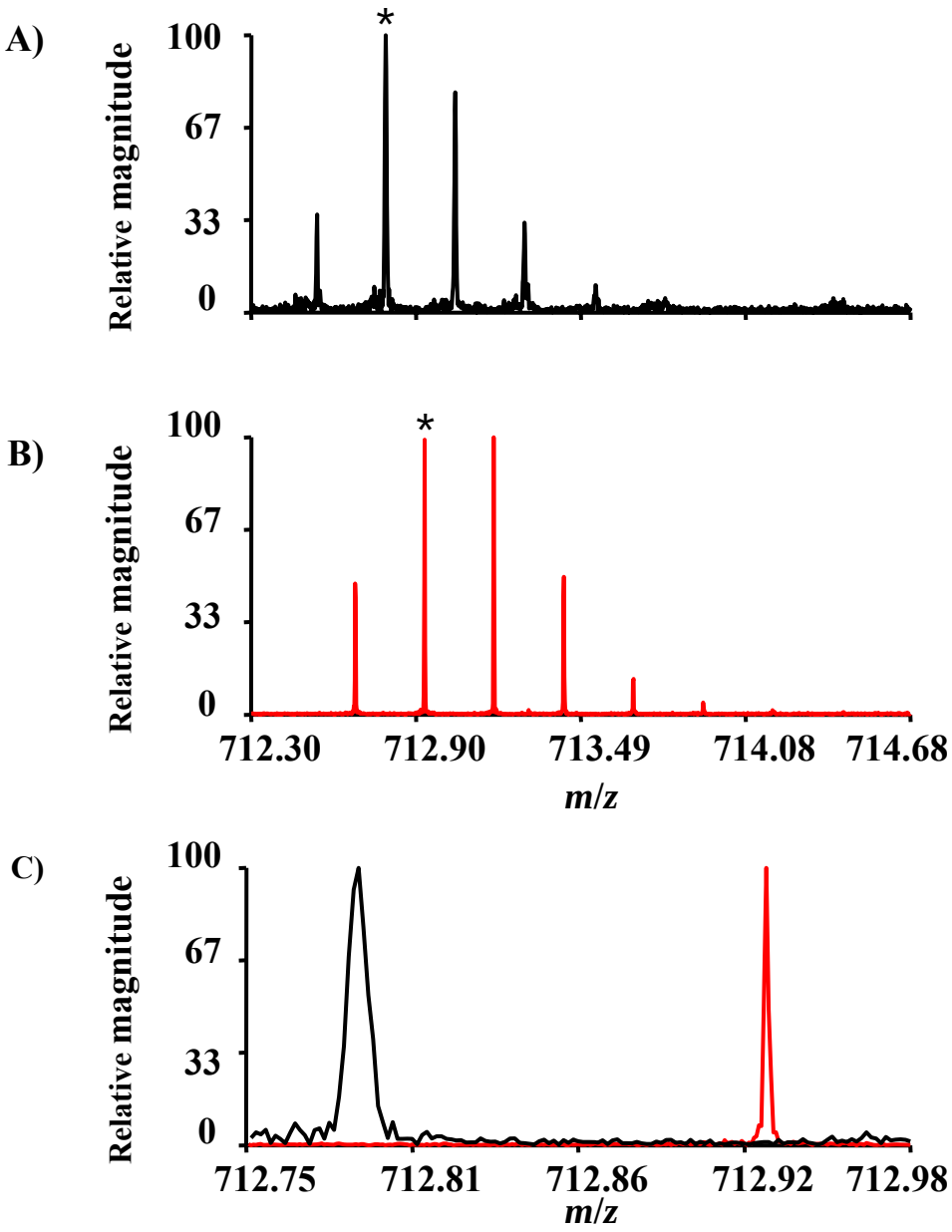

Figure 4. Melittin $(M+4H)^{4+}$ spectra acquired with the TREC cell, all spectra are single scan. A) Optimized conditions for non-TREC conditions (all rings have the same potential). B) Optimized conditions for TREC with a voltage profile of 0.2, 1.2, 2.0, 2.4, and 2.8 V from inner most ring out.

Figure 5

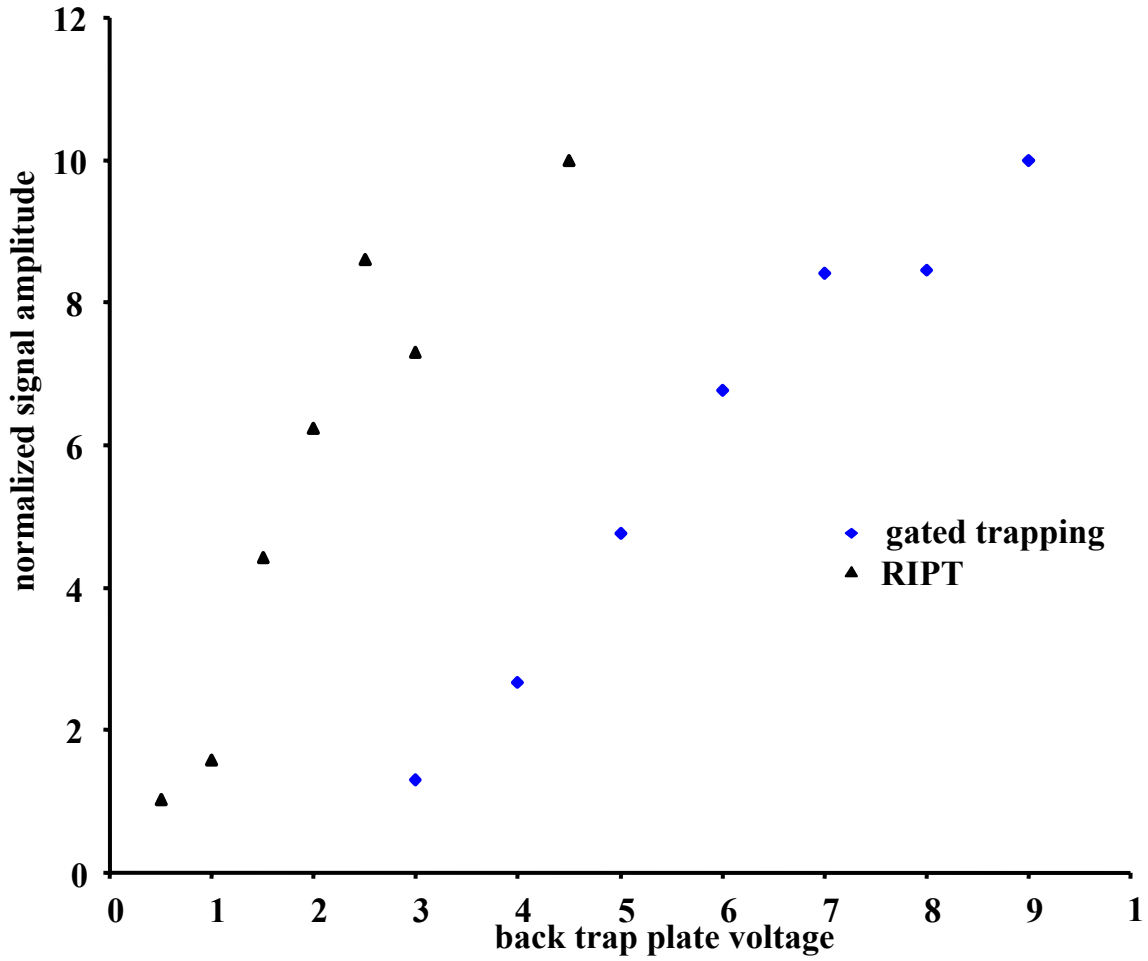

Figure 5. Comparison of kinetic energy between gated trapping and RIPT of ions entering the ICR cell.

Chapter 8

Conclusions

In CHAPTER 2 we presented a method to correct space charge induced frequency shifts in FTICR measurements which pertains to MS/MS fragment ions. In follow-up experiments that aim to minimize these frequency shifts, we produced a low energy electron beam along the *z*-axis of the ICR cell during detection. The results we obtained were unexpected; the duration of the time-domain signal increased dramatically. Characterizing and explaining this phenomenon formed the basis for the rest of my thesis work. The initial observations of this method, called Electron Promoted Ion Coherence or EPIC, had on the observed ICR signal was described in CHAPTER 3. The lifetime of the observed time-domain signal depends upon the coherent motion of ions. Through a number of experiments and deductions we were able to demonstrate that application of EPIC results in altered electric fields within the ICR cell. In depth characterization of EPIC was present in CHAPTER 4, which described how the space charge conditions and magnetron motion was altered. In the literature, one of the major causes of ion cloud de-phasing is attributed to inhomogeneity of the electric fields. Though these electric field inhomogneities have been described in theoretical work, experimental work consists mainly of axialization and reduction of trapping voltage. It was known that increasing the trapping potentials induce faster signal decay rates. In CHAPTER 5, we presented a detailed study of electric field inhomogeneity and EPIC, and how these inhomogeneities affect ion cloud stability. In most ICR cell designs, the magnitude of the radial electric

force which drives magnetron motion is not constant along the *z*-axis. When ions are trapped in the ICR cell they will exhibit a distribution of *z*-axis kinetic energy. Therefore, ions with different *z*-axis kinetic energy will exhibit different magnetron frequencies. This will lead to de-phasing of the ion packet. All ions will be in-phase after excitation but different magnetron frequencies will result in de-phasing of ion motion and the signal amplitude will decrease with time. By turning on the electron beam, we are minimizing changes in radial fields along the *z*-axis. This results in observed cyclotron frequency that is independent of *z*-axis kinetic energy. This work provides further insight into ion cloud de-phasing mechanisms.

However, it is noted in CHAPTER 4 that the observed cyclotron frequency is very sensitive to the number of electrons being sent through the ICR cell. With our current hardware, the reproducibility of the electron current from experiment to experiment was found to be inadequate, thus limiting the utility of EPIC as an analytical technique. However, the technique has proved to be extremely useful tool to study ion cloud de-phasing. All my work with EPIC has led us to develop an ICR cell which is capable of mimicking the electric fields with more flexibility and great stability than those produced with EPIC. This ICR cell design gives us the unique capability of tailoring the electric fields.

My other research objective was focused on eliminating time-of-flight effects and transferring cooled ion packets to the ICR cell. Thus, eliminate ion cooling events which require lengthy time periods. The RIPT ion guide I built to accomplish this was described in detail in CHAPTER 6. Ions were accumulated in a quadrupole at high pressure which cools the ions translational energy. Through computer modeling we were

able to illustrate that the kinetic energy imparted to the ions during the transfer process was minimized by the transfer waveform applied to the segments of the ion guide. Also, since ions are contained during the entire transfer process there are no time-of-flight effects. The ion guide was tested on a novel FTICR instrument under-developed in our laboratory. The RIPT ion guide was only one of the novel components implemented into the instrument. A full description of the instrument is available in CHAPTER 7. These novel features employed in the lab, such as EPIC, RIPT and TREC, have advanced FTICR mass spectrometry technology, and provide further insight into ion motion in the ICR cell.